Magnetic and Dielectric Studies on Cobalt Substituted BiFeO$_3$

A THESIS SUBMITTED FOR THE AWARD

OF THE DEGREE

OF

DOCTOR OF PHILOSOPHY

IN PHYSICS

By

JASHASHREE RAY

ROLL NO. - 509PH302

UNDER THE SUPERVISION OF
Dr. PRAKASH NATH VISHWAKARMA

DEPARTMENT OF PHYSICS & ASTRONOMY,

NATIONAL INSTITUTE OF TECHNOLOGY, ROURKELA-769008

ODISHA, INDIA, DECEMBER- 2014

Dedicated

To

My Parents

DECLARATION BY THE CANDIDATE

*I declare that the thesis entitled "***Magnetic and Dielectric Studies on Cobalt Substituted** $BiFeO_3$*" is my own work, conducted under the supervision of* **Dr. Prakash Nath Vishwakarma** *at NIT Rourkela, Odisha, India and approved by the Doctoral Scrutiny Committee.*

I further declare that to the best of my knowledge the thesis does not contain any part of the work which has been submitted for the award of any degree either in this Institute or in any other University/ Deemed University without proper citation. I have adhered to the norms and guidelines given in the ethical code of conduct of the Institute.

Jashashree Ray

Signature of the Candidate

CERTIFICATE

Dr. P. N. Vishwakarma
Assistant Professor
Department of Physics &Astronomy,
National Institute of Technology
Rourkela, India
Email id: prakashn@nitrkl.ac.in
pnviisc@gmail.com
Telephone: (+91) -661-2462728

This is to certify that the research work embodied in the thesis entitled "**Magnetic and Dielectric Studies on Cobalt Substituted $BiFeO_3$**" is done by **Ms. Jashashree Ray** under my supervision, towards the degree of Doctor of Philosophy at NIT Rourkela, Odisha, India. To the best of my knowledge and belief, the thesis embodies the work of the candidate herself and fulfills the requirements of the ordinance relating to the Ph. D degree of the Institute. The contents of the thesis, in full or in parts, have not been submitted to any other Institute or University for the award of any degree.

Date: **Dr. P. N. Vishwakarma**

ACKNOWLEDGEMENTS

✍ ……… *This doctoral thesis has been possible with the help and support of the kind people around me, to only some of whom it is possible to give particular mention here.*

First and foremost, I would like to acknowledge and extend my gratitude to my thesis supervisor ***Dr. P. N. Vishwakarma*** *for his patience, constant support and encouragement, without which this work could not attain the shape which it has taken. While joining Ph. D, I had a little knowledge in the field of experimental research, but he showed his enormous patience and spent sufficient time to teach me instruments, data analysis, etc. His immense knowledge, logical approach to tackle any problem and the sense of presentation has been a great motivation to me. His kind presence and advices during my adverse situation is highly respectable.*

Dr. V. Siruguri, Dr. V. Ganesan, Dr. P. D. Babu, Dr. Alok Banerjee, Dr. V. R. Reddy and Dr. M. K. Gupta is highly acknowledged for providing AFM, XRD, Magnetization, Neutron diffraction, PE loop measurements.

I would like to express my gratitude to all my Doctoral Scrutiny Committee members, Dr. S.C. Mishra (MM), Dr. D. K. Bisoyi (PH), Dr. D. Behera (PH) and Dr. P. Kumar (PH) for their useful discussions and constructive suggestions to improve the quality of this research work.

I am grateful to Dr. P. Kumar for providing me his muffle furnace for initial sintering of my sample.

I am thankful to the Dept. of Metallurgy and Materials Engineering, Dept. of Ceramic Engineering and Dept. of Physics and Astronomy for providing the XRD facility.

It gives me a great pleasure to thank my labmate Mr. Achyuta Kumar Biswal for his cooperation and companionship during my Ph.D. work. His technical knowledge and timely support helped me to carry out the experiments in our lab.

I gratefully acknowledge my labmates Mrs. Sanghamitra Acharya and Mr. Sourav Kuila for their help and for creating cordial and jolly environment in the lab.

I would like to thank to all the members of the Department of Physics & Astronomy, NIT Rourkela.

NIT Rourkela is also acknowledged for providing me the financial support for attending conferences in India as well as at Italy.

I am also thankful to UGC- DAE CSR, Indore, DST and CSIR for the financial support during my Ph. D tenure.

I am also thankful to all the research scholars of the Department of Physics & Astronomy, NIT Rourkela.

Finally, I am forever indebted to my parents, my sister, my brother-in-law, my brother for their constant encouragement, support and persistent love. I would forever relish the company of Siddhi and Sriyan.

Date: **Jashashree Ray**

NIT, Rourkela, Odisha.

Preamble

This thesis presents the study of structural, surface morphology, electric, magnetic, magnetoelectric and magnetodielectric properties of Cobalt substituted multiferroic $BiFeO_3$.

Since their discovery, multiferroics have brought tremendous interest among the researchers due to the coexistence of various ferroic order parameters. The synchronization of the magnetic and electric order parameter, hence generating magnetoelectric coupling, has been of importance in particular. Various functional devices aiming at the coupling between the ferroelectric and ferromagnetic order parameter are underway. Among all, the perovskite oxides (ABO_3) based multiferroics are of prime interest due to their ease of synthesis and easy to understand physical interactions due to their simple structure.

Bismuth Ferrite ($BiFeO_3$), is a prototype ABO_3 type multiferroic material, possessing the ferroelectric Curie temperature (Tc) ~ 1103K and antiferromagnetic Neel temperature (T_N) ~ 643K. It exhibits a weak net magnetization as the G- type magnetic ordering is superimposed with an incommensurate cycloidal spin structure having the periodicity of 62nm. The chemical substitution is considered as one of the alternatives for enhancing the net magnetization via disruption of the cycloidal chain. Among the various B–site substitution, the Co substituted $BiFeO_3$ is found to be very rare in the literature.

In this context, Co is chosen for the substitution at the Fe- site as the ionic radius of both Fe and Co are similar. On top of that Co^{3+} exhibits thermally stimulated spin state transitions from a low spin (LS; $T < 100$ K) to high spin (HS; $T > 500$ K) via an intermediate spin (IS; $100K < T < 300$ K). Thus the effect of spin state transition on the magnetic as well as on the electric properties has been explored.

The Co substituted $BiFeO_3$ ($BiFe_{1-x}Co_xO_3$; x=0, 0.01, 0.02, 0.03, 0.1, 0.2, 0.3, 0.35, 0.4, 0.5, 0.6, 0.7, 0.8, 0.9 and 1) are prepared by the sol gel auto combustion method. The phase confirmation is done via the x-ray diffraction (XRD) measurement. The refinement of XRD data via Reitveld technique confirms the rhombohedral crystal structure (space group R3c) of the pristine sample with no trace of secondary phases. The R3c structure remains stabilized for x = 0.01 and x = 0.02. From x = 0.03 onwards, peaks related to another phase (cubic, space group I23) are also seen along with the rhombohedral phase. On further increasing the Co concentration, the x-ray data shows that from x = 0.35, the sample is again in single phase, but this time, crystallized in a cubic structure (I23). However, the present study deals only with the single phase $BiFe_{1-x}Co_xO_3$ which comprises the dilute concentration of Co viz. x = 0, 0.01, 0.02 and the higher concentration of Co viz. x = 1, x = 0.5.

The surface morphology study carried out via atomic force microscopy shows that the particles sizes for all the samples are of nano-order (100 – 200nm). The temperature dependent DC magnetization study on the dilute Co (x = 0, 0.01, 0.02) substituted $BiFeO_3$, reveals various magnetic states viz. superparamagnetic, antiferromagnetic and ferromagnetic states along with the signature of the spin glass transition. Presence of glassy behaviour is also seen in the magnetic relaxation measurements, done at various static temperatures. The temperature dependent neutron diffraction measurements are done on all the three samples. At room temperature the Co^{3+} ions are found to be in an intermediate spin state corresponding to magnetic moment 2.828 μ_B, whereas that of Fe^{3+} as 3.848μ_B. Lowering of temperature shows signature of possible spin state transition from an intermediate spin (S = 1) to low spin (S = 0) of Co^{3+} ion. Apart from this, from the magnetic ordering point of view, substitution of Co^{3+} is found to increase magnetic anharmonicity with more spin canting. This magnetic anharmonicity decreases with lowering of temperature and the magnetic cycloidal structure revives.

Measurement of room temperature longitudinal ME coupling coefficient (α) displays a hysteresis as a function of magnetic field (H) for the pristine sample whereas the hysteresis disappears for x =0.02. The variation of α in x = 0.02 becomes linear in H which is well sought for device applications, especially where α must follow the applied magnetic field linearly, e.g., transistors, transducers, etc. A close correlation is observed among the magnetoelectric coefficient, polarization and magnetodielectricity in Co-substituted $BiFeO_3$.

The electrical transport measurements suggest Mott’s variable range hopping as the conduction mechanism at low temperature. The calculated average hopping range also is in agreement with the increase in conductivity of $BiFeO_3$ on cobalt doping.

The low temperature dielectric measurement on x = 0, 0.01, 0.02 shows the joint contribution of Haverliak – Negami (HN) and Maxwell Wagner (MW) type relaxations, such that near room temperature region is dominated by the MW. The dielectric relaxations are found to be obeyed by polaronic variable range hopping model. Various magnetic transitions are observed via the magnetodielectric measurement. In addition, a new relaxor type behavior is also observed in $BiFe_{0.98}Co_{0.02}O_3$ above the room temperature (~ 475K).

The Bismuth cobaltite $BiCoO_3$ (x = 1) and 50% Fe- substituted $BiCoO_3$ (x =0.5) are synthesized under ambient condition via sol – gel method. The Reitveld refinement of XRD data confirms cubic crystal structure where Co ions at 2a sites are tetrahedrally bonded to four oxygen ions and those sharing the 24f positions with Bi are bonded in square pyramidal configuration. The temperature dependent DC magnetization shows the paramagnetic nature of x =1 at room temperature and a hint of possible antiferromagnetic magnetic ordering at 30K without any magnetic disorder. On the other hand, x = 0.5 shows huge magnetic disorder with a ferromagnetic ground state. Dielectric measurements on x = 1 sample shows dominant extrinsic contributions to dielectric with negligible intrinsic contributions, whereas x = 0.5 sample shows both intrinsic and extrinsic contributions to dielectric.

CONTENTS

Chapter 1

Introduction

This chapter deals with the introduction of multiferroics and magnetoelectrics. The importance of these multiferroics in various technological applications is highlighted. Among the several multiferroics, the multiferroicity in perovskite oxides have been specially emphasized. In the present work, single phase Bismuth ferrite is the focus of study. The underlying physics of various cobaltates is discussed. The mechanism of the spin state transition of these cobaltites is also taken into consideration. Then the motivations and aim of the present work are highlighted.

1.1 Multiferroics and Magnetoelectrics

In the current age of device miniaturization, multiferroics are technologically significant. It involves the coexistence of two or more ferroic order parameters viz. ferroelectricity, ferromagnetism and ferroelasticity in a single phase[1]. The possible potential applications along with the rich underlying physics, renders a new scope for the researchers to explore. The underlying complex physical phenomena involving spin dynamics, charge ordering, phonon interactions and their mutual dependency holds a lot of grey areas for the researchers.

Multiferroics involve coupling between the electric and magnetic order parameters. Magnetoelectric coupling allows the electric polarization of multiferroics to be tuned by external magnetic field and vice versa[2]. The strong magnetoelectric coupling is the ultimate goal for device application[3]. This magnetoelectric coupling can be parameterized by the expansion of free energy[2] as given in eq. 1.1.

$$F(E,H) = F_0 - P_i^s E_i - M_i^s H_j - \frac{1}{2}\varepsilon_0 \varepsilon_{ij} E_i E_j - \frac{1}{2}\mu_0 \mu_{ij} H_i H_j - \alpha_{ij} E_i H_j - \frac{1}{2}\beta_{ijk} E_i H_j H_k - \frac{1}{2}\gamma_{ijk} H_i E_j E_k - \cdots \quad \text{------------------- (Eq. 1.1)}$$

The electric polarization 'P' and magnetic magnetization 'M' are obtained by taking the derivative of free energy w.r.t electric field 'E' and magnetic field 'H' respectively,

$$P_i = -\frac{\partial F}{\partial E_i} = P_i^s + \varepsilon_0 \varepsilon_{ij} E_j + \alpha_{ij} H_j + \frac{1}{2}\beta_{ijk} H_j H_k + \gamma_{ijk} H_i E_j - \cdots \quad \text{------------ (Eq. 1.2)}$$

$$M_i = -\frac{\partial F}{\partial H_i} = M_i^s + \mu_0 \mu_{ij} H_j + \alpha_{ij} E_i + \beta_{ijk} E_i H_j + \frac{1}{2}\gamma_{ijk} E_j E_k + \cdots \quad \text{------------- (Eq. 1.3)}$$

where ε_0 is the permittivity of the free space, ε_{ij} is the relative permittivity, E is the applied electric field, μ_0 is the permeability of the free space, μ_{ij} is the relative permeability and H is the applied magnetic field. The first term of the eq. 1.2 represents the electrical response due to the electric field and that in eq. 1.3 is the magnetic response due to the magnetic field. The second term in (eq. 1.2) is linear in magnetic field and similarly in (eq. 1.3) linear in electric field, which signifies that electric polarization may also be obtained via magnetic field and magnetic polarization via electric field. Third term onwards contains the higher orders of magnetic field (eq. 1.2) and electric field (eq. 1.3), thus contributes nonlinear coupling. The parameters α_{ij} is the measure of linear magnetoelectric coupling and β_{ijk} & γ_{ijk} for nonlinear magnetoelectric coupling.

The coefficients α and β determines the coupling strength and can be measured directly (discussed in chapter 5). Another way of measuring the magneto electric coupling is by indirect method which involves measurement of magnetization near the ferroelectric transition temperature or vice versa[4, 5].

1.2 Applications of Multiferroics:

The confluence of various ferroic order parameters in multiferroics enhances the possibility for large scale applications. The multilayered multiferroics also can be used as electrically tunable microwave applications such filters, oscillators, phase shifters and low frequency with high resolution magnetic field sensors[6]. Furthermore, the magnetoelectric coupling increases the possibility for extensive use in spintronic devices[7]. The spintronic device includes actuators, transducers with magnetically modulated piezoelectricity and multiple state memory devices[8]. The memory device essentially needs strong coupling between the polarization and magnetization, so that ferroelectric data storage may be combined with magnetic read[9]. However, for the best realization of these applications, strong coupling coefficients are highly desirable. Fig. 1.1 shows the schematic diagram of one such possible device application of multiferroics.

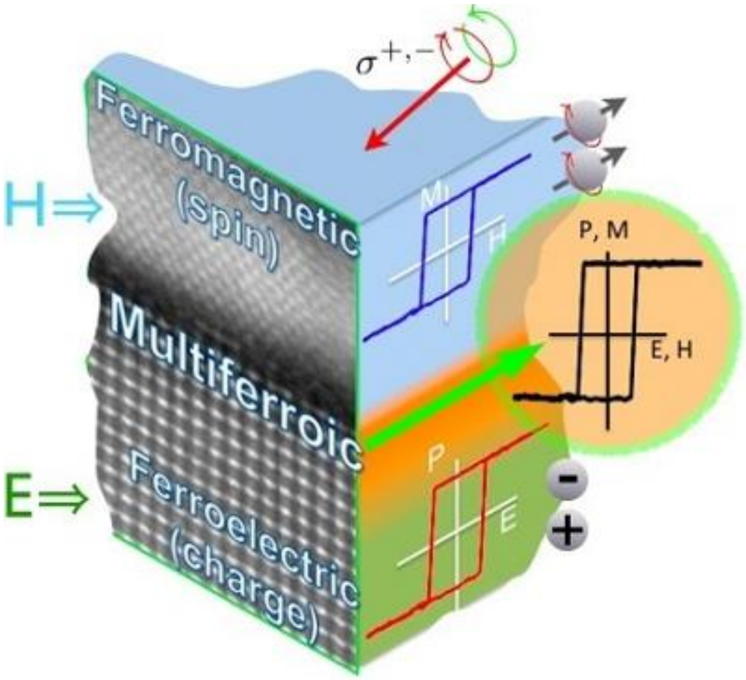

Fig. 1.1. A possible application of mutiferroics at the interface of ferroelectric and ferromagnetic material [10,11].

1.3 Multiferroic effect in perovskite oxides:

Multiferroic oxides like $BiFeO_3$, $TbMnO_3$, $YMnO_3$, $BiMnO_3$, $BiCrO_3$ etc. are crystallized in the perovskite type structure (ABO_3) as shown in fig. 1.2. These oxides have brought considerable attention due to their structural simplicity and they can easily grow. In the quest for perovskite multiferroic oxide, $(1-x)Pb(Fe_{2/3}W_{1/3})O_3$ - $xPb(Mg_{1/2}W_{1/2})O_3$ is found to be the first ferromagnetic ferroelectric synthetic material[12] in which Mg and W causes the ferroelectricity whereas Fe^{3+} (d^5) ion is responsible for the ferromagnetism. Similarly, the perovskite Pb based oxides such as $Pb_2(CoWO_6)$[13], and $Pb_2(FeTa)O_6$[14] are the ferroelectric-ferromagnetic and ferroelectric-antiferromagnetic materials respectively. However the recent trend of Pb – free research urged the researchers to explore for new multiferroics. Perovskite manganites such as $BiMnO_3$ is considered as ferromagnetic and ferroelectric [15, 16], $YMnO_3$ is antiferromagnetic and ferroelectric [17]. Furthermore, the Bi based chromite viz. $BiCrO_3$[18], Bi_2CrFeO_6[19] also exhibits the multiferroicity.

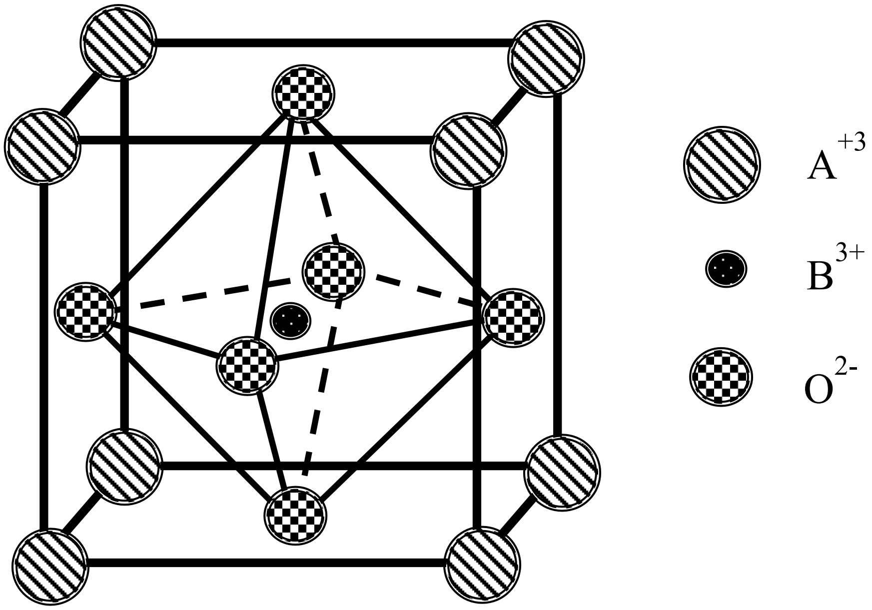

Fig. 1.2. The Schematic diagram of a perovskite structure. The large A-cations occupies the corners positions and the smaller B cations are at the center of the oxygen octahedron (at face center positions).

1.3.1 Reason of mutually exclusiveness of multiferroic perovskite oxides:

There are various limiting factors that prevent the coexistence of the ferroelectricity and ferromagnetism in a single phase. The ferroelectricity and ferromagnetism have contrasting origins. These two ferroic ordering depends on the d electronic state of the central transition metal cation of the perovskite oxide. The empty d orbital (d^0) of the central metal cation of perovskite oxide can be possibly one reason for the noncentrosymmetric lattice distortion. The hybridization among the central empty d cation and p orbital of anion forms the covalent bond that stabilizes the distortion and hence ferroelectricity develops in the material. The cations such as Ti^{+4}, V^{+5}, Nb^{+5}, Ta^{+5}, W^{+6} etc. are exhibiting the d^0 – ness, thus the perovskite oxide containing these cations shows ferroelectricity.

On the other hand, magnetism in the perovskite oxide requires unpaired itinerant d electronic state (d^n, where n = 1, 2, 3….) of the central metal ion. These partially filled d electron comprises a net magnetic moment. The cooperative coupling of these magnetic moments results the magnetism.

Due to the above mutual exclusiveness of d^0 vs. d^n, the existence of ferroelectricity and magnetism in a single phase is very rare [9, 20].

1.3.2 Several alternatives for coexistence of multiferroicity in perovskite oxides:

Despite the above discussed mutual exclusiveness of ferroelectricity and ferromagnetism in perovskite oxides, there exist several alternative mechanisms for combining these two ferroic orders in a single phase. Keeping the d^n ness as the source of magnetism in perovskite oxide, ferroelectricity can have different origins. The different mechanisms for the origin of ferroelectricity with magnetic central cation are the following:

Ferroelectricity due to lone pairs:

The ferroelectricity in Bi^{3+} or Pb^{2+} based compounds can be generated due to the stereochemically active $6s^2$ lone pair. Instead of forming any chemical bond with the oxygen ligand, the lone pair of electrons forms an asymmetric electron density around it. This asymmetric electron density causes the dangling of the bonds in perovskite oxide resulting the noncentrosymmetric lattice distortion. Hence a polarization develops in the material[9]. Few perovskite oxides viz. $BiFeO_3$, $BiMnO_3$, $PbVO_3$ etc. exhibit ferroelectricity due to this lone pair mechanism.

Ferroelectricity due to charge ordering:

The ferroelectricity can also be possible by the charge ordering which is mostly observed in transition metal compounds having different valence of the central metal cation. The charge ordering implies inequivalent bonds of the transition metal ion hence produce ferroelectricity[21]. The ferroelectricity in manganites and nicklates arises due to this charge ordering. In addition to these, ferroelectricity in $LuFe_2O_4$ arises because of polarized Fe-O bilayers due to charge ordering.

Geometric ferroelectricity:

The tilting of the central transition metal ion and oxygen block (BO_5) generates geometric ferroelectricty[22]. $YMnO_3$ exhibit the geometric ferroelectricity. Due to the tilting of the MnO_5 block, the positive and negative charge centers get separated, thus creating a net dipole moment.

Among these perovskite oxides Bi based perovskites have been highly studied since the 19th century. The coexistence of lone pair based ferroelectricity along with complex magnetic ordering provides a great platform for the research community. In $BiFeO_3$, the ferroelectricity originates due to the $6s^2$ lone pair of Bi^{3+} whereas the magnetic ordering generates due to the partially filled Fe^{3+} cation. Due to this different origin of the ferroic ordering, multiferroicity exist in the single phase. The material can possibly be applied for the development of devices as the ferroelectric and magnetic transition lies above room temperature [23].

1.4 Bismuth Ferrite

Among all the novel multiferroics, Bismuth ferrite ($BiFeO_3$: BFO) is a prototype multiferroic that possess various kinds of ferroic ordering in the single phase. The rich physics involved in the material brought the tremendous attention of the researchers. There are still numerous studies going on for the depth understanding of the underlying physics and to improvise its ferroic orderings.

BFO crystallizes in the rhombohedrally distorted perovskite structure with the space group R3c. The unit cell can be represented in the hexagonal structure with the lattice parameter a = 5.587Å and c = 13.867Å[24] as shown in fig. 1.3. The oxygen octahedra of the perovskite tilted with $[\bar{a}\bar{a}\bar{a}]$ system[25] and rotated in anticlockwise around the $[111]_c$ direction[26] with the angle of distortion ~ 11^0 - 14^0 [27, 28, 29]. The lone pair of Bi may be the possible reason behind the distortion of the octahedra as both Bi^{3+} and Fe^{3+} cations are shifted from their centrosymmetric positions. So there are two inequivalent O-O bond lengths i.e. 2.71 Å and 3.02 Å[28] in the octahedra. The noncentrosymmetric arrangement of the octahedra results polarization and is directed along the $[001]_{hex}$ or $[111]_{cub}$ direction. At room temperature, BFO is a commensurate ferroelectric[30]. It possesses a large leakage current which hinders it for the practical applications. The spontaneous polarization in bulk single crystal BFO is obtained ~ 6.1 μCcm^{-2} at 77K along [111] direction[30]. The actual polarization of BFO obtained from the theoretical calculation is of one order higher magnitude than the experimentally observed one [30]. However, a large polarization is obtained ~ 90 -100 μCcm^{-2} for BFO thin film [31, 32]. The ferroelectric Curie temperature (T_c) is ~ 1103K [33].

The bulk BFO is considered as an incommensurate antiferromagnet having Neel temperature (T_N) ~ 643K [27, 33, 34]. The magnetic moment of Fe^{3+} is coupled ferromagnetically within the $(001)_h$ planes and antiferromagnetically between the adjacent planes, hence results G-type antiferromagnetism [35].

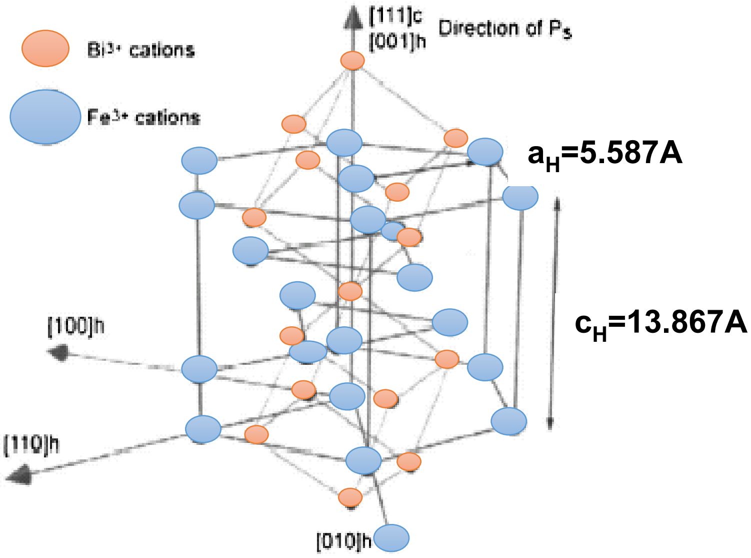

Fig. 1.3. Schematic diagram showing the direction of spontaneous polarization in the hexagonal unit cell of $BiFeO_3$ [36].

However, a spiral spin structure is found to superimposed on the antiferromagnetic order having periodicity of 62nm [35] (as shown in fig. 1.4) along the [110] direction. This spiral spin arrangement results the cancellation of the net magnetization and thus by hampering the linear magnetoelectric effect [37, 38]. The spiral spin arrangement of Fe^{3+} was introduced by Sosnowska et.al.[35] while performing the high resolution time of flight neutron diffraction measurement. The most intense magnetic satellite peaks were obtained around (101) and (003) plane at about 9.2 Å (as shown in fig. 1.5) [35].These peaks were attributed to antiferromagnetically arranged spiral spin order. The length of the spiral was obtained from the span of the (101) triplet, the orientation of the propagation vector was obtained from the shape of the magnetic peaks and the intensity of (101) and (003) peaks defines the type of spiral spin structure [35]. Numerous debates are still prevailing for explaining the modulated structure by performing neutron diffraction [39], NMR study [40, 41], Mossbauer spectroscopy [42] etc. In spite of the several available literatures dealing with the modulated structure, still it is an open area of research.

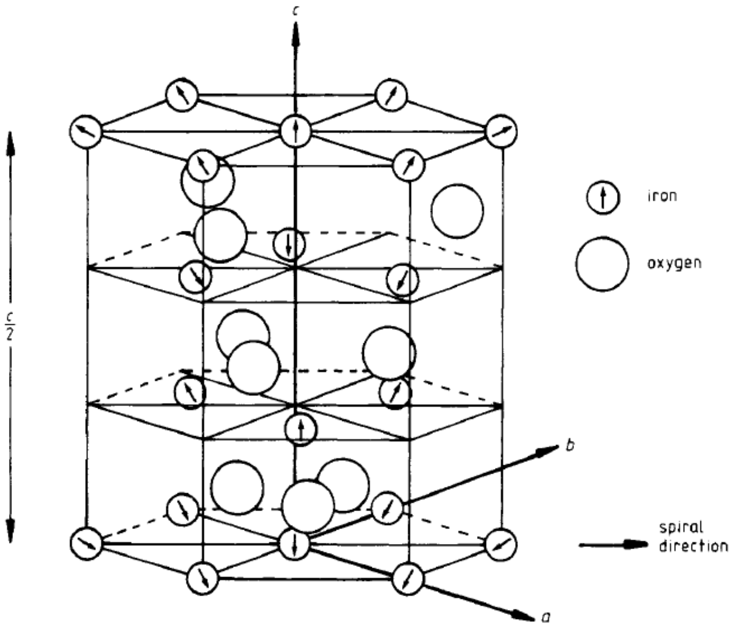

Fig. 1.4. Schematic diagram of a portion of $BiFeO_3$ lattice showing spiral arrangement of spin [35].

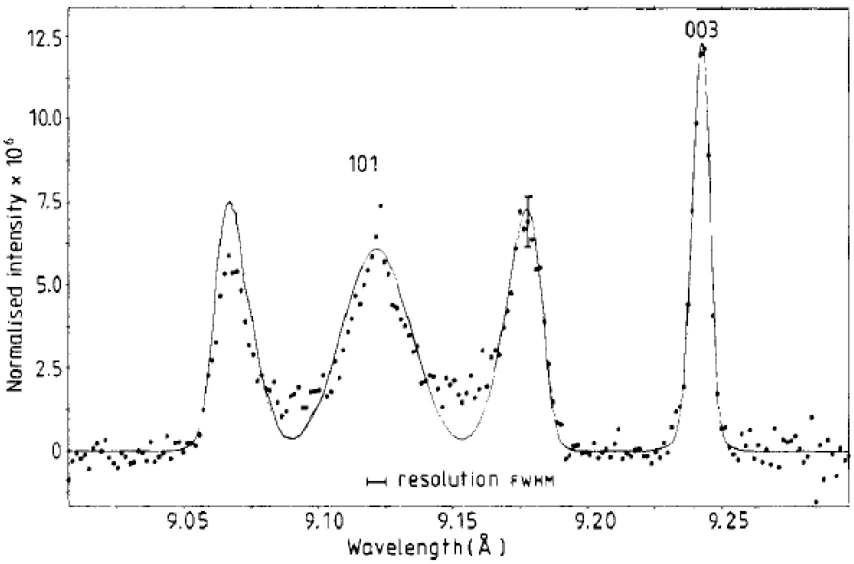

Fig. 1.5. Normalized time of flight spectrum of $BiFeO_3$ powder sample at about 9.2Å. The full curve represents the spectrum calculated for the proposed model of spin configuration[35].

In addition to this, the weak magnetization exhibited by BFO makes it unsuitable for the practical applications. Hence various attempts have been taken by the researchers to improvise its magnetization. According to the literatures, the spiral spin can unwind by applying a large magnetic field ~ 18T [43]. Instead of this huge magnetic field, the application of strain [44] or the chemical substitution [45, 46] by various suitable elements is also able to improve the magnetization. Besides the bulk antiferromagnet, researchers observed that the weak magnetic ordering can be improved by synthesizing the phase pure BFO in various lower dimensions such as thin film (2D), nanopowders, nanowires etc. [45, 47, 48]. The magnetic ordering shows a strong correlation with the dimensions. The nanoparticles of BFO are able to interrupt the spiral spin arrangement hence resulting uncompensated spins. These uncompensated spin improves the magnetization. The surface to volume ratio becomes larger as the particle size reduces, thus the net magnetization is enhanced resulting ferromagnetic ordering by the uncompensated spins at the surface [47].

Recent research reveals that BFO exhibits various anomalies at the cryogenic temperatures. Various phase transitions at 50K, 140K, 200K and 230K have been witnessed from the

Raman scattering and dielectric measurements on single crystal and polycrystalline BFO (as shown in fig. 1.6) [49- 51].

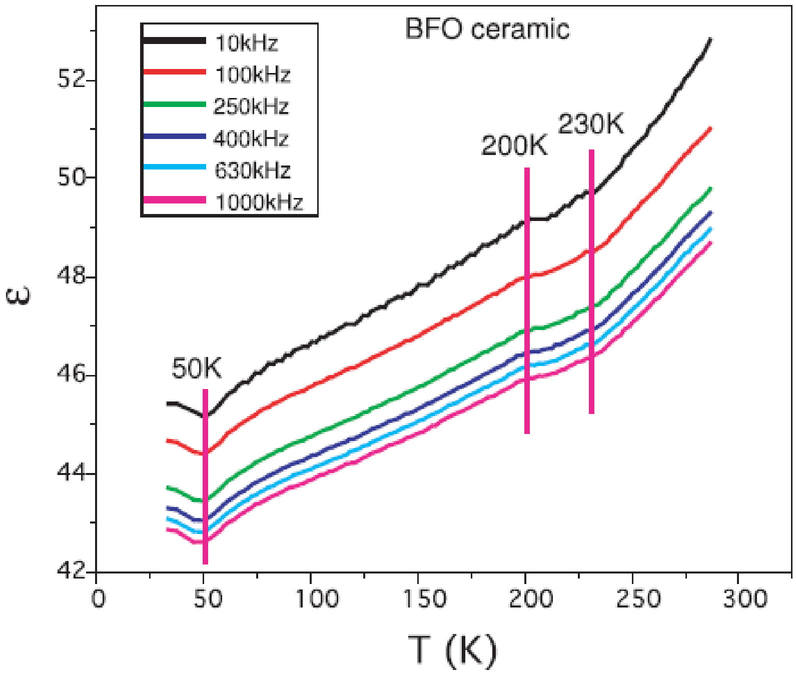

Fig. 1.6. Dielectric constant of $BiFeO_3$ ceramic at low temperature, shows anomaly at 50K, 200K and 230K at several frequencies [49].

Most of these phase transitions have also been observed as dielectric anomalies and are inferred as: 50 K, (magnetic, but glassy and with magnetoelectric coupling), 140 K (dominantly magnetic), 200 K (magnetoelastic with small coupling to polarization) and 230 K (magnetic; glassy and also weakly coupled to polarization)[49]. In reduced dimensions, for instance thin film, “one magnon” scattering is observed at 90K and also a kink in magnon intensity at 150 K and a strong anomaly near 210 K as a representation of spin reorientation transition inferred from Raman spectroscopy [52]. For samples prepared under vacuum annealed condition, additional two dielectric anomalies have been reported at 25K and 281K. The anomaly at 25K has been found to be due to structural distortion, which affects charge, spin, and structural degrees of freedom and that at 281K is due to the antiferromagnetic to spin glass transition [53].

Spin glass behavior is also observed by Nakamura in amorphous $BiFeO_3$ below T = 220K[54]. In single crystal $BiFeO_3$, the spin glass transition is observed below 250K with a sharp cusp representing the blocking temperature (T_B) at ~ 50K [55]. There are literatures available that may explain the spin glass transition in $BiFeO_3$[55, 56]. The band gap calculated from the optical measurement is ~ 2.3 – 2.8eV and is a direct band gap at room temperature [57].

From the above literatures, it is inferred that BFO exhibits multiple transitions as observed from various measurements viz. Raman spectroscopy, NMR, neutron diffraction, dielectric measurements, etc. The modulated spiral spin structure captivates the scientific community. The interruption of the spiral spin can be possible by the substitution of magnetic ion at Fe site or by divalent ions and rarer earth ions at Bi site, hence improving the magnetization. Substitution might improve the leakage current problem with improved ferroelectricity. The above peculiar characteristic of BFO certifies it to be a potential multiferroic.

1.5 Cobaltites

In recent years the cobaltites have brought considerable attention due to their peculiar properties. The cobaltites which are crystallized in the perovskite structure with Co^{3+} as the central transition metal ions are surrounded by the oxygen octahedral. The CoO_6 octahedral is mainly responsible for the spin state transition[58, 59], metal- insulator transition, etc[60-62]. The magnetic state of these cobaltites, in particular, is very unique. The electronic state of the Co^{3+} ion contains six electrons in the outer most d orbital (d^6). The hybridization between the five d orbitals with the surrounding oxygen ligands takes place. However, according to the crystal filed theory, the electrostatic repulsion from the negatively charged oxygen octahedral environment results the d orbitals in two classes. The d_{xy}, d_{yz} and d_{xz} orbital constitute the t_{2g} orbitals and $d_{x^2-y^2}$ and d_{z^2} together forms e_g orbitals. Depending upon the extent of overlapping between the five d orbitals and oxygen p orbitals, the energy of the t_{2g} is less as compared to e_g. Hence, the five orbitals split with threefold t_{2g} levels and two fold e_g levels.

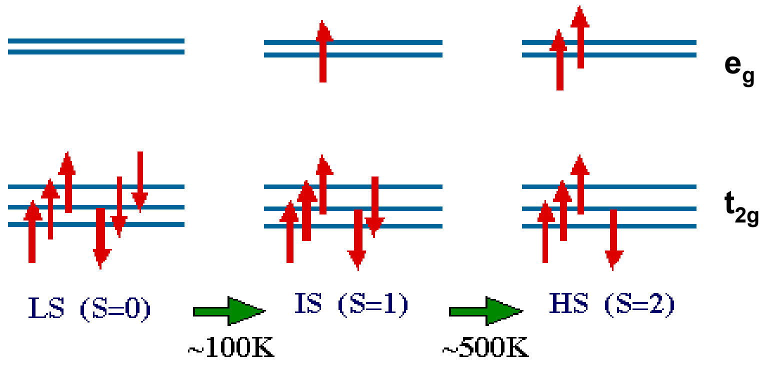

Fig. 1.7. Schematic diagram of spin state transition exhibited by Co^{3+} in the octahedral coordination [56].

Co^{3+} in this octahedron (e.g., $LaCoO_3$) exhibits thermally stimulated spin state transitions from low spin (LS; T < 100 K) to high spin (HS; T > 500 K) via an intermediate spin (IS; 100K < T < 300 K) as shown in fig. 1.7 [63]. This behavior is attributed to the comparable energy of crystal field splitting of Co-d states (Δ_{CF}) and Hund's exchange energy (Δ_H) which results a small separation between t_{2g} and e_g levels, of the order of k_BT. Hence variation of temperature or application of pressure can lead to the occupation of a higher spin state[63].

1.6 Motivations

The synthesis of single phase BFO is more challenging. Since its discovery, researchers have attempted various synthesis conditions, such as, in solid state process the sintering temperature is vital whereas in solution method, the fuel used is found to be very much crucial. In addition to this, during the synthesis of BFO, more emphasis is given to avoid the Bi loss. The dopant may create the secondary phase due to ionic radius mismatch. A plenty of research has been carried out to improve both magnetic and electric ordering by various composites, elemental substitutions, etc. The reports of Co^{3+} substitution (available till now), deals only with the magnetic part, leaving the dielectric or magnetoelectric properties unaddressed. Among the various reports of B-site substitution, substitutions via Co are very few. The Co^{3+} ion in an octahedral arrangement undergoes spin state transitions. The effect of spin state transition on the magnetic as well as on the electric properties is an area to be explored.

1.7 Objectives of the present work:

- Synthesis of single phase nanoparticles of BFO.
- The lone pair of electrons of Bi is mainly responsible for the observed ferroelectricity in $BiFeO_3$. Thus, it won't be a good idea to replace Bi by other elements and hence we restricted ourselves to the Fe site only.
- Initially, a very dilute substitution of Co at the Fe site is chosen, so that any lattice distortion due to ionic radius mismatch may be minimized.
- The synthesis procedure is restricted to the single phase of BFO and its Co substituted compounds so that we may address (i) the spin cycloid in nano BFO (ii) the effect of Co^{3+} substitution on the magnetic cycloid of BFO (iii) the evolution of Co^{3+} substituted BFO with decrease in temperature.
- As Co^{3+} exhibits thermally induced spin state transitions, so its effect on magnetic ordering is also expected below room temperature.
- The effect due to cobalt on the crystal or magnetic lattice and hence leading to the magnetoelectric property is also expected to be revealed.
- Due to multiple transitions exhibited by BFO, we have focused our attention on both low and high temperature dielectric and magnetodielectric response of BFO as well as its Co substituted compounds.
- Similar to BFO, synthesis of $BiCoO_3$ ($x = 1$) is done under ambient condition and its magnetic and dielectric behaviour is studied. The magnetic and electric properties as a function of temperature are studied especially below 100K. In addition, we have also addressed the effect due to partial substitution of Fe at Co site of $BiCoO_3$.

References:

1. H. Schmid, *Ferroelectrics*, **162** 665 (1994)
2. M. Fiebig, *J. Phys. D: Appl. Phys.*, **38** R123 (2005)
3. L W Martin, S. P. Crane, Y. -H. Chu, M. B. Holcomb, M. Gajek, M. Huijben, C. -H. Yang, N. Balke and R. Ramesh, *J. Phys.: Condens. Matter*, **20** 43420 (2008)
4. T. Kimura, S. Kawamoto, I. Yamed, M. Azuma, M. Tanky, and Y. Tokura, *Phys. Rev. B*, **67** 180401R (2003)
5. V. R. Palkar, J. John, and R. Pinto, *Appl. Phys. Lett.*, **80** 1628 (2002)
6. S. Dong, J. Cheng, J. F. Li, and D. Viehland, *Appl. Phys. Lett.*, **83** 4812 (2003)
7. R. Ramesh and N. Spaldin, *Nature Mater.*, **6** 21 (2007)
8. N. A. Hill, *J. Phys. Chem. B*, **104** 6694 (2000)
9. Y. Jian and C. JunHao, *Chin. Sci. Bull.*, **53** 2097 (2008)
10. S. Valencia, A. Crassous, L. Bocher, V. Garcia, X. Moya, R. O. Cherifi, C. Deranlot, K. Bouzehouane, S. Fusil, A. Zobelli, A. Gloter, N. D. Mathur, A. Gaupp, R. Abrudan, F. Radu, A. Barthelemy and M. Bibes *Nat. Mater.*, **10** 753 (2011).
11. V. Garcia, M. Bibes, L. Bocher, S. Valencia, F. Kronast, A. Crassous, X. Moya, S. Enouz-Vedrenne, A. Gloter, D. Imhoff, C. Deranlot, N. D. Mathur, S. Fusil, K. Bouzehouane, A. Barthelemy, *Science*, **327** 1106 (2010).
12. G. A. Smolensky, V. A. Isupov, N. N. Krainik, A. I. Agranovskaya, *Isvest. Akad. Nauk SSSR, Ser. Fiz*, **25** 1333 (1961)
13. W. Brixel, J.P. Rivera, A. Steiner, H. Schmid, Ferroelectrics, **79**201(1988)
14. D. N. Astrov, B. I. Al'shin, Y. Y. Tomashpol'skii, Y. N. Venevtsev, *Sov. Phys. JETP*,**28** 1123 (1969)
15. N. A. Hill, K. M. Rabe, *Phys. Rev. B*, **59** 8759 (1999)
16. A. M. dos Santos, S. Parashar, A. R. Raju, Y. S. Zhao, A. K. Cheetham and C. N. R. Rao, *Solid State Comm.*, **122** 29 (2002)
17. Z. J. Huang, Y. Cao, Y. Y. Sun, Y. Y. Xue and C. W. Chu, *Phys. Rev. B*, **56** 2623 (1997)
18. N. A. Hill, P. Battig and C. Daul, *J. Phys. Chem. B*, **106** 3383 (2002)
19. P. Baettig, C. Ederer and N. A. Spaldin, *Phys. Rev. B*, **72** 214105 (2005)
20. D. Khomskii, *Physics*, **2** 20 (2009)

21. J. V. D Brink and D. I. Khomskii, *J. Phys.: Condens. Matter*, **20** 434217 (2008)
22. B. B. V. Aken, T. T. M. Palstra, A. Filippetti and N. A. Spaldin, *Nature Mater.*, **3** 164 (2004)
23. D. Pandey and A. Singh, *Bull. Mater. Sci.*, **32** 361 (2009)
24. C. Michel, J. M. Moreau, G. D. Achenbechi, R. Gerson and W.J. James, *Solid State Comm.*, **7** 701 (1969)
25. A. M. Glazer, *Acta Crystallogr.*, **B28** 3384 (1972)
26. A. J. Jacobson and B. E. F. Fender, *J. Phys. C: Solid State Phys.*, **8** 844 (1975)
27. J. M. Moreau, C. Michel, R. Gerson and W. J. James, *J. Phys. Chem. Solids*, **32** 1315 (1971)
28. F. Kubel and H. Schmid, *Acta Cryst. B*, **46** 698 (1990)
29. H. D. Megaw and C. N. W. Darlington, *Acta Cryst. A*, **31** 161 (1975)
30. J. R. Teague, R. Gerson and W.J. James, *Solid State Comm.*, **8** 1073 (1970)
31. J. B. Neaton, C. Ederer, U. V. Waghmare, N. A. Spaldin, and K. M. Rabe, *Phys. Rev. B*, **71** 014113 (2005)
32. J. Li, J. Wang, M. Wuttig, R. Ramesh, N. Wang, B. Ruette, A. P. Pyatakov, A. K. Zvezdin and D. Viehland, *Appl. Phys. Lett.*, **84** 5261 (2004)
33. G. A. Smolenskii, I. E. Chupis, *Sov. Phys.- Usp.*, **25** 475 (1982)
34. I. Sosnowska, M. Loewenhaupt, W.I.F. David and R.M. Ibberson, *Physica B*, **180 -181** 117 (1992)
35. I. Sosnowska, T. P. Neumaier and E. Steichele, *J. Phys. C:Solid State Phys.*, **15** 4835 (1982)
36. V V Lazenka, G Zhang, J Vanacken, I I Makoed, A F Ravinski and V V Moshchalkov, *J. Phys. D: Appl. Phys.* **45** 125002 (2012)
37. W. Eerenstein, N. D. Mathur and J. F Scott, *Nature*, **442** 759 (2006)
38. Y. F. Popov, A. K. Zvezdin, G. P. Vorobev, A. M. Kadomtseva, V. A. Murashev and D. N. Rokov, *JETP Lett.*, **57** 169 (1993)
39. I. Sosnowska and R. Przenioslo *Phys. Rev. B*, **84** 144404 (2011)
40. A. Zalesskii, A. Frolov, T. Khimich, A. Bush, V. Pokatilov and A. Zvezdin, *Euro Phys. Lett.*, **50** 547 (2000)
41. V. S. Pokatilov and A. S. Sigov, *JETP*, **110** 440 (2010)

42. D. Lebeugle, D. Colson, A. Forget, M. Viret, P. Bonville, J. F. Marucco and S. Fusil, *Phys. Rev. B*, **76** 024116 (2007)
43. B. Ruette, S. Zvyagin, A. P. Pyatakov, A. Bush, J. F. Li, V. I. Belotelov, A. K. Zvezdin and D. Viehland, *Phys. Rev. B*, **69** 064114 (2004)
44. J. Wang, J. B. Neaton, H. Zheng, V. Nagarajan, S. B. Ogale, B. Liu, D. Viehland, V. Vaithyanathan, D. G. Schlom, U. V. Waghmare, N. A. Spaldin, K. M. Rabe, M. Wuttig, R. Ramesh, *Science*, **299** 1719 (2003)
45. I. Sosnowska, W. Schafer, W. Kockelmann, K.H. Andersen, I. O. Troyanchuk, *Appl. Phys. A*, **74** 1040 (2002)
46. Z. X. Cheng, X. L. Wang, Y Du and S. X. Dou, *J. Phys. D: Appl. Phys.*, **43** 242001 (2010)
47. T. Park, G. C. Papaefthymiou, A. J. Viescas, A. R. Moodenbaugh, S. S. Wong, *Nano Letters*, **7** 766 (2007)
48. F. Gao, Y. Yuan, K. F. Wang, X. Y. Chen, F. Chen, J. M. Liu and Z. F. Ren, *Appl. Phys. Lett.*, **89** 102506 (2006)
49. S. A. T. Redfern, C. Wang, J. W. Hong, G. Catalan, and J. F. Scott, *J. Phys: Condens Matter*, **20** 452205 (2008)
50. M. K. Singh, R. S. Katiyar and J. F. Scott, *J. Phys: Condens Matter.*, **20** 252203 (2008)
51. J. F. Scott, M. K. Singh and R. S. Katiyar, *J. Phys: Condens Matter.*, **20** 322203 (2008)
52. A. Kumar, N. M. Murari and R. S. Katiyar, *Appl. Phys. Lett.*, **92** 152907 (2008)
53. B. Ramachandran, A. Dixit, R. Naik, G. Lawes and M. S. Ramachandra Rao, *J. Appl. Phys.*, **110** 104105 (2011)
54. S. Nakamura, S. Soeya, N. Ikeda and M. Tanaka, *J. Appl. Phys.*, **74** 5652 (1993)
55. M. K. Singh, W. Prellier, M. P. Singh, R. S. Katiyar, J. F. Scott, *Phys. Rev. B*, **77** 144403 (2008).
56. M. K. Singh, R. S. Katiyar, W. Prellier and J. F. Scott, *J. Phys.: Condens. Matter*, **21** 042202 (2009).
57. G. Catalan and J. F. Scott, *Adv. Mater.*, **21** 2463 (2009)
58. M. A. Korotin, S. Y. Ezhov, I. V. Solovyev, V. I. Anisnmov, D.I. Khomskii, and G. A. Sawatzky, *Phys. Rev. B*, **54** 5309 (1996).
59. R. H. Potze, G. A. Sawatzky and M. Abbate, *Phys. Rev. B*, **51** 11501 (1995).
60. A. A. Taskin, A. N. Lavrov and Y. Ando, *Phys. Rev. Lett.*, **90** 227201 (2003)

61. C. Frontera, J. L. Garcia-Munoz, A. Llobet and M. A. G. Aranda, *Phys. Rev. B*, **65** 180405 (2002)
62. T. Saito, T. Arima, Y. Okimoto, and Y. Tokura, *J. Phys. Soc. Jpn.*, **69** 3525 (2000)
63. J. C. Burley, J. F. Mitchell and S. Short, *Phys. Rev. B*, **69** 054401 (2004)

Chapter 2

Sample Preparations and Characterizations

This chapter describes the methodology adopted for the synthesis of $BiFeO_3$. A brief review of the preparation techniques adopted by various workers is also presented. The synthesized polycrystalline samples are examined for their crystallographic phase(s) via X- ray diffraction (XRD). The Reitveld refinement method of XRD data is adopted to extract the detailed crystal structural information. The Atomic force microscopy is carried out for getting the information of particle size.

2.1 Introduction

Synthesis of $BiFeO_3$ (BFO) from its constituent oxides is very critical due to the very narrow range of its stability as a single phase compound[1]. Thus, even a slight change in the stoichiometry while preparation, leads to secondary phases such as Bi_2O_3, $Bi_2Fe_4O_9$ and $Bi_{25}FeO_{40}$[2]. Volatile nature of Bi makes the high temperature synthesis of BFO difficult as the chances of stoichiometric disturbances are high. Thus the appearance of secondary phases and non-stoichiometry makes the synthesis of phase pure BFO is a daunting task. The optimizations of temperature as well as the synthesis methods are very crucial. Various synthesis methods used by the researchers viz. solid state method, wet chemical method, etc. are briefly reviewed in the following section.

2.2 Literature reviews on synthesis of $BiFeO_3$

2.2.1 Solid State method

The conventional solid state method is one of the most commonly used methods for the synthesis of the polycrystalline metallic oxides. In this method, physical diffusion of the raw materials at high temperature leads to reaction among them and product formation happens. Hence this method needs relatively high temperature. The solid state synthesis of $BiFeO_3$ is schematically explained via the phase diagram of Bi_2O_3/Fe_2O_3 in fig. 2.1 [3].

The preparation of single phase BFO via this method is challenging even by extensive variation of sintering temperature, soaking time and atmosphere, etc. As the solid state synthesis requires the high formation temperature, hence it allows the possibility of the Bi loss, which may be compensated by the addition of excess of Bi_2O_3 during the synthesis followed by leaching with HNO_3 to remove the secondary phase [4].

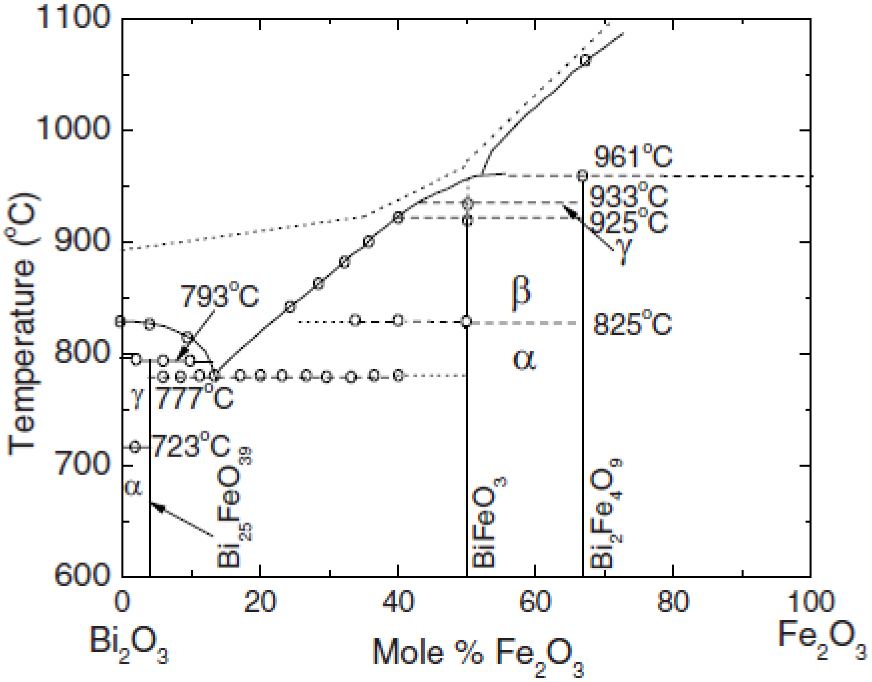

Fig. 2.1. Compositional phase diagram of bismuth ferrite using Bi_2O_3 and Fe_2O_3 as precursors [3]

Lu et. al. prepared BFO by the solid state reaction method by using Bi_2O_3 and Fe_2O_3 as the precursors. The mixed product was heated at 800^0C for 48hrs which is followed by leaching three times. Finally, no traces of any secondary phases are seen in both single crystal and polycrystalline powder[5]. The oxides of Bi and Fe are mixed and calcined at 820^0C for 3h followed by a second calcination to get an impurity free BFO phase[6, 7]. Kothari et. al. have synthesized the BFO by the solid state reaction method. They adopted two calcination, one at 650^0C for 1 hr and the second at 810^0C at 1hr with intermediate grinding. The final calcined powder is leached with dilute HNO_3 to remove the impurity phases. During the phase confirmation, they observed the peaks corresponding to impurity phases viz. $Bi_{36}Fe_2O_{57}$, $Bi_{46}Fe_2O_{47}$ along with that of BFO in the XRD plot of unleached powder. Even after leaching, small traces (~1%) of $Bi_{36}Fe_2O_{57}$ remained in the BFO sample[8].

2.2.2 Wet chemical method

Besides the solid state synthesis, researchers have also adopted the wet chemical method as it requires comparatively lesser heat treatment. In this method the chemical diffusion of the raw materials results the product. Due to certain advantages viz. smaller crystallites, low temperature and the short duration of synthesis, this method is of particular importance. BFO has also been prepared by various wet chemical method, e.g. pechini method, hydrothermal method, sol- gel method, etc.

Jiang et. al. have adopted the Pechini method by using bismuth nitrate ($Bi(NO_3)_3.5H_2O$) and iron nitrate ($Fe(NO_3)_3.9H_2O$) as the precursor with citric acid ($C_6H_8O_7$) as fuel. The product was heated at 700^0C for 1hr. They observed that the pH of the solution has a vital role in getting the pure BFO sample. The appearance of secondary phase ($Bi_2Fe_4O_7$) was monitored at various pH values and at pH=1 the phase pure sample was obtained[9].

In the hydrothermal method, the mixture of $Bi(NO_3)_3.5H_2O$ and $FeCl_3.6H_2O$ dissolved in ethanediol, are allowed for the hydrothermal reaction with NaOH as mineralizer. The product was washed with de-ionized water until the neutral condition achieved. The synthesized powder was calcined at $140\text{-}220^0C$ for 12 hrs. The phase pure BFO was obtained on calcining the powder at 180^0C at 12hrs. For all other calcined temperatures, secondary phases ($Bi_{25}FeO_{40}$, $Bi_2O_{2.33}$) appeared [10].

BFO has also been synthesized by ethanol mediated sol – gel process with the bismuth nitrate ($Bi(NO_3)_3.5H_2O$) and iron nitrate ($Fe(NO_3)_3.9H_2O$) as the precursor. The nitric acid (HNO_3) and hydrogen peroxide were added to the solution and the solution was subjected to stir. The obtained powders were calcined at 550^0C - 650^0C and the final sintering was done at 850^0C. Though the powders were found to be phase pure, the grain sizes measured through FESEM were ~10-30μm [11].

Wei et. al. synthesized BFO in sol- gel process by using EDTA as fuel and calcined the product at 300^0C- 600^0C [12]. Ghosh et. al. have prepared nanosize BFO by a soft chemical method using tartaric acid as the complexing agent [13].

As per the numerous literature survey, it is observed that various complexing agent viz. citric acid, EDTA, 2 – methoxy ethanol and ethylene glycol, hydrogen peroxide etc. are needed for the synthesis of BFO.

2.3 Inferences

From the above discussions, it is observed that mostly the solid state method and wet chemical method are favorable for the synthesis of $BiFeO_3$. During the synthesis of BFO, the appearance of undesirable secondary phases is comparatively less in the wet chemical method than the solid state method. As the nanoparticles of BFO are highly desired for improving the electric as well as magnetic ordering of BFO, the researchers have adopted various techniques for synthesis of the pure BFO nanoparticles. The preparation of these nanoparticles is carried out mostly via wet chemical method. The chelating agents/complexing agents used in the above mentioned literatures, are found be associated with the secondary phases. However, glycine (NH_2CH_2COOH) is found to be a suitable fuel for synthesizing nanoparticles [14] and relatively less impurity is found in the samples prepared by the use of glycine [15]. So in the present work, BFO is optimized with the use of glycine for the preparation of pure BFO nanoparticles.

2.4 Preparation and characterization of $BiFe_{1-x}Co_xO_3$ (x=0, 0.01, 0.02, 0.03, 0.1, 0.2, 0.3, 0.35, 0.4, 0.5, 0.6, 0.7, 0.8, 0.9 and 1)

The $BiFe_{1-x}Co_xO_3$ samples are prepared by the sol-gel auto combustion technique with bismuth nitrate (Bi $(NO_3)_3.5H_2O$), iron nitrate (Fe $(NO_3)_3.9H_2O$) and Co $(NO_3)_3.6H_2O$ as precursors and glycine (NH_2CH_2COOH) as a fuel. Aqueous solutions of Bi $(NO_3)_3.5H_2O$ and Fe $(NO_3)_3.9H_2O$ made separately are mixed together with the appropriate amount of fuel in it. The glycine to nitrate ratio of 1 is optimized for the synthesis of phase pure BFO. The solution is heated under continuous stirring, to obtain the gel, which eventually burnt to form xerogel powder. This as-prepared xerogel powder is then properly ground and pressed into pellets of 10mm diameter by applying 6×10^7 kgm^{-2} pressure in a hydraulic press. These pellets are subjected for sintering at temperature of 700^0C for $BiFe_{1-x}Co_xO_3$ (x=0, 0.01, 0.02, 0.03, 0.1, 0.2, 0.3) and 780^0C for $BiFe_{1-x}Co_xO_3$ (x=0.35, 0.4, 0.5, 0.6, 0.7, 0.8, 0.9 for 1) 1h. The phases of the obtained samples are characterized by x-ray diffraction (XRD) (Bruker D8 Advance X-ray diffractometer) in a wide range of Bragg angle 2θ ($20^0 \leq 2\theta \leq 80^0$) using CuK_α (1.5406Å) radiation with a step size of 0.02^0. The x-ray diffraction data are analyzed via Reitveld method using FULLPROF software.

2.4.1 Flow chart of the synthesis procedure adopted for $BiFe_{1-x}Co_xO_3$

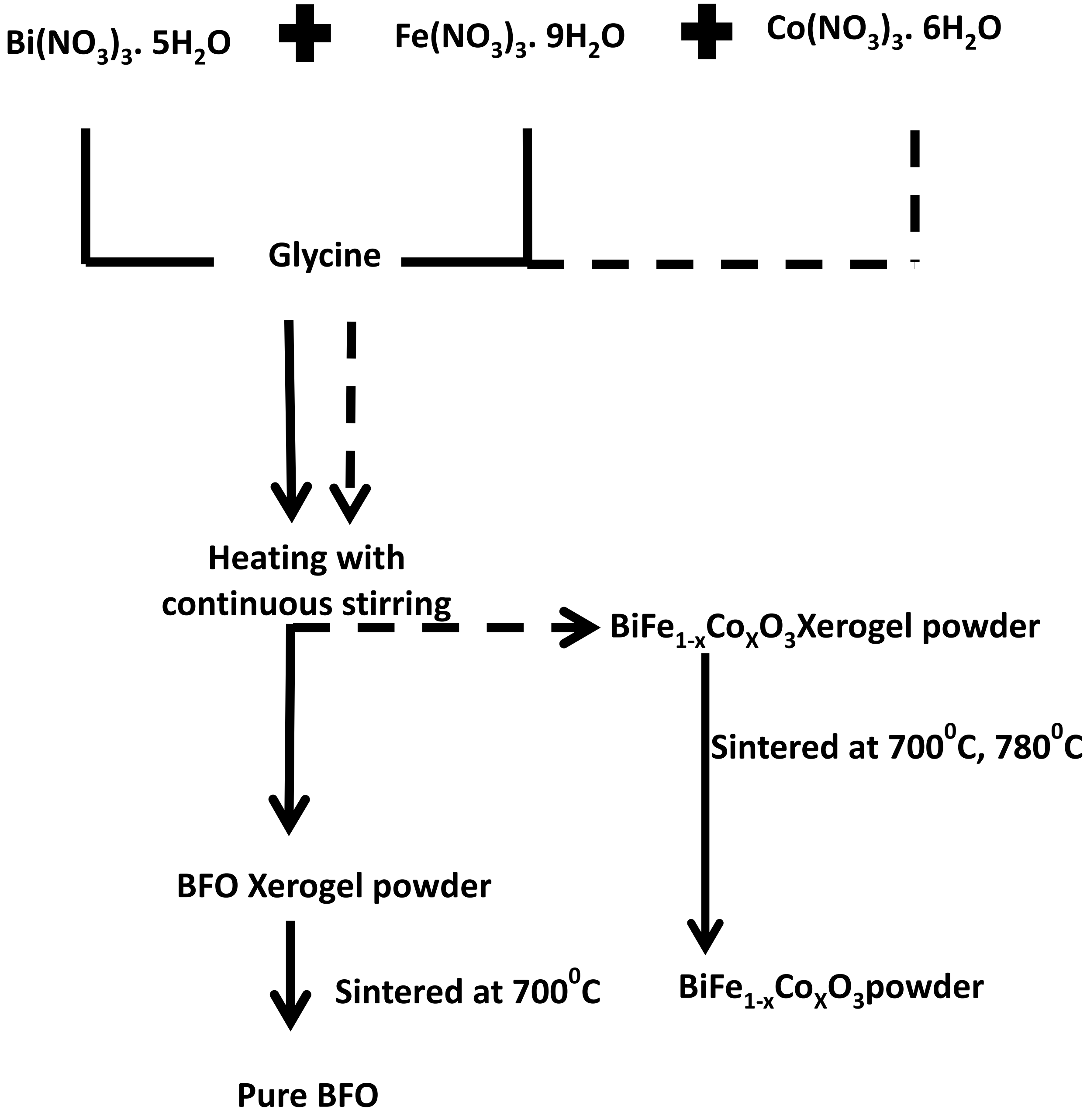

2.4.2 Analysis of XRD patterns of $BiFe_{1-x}Co_xO_3$ (x=0, 0.1, 0.2, 0.3, 0.35 and 1)

Fig. 2.2 shows the XRD pattern of $BiFe_{1-x}Co_xO_3$ (x=0, 0.1, 0.2, 0.3, 0.35 and 1). The pristine sample (x= 0) is found to be crystallized in rhombohedral structure with space group R3c without any appearance of secondary phases. This rhombohedral structure is found stable also for x= 0.01 and 0.02 with a slight shifting of the peak positions. This may be due to the substitution of Co at Fe site as the ionic radius of Co^{3+} (54.5pm in low spin state and 61pm in the high spin state) is slightly less than that of Fe^{3+} (55pm in low spin state and 64.5pm in the high spin state). From x = 0.03 onwards, additional peaks corresponding to the cubic phase (space group I23) along with that of rhombohedral phase, surfaced up in the XRD plot. However, the pure cubic phase is completely stabilized from x = 0.35 onwards with no trace of rhomobohedral phase. Hence a clear structural transition is observed from rhombohedral phase ($x \leq 0.02$) to cubic phase ($x \geq 0.35$) via intermediate mixed phase ($0.03 \leq x \leq 0.3$). The detailed analysis of the crystal structure is carried out via Reitveld refinement as described in the following sections.

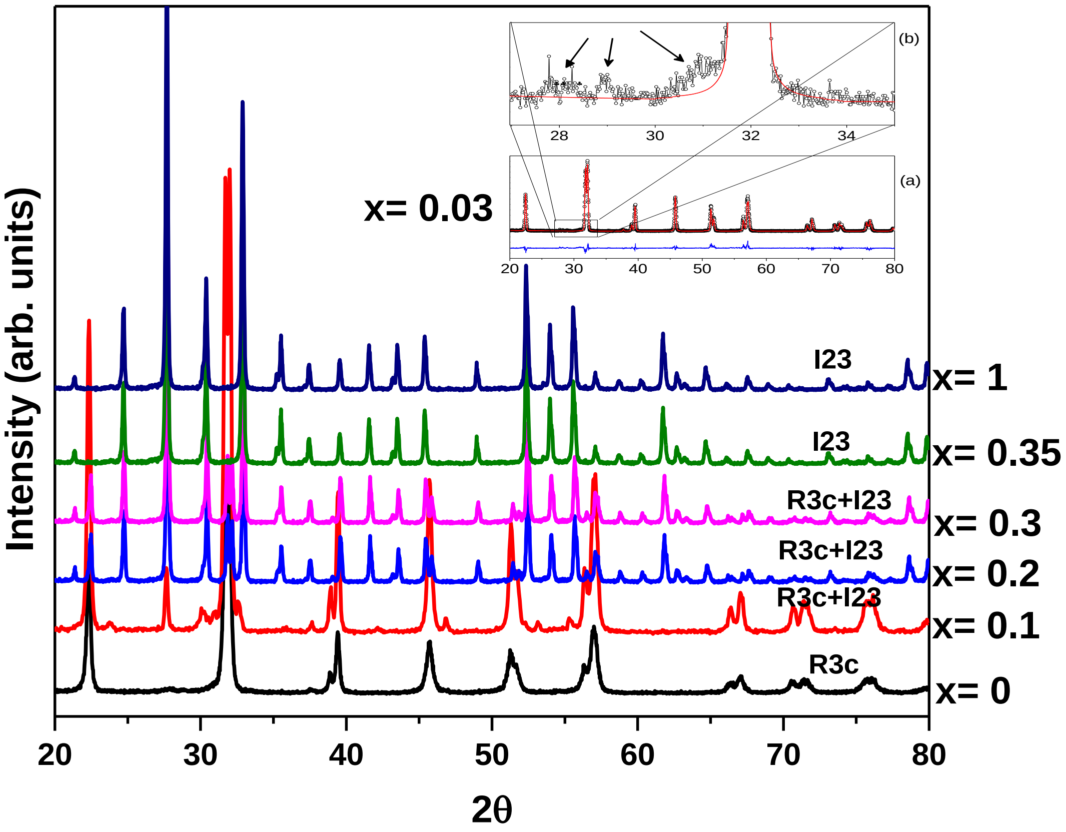

Fig. 2.2 XRD plot of BiFe$_{1-x}$Co$_x$O$_3$ (x=0, 0.1, 0.2, 0.3, 0.35 and 1). The inset shows the appearance of the cubic phase from x = 0.03 onwards.

2.4.3 Analysis of XRD patterns of BiFe$_{1-x}$Co$_x$O$_3$ (x= 0, 0.01, 0.02, 0.5 and 1) through Reitveld method

Fig. 2.3 a, b and c shows the Reitveld refined XRD data for x = 0, x = 0.01 and x = 0.02 respectively. The refinement reveals that all the three samples are crystallized in rhombohedral structure with space group (R3c) with no indication of any detectable secondary phases. Fig 2.4 shows the schematic diagram of a portion of the hexagonal unit cell of x = 0 (BFO) where the FeO$_6$ octahedrons are arranged in a tilted fashion. Since, the ionic radius of Co^{3+} (54.5 pm in LS and 61.0 pm in HS) is slightly less than Fe^{3+} (55 pm in LS and 64.5 pm in HS), a shrinkage in lattice parameter hence in the volume may be expected. The lattice parameters so obtained from the structural refinement for all the above samples are a = 5.5467(2) Å, c = 13.7909(6) Å (x = 0), a = 5.5413(1) Å, c = 13.7755(3) Å (x = 0.01) and a = 5.5373(1) Å, c = 13.7640(4) Å (x = 0.02). The plot of cell volume as a function of cobalt concentration (fig. 2.5) shows a systematic decrease in lattice volume, indicating successful substitution of cobalt at Fe site. On the other hand, according to fig. 2.2 it is clearly observed that at x = 0.35, a structural transition takes place from rhombohedral to cubic structure.

The confirmation of the crystal structure has been done by the Reitveld refinement of x= 0.5 and x = 1. The sintered samples are subjected to x-ray diffraction (XRD) for the phase identification as shown in fig. 2.6. Reitveld analysis of the XRD data shows that the sample is crystallized in a cubic structure (space group I23) in the sillenite $(Bi,Co)_{25}CoO_{40}$ phase[16, 17]. The 2a (0, 0, 0) positions are occupied by Co ions and the Bi ions shares the 24f site (x, y, z) along with remaining Co ions. The oxygen ions are distributed over 24f site and two sets of 8c (x, x, x) sites with 100% occupancy in each. The lattice constant along with other parameters obtained from the refinement are tabulated in table 2.1. The crystal structure (shown in fig. 2.7) shows that the Co ion at 2a site is tetrahedrally bonded to four oxygen ions and those sharing the 24f positions with Bi are bonded in square pyramidal configuration, which may be visualized as octahedral configuration with the sixth vertex absent. This unusual square pyramidal configuration is due to Bi^{3+} ions, which is bonded in octahedral configuration to five oxygen and the sixth one being the lone pair of electrons[16]. Since 24f site is jointly shared by Bi^{3+} and Co^{3+} and our inability to distinguish between those occupied by Bi^{3+} and those by Co^{3+}, the software has shown all the 24f sites as square pyramidal bonding. Probably a detailed crystal structure study on single crystals might be needed to distinguish the positions occupied by Bi^{3+} and Co^{3+}.

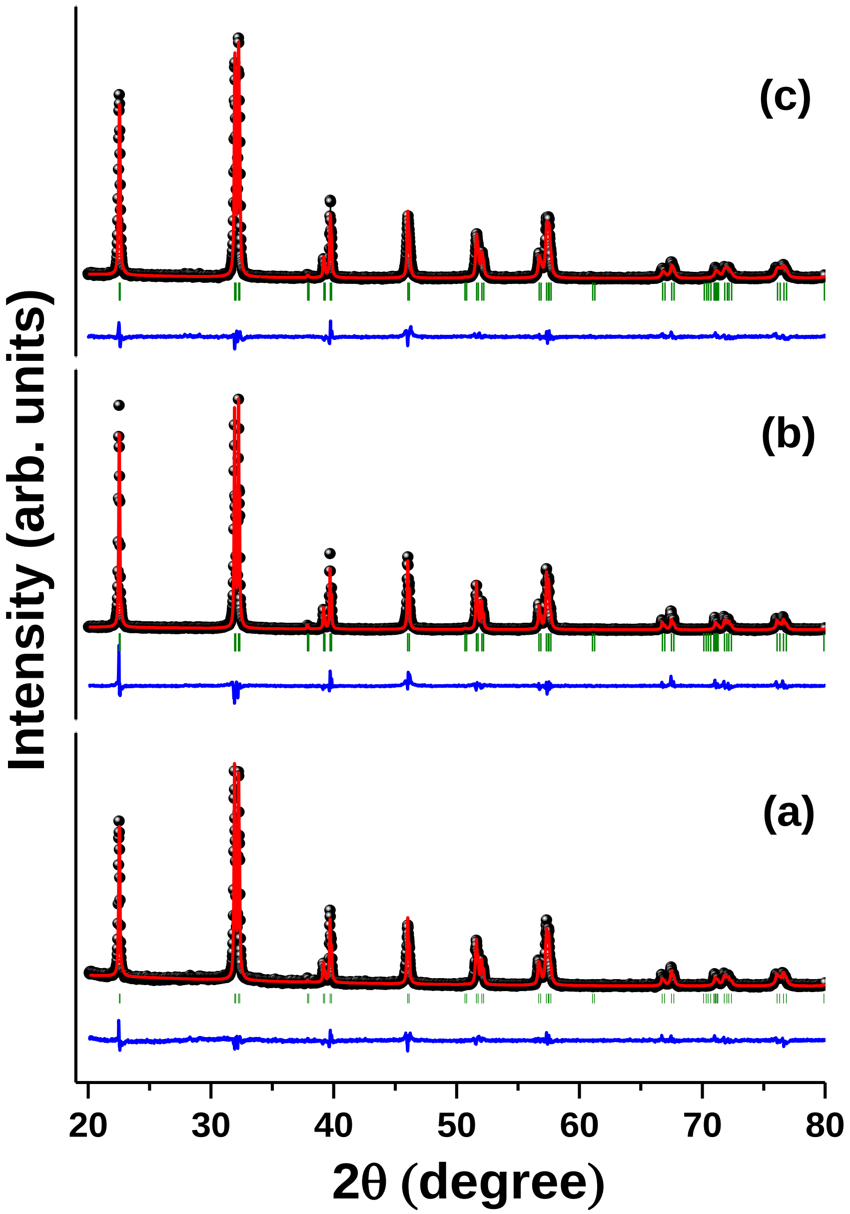

Fig. 2.3. XRD data of a) x = 0, b) x = 0.01 and c) x = 0.02 refined via Reitveld method. Refinement confirms the single phase of the compounds synthesized.

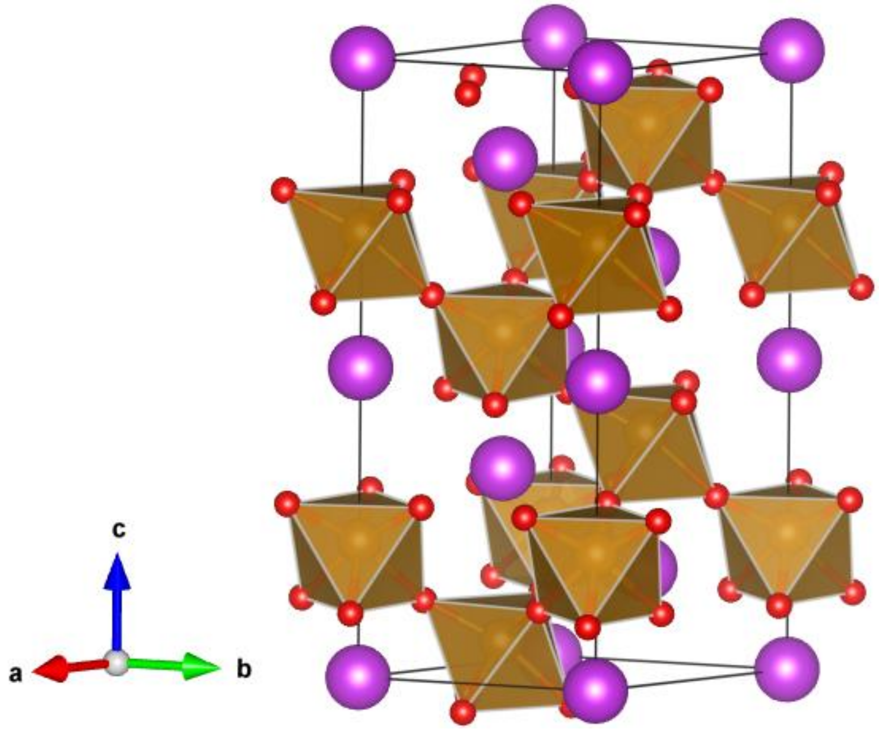

Fig. 2.4. The crystal structure of BFO is represented as a small portion of the hexagonal unit cell.

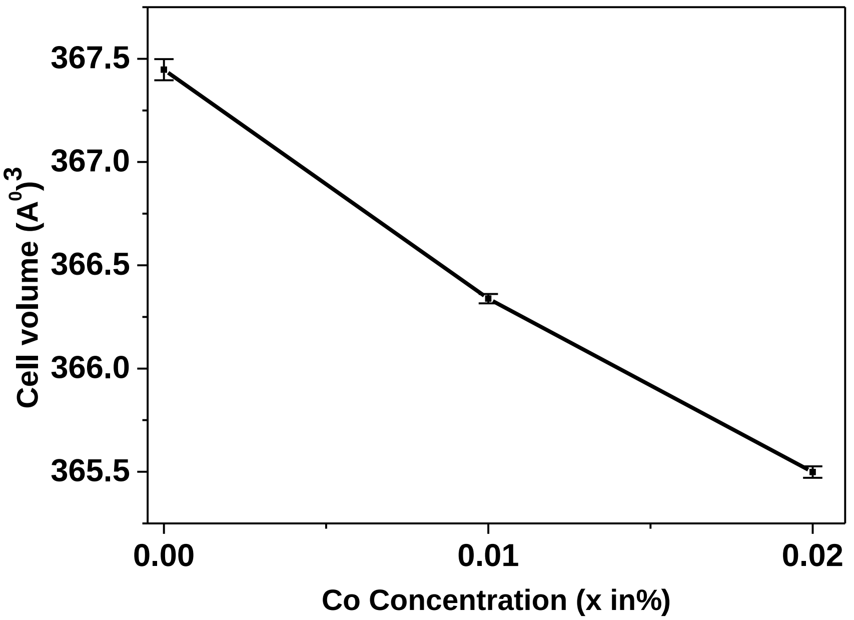

Fig. 2.5. Variation of cell volume (obtained from the refinement of XRD data) as a function of Co concentration in $BiFe_{1-x}Co_xO_3$ (x= 0, 0.01, 0.2). The vertical bars in the plot marks the respective errors associated.

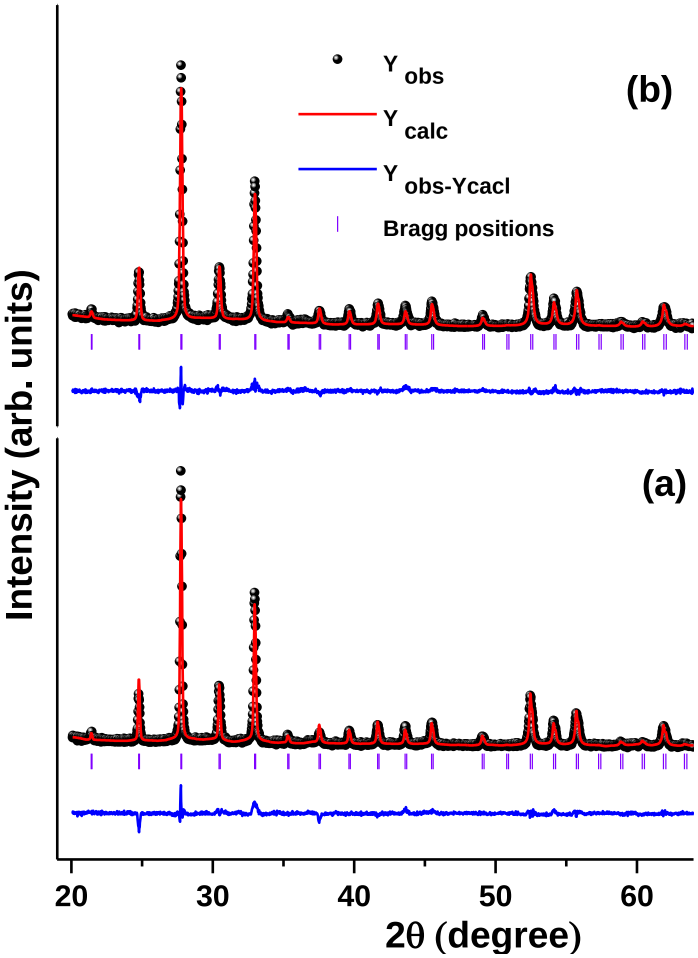

Fig. 2.6. Reitveld refinement of a) x=1 $(Bi_{13}Co_{12})CoO_{40}$ b) x = 0.5 $(Bi_{13}Co_{5.5}Fe_{6.5})CoO_{40}$ samples shows that both the samples are crystallized in cubic structure with the space group I23.

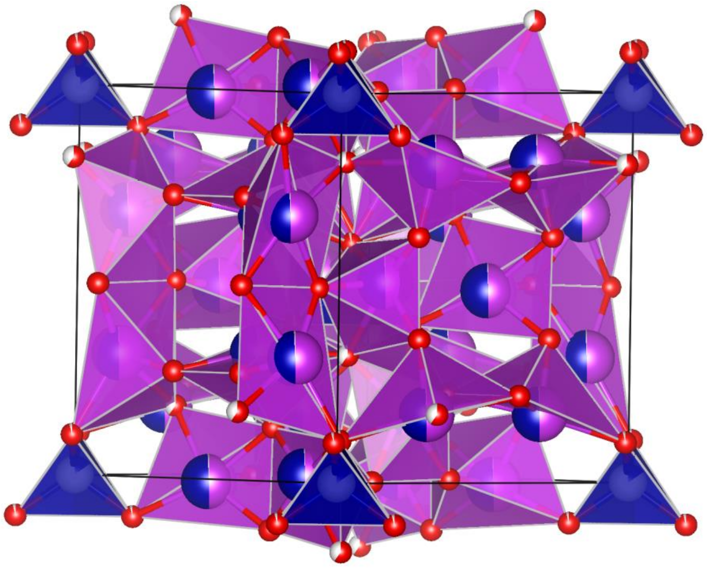

Fig. 2.7. The cubic crystal structure in which corner positions of Co ions are tetrahedral (blue) and the octahedral sites (magenta) within the unit cell.

Table 2.1 : Structural parameters obtained from refinement of XRD data.

	$(Bi_{13}Co_{12})CoO_{40}$	$(Bi_{13}Co_{5.5}Fe_{6.5})CoO_{40}$
Bi/Co (x, y, z)	0.17616 0.31739 0.01426	0.17805 0.31858 0.01438
Co/Fe(x, x, x)	0.00000 0.00000 0.00000	0.00000 0.00000 0.00000
O1(x, y, z)	0.12947 0.23039 0.44194	0.15090 0.22371 0.45660
O2(x, x, x)	0.19650 0.19650 0.19650	0.20652 0.20652 0.20652
O3(x, x, x)	0.90600 0.90600 0.90600	0.86134 0.86134 0.86134
a	10.1628(4)Å	10.1583 (4) Å
(Bi-O1)	2.16286(8) Å	2.86968(9) Å
(Bi-O1)	1.81020(5) Å	2.23626(7) Å
(Bi-O1)	2.23211(7) Å	2.65254(8) Å
(Bi-O1)	2.65740(8) Å	2.09465(7) Å
(Bi-O3)	2.90168(9) Å	2.02657(6) Å
(Co-O3)	1.65463(4) Å	1.65393(4) Å
(O3-Co-O3)	109.4712(0) deg.	109.4712(0) deg.

2.4.4 Atomic force microscopy (AFM) study of $BiFe_{1-x}Co_xO_3$ (x= 0, 0.01, 0.02, 0.5 and 1)

The AFM study is carried out for all the three samples for getting the information about the morphology of the pristine sample as well as the Co doped sample. A non-uniform distribution of the particle sizes for x =0, x = 0.01 and x = 0.02 samples are obtained (fig. 2.8 a, b and c). It has been observed that the average particle size of the three samples is ~ 100nm -200nm. However the particle size for x = 0.01 is found to be slightly larger in comparison to the other two samples. Fig. 2.8 d, e shows the surface morphology of the samples $(Bi_{13}Co_{5.5}Fe_{6.5})CoO_{40}$ (x = 0.5) and $(Bi_{13}Co_{12})CoO_{40}$ (x = 1) seen via atomic force microscopy shows uniform size distribution with the average particle size ~75nm for x = 0.5 and ~100nm for x =1. It has been observed that the particles are of spherical shape.

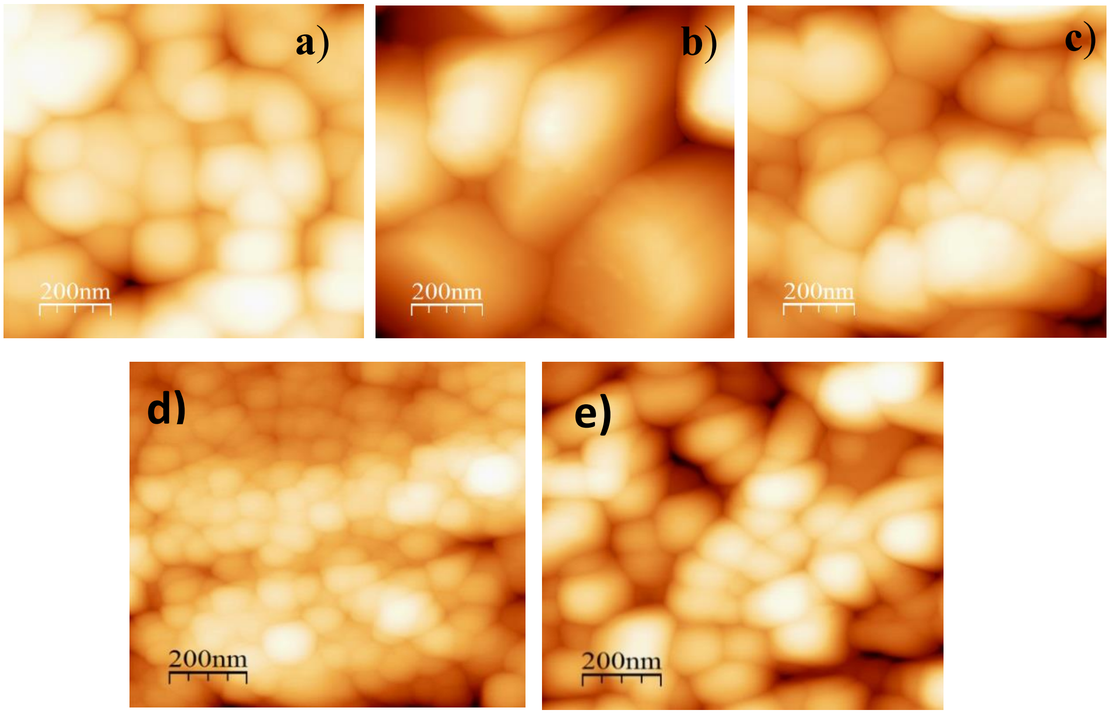

Fig. 2.8. AFM image of a) x = 0, b) x = 0.01 and c) x = 0.02, shows the particle sizes are ~ 100 – 200 nm and d) x = 0.5 and e) x =1 shows the particle size ~ 75nm and 100nm respectively.

2.4.5 DC Magnetization measurement of $BiFe_{1-x}Co_xO_3$ (x= 0, 0.01, 0.02, 0.5 and 1)

The magnetic measurements are carried out with 14T physical property measurement system vibrating sample magnetometer (PPMS VSM) of Quantum design, USA in the temperature range 4K to 300K.

2.4.6 Neutron Diffraction measurement of $BiFe_{1-x}Co_xO_3$ (x= 0 and 0.02)

The ND measurements at room temperature and low temperatures are carried out in the 2θ range 6^0 to 120^0, at a wavelength of 1.48 Å on the focusing crystal based powder neutron diffractometer setup by UGC-DAE CSR Dhruva Reactor, BARC Mumbai, India. To see the effect of Co^{3+} in BFO and for further insight of spinoidal arrangement, ND measurements are done on BFO & BFCO2 at room temperature (300K), 100K, 50K and 2K.

2.4.7 Magnetoelectric measurement of $BiFe_{1-x}Co_xO_3$ (x= 0, 0.01 and 0.02)

The magnetoelectric study is carried out in a homemade setup (based on the dynamic method) [18], whose schematics are shown in fig. 2.9. The DC magnetic bias field up to 1T (measured using Hall probe) is applied using an electromagnet (GMW 5403) equipped with bipolar dc power supply. The sample is excited with AC magnetic field of ~2.3 Oe and frequencies ranging from 100 Hz to 6 kHz, superimposed with the applied dc field. The AC magnetic field is produced by a solenoidal coil of 200 turns with an average diameter 6mm and length of 15mm. The solenoidal coil (connected to the sin-out of lock-in amplifier) is placed longitudinally between the two pole pieces of the electromagnet. The rod shaped sample of thickness 0.5 mm and length 5 mm is placed longitudinally (faces towards magnet pole) inside the core of the solenoid, with the ends of the sample electrically connected to the lock-in amplifier (SR 830). The magnetoelectric (ME) output voltage (V_{out}) is measured in the differential mode to nullify the effect of induced voltage[19]. The magnetodielectric measurement as a function of temperature and magnetic field is carried out for both the samples using lock in amplifier and electromagnet. The temperature dependent electrical transport measurements are done in closed cycle refrigerator (Janis), using an electrometer (Keithley 6517B) and temperature controller (Lakeshore 331). The electrical point contacts were made using conducting silver epoxy.

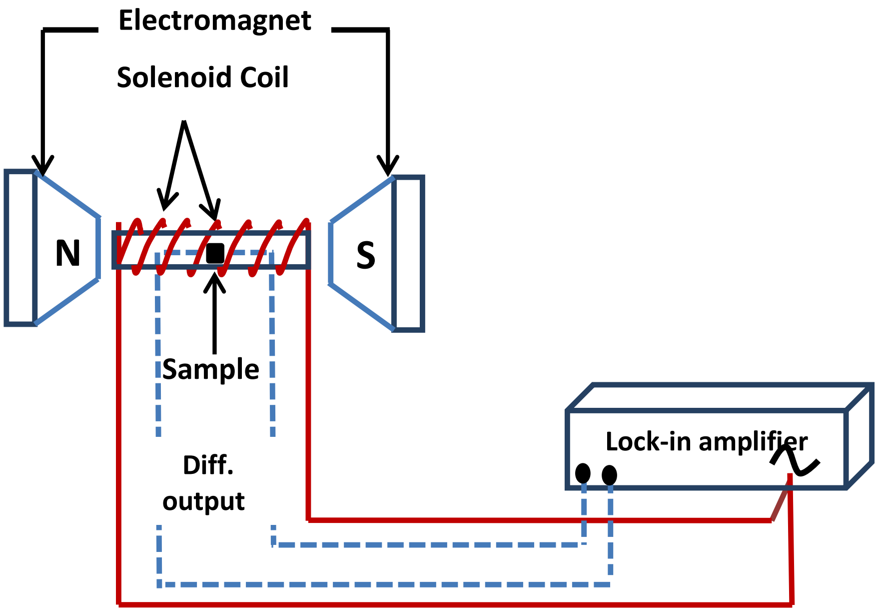

Fig. 2.9. Schematic diagram of dynamic magnetoelectric measurement set-up.

2.4.8 P-E loop measurement of $BiFe_{1-x}Co_xO_3$ (x= 0 and 0.02)

The room temperature ferroelectric studies (P – E measurements) are done using Ferroelectric loop tracer (Radiant Tech, USA). In the present case, the sample thickness is ~ 1.2mm and the applied voltage is ~ 0.36kV.

2.4.9 Dielectric and magnetodielectric measurement of $BiFe_{1-x}Co_xO_3$ (x= 0, 0.01, 0.02, 0.5 and 1)

The low temperature dielectric measurements are done with Stanford SR 830 Lock in Amplifier in a frequency range of 100 Hz - 100 KHz. The temperature variation from 70K-300K is achieved using closed cycle refrigerator (Janis, USA). The temperature dependent high temperature dielectric measurements are performed using a Hioki impedance analyzer (IM3570) in a wide frequency range (100Hz-1MHz) from 300K to 620K. Magnetodielectric measurement is performed using the DC magnetic bias field up to 1.3T (measured using Hall probe) is applied using an electromagnet (GMW 5403) equipped with bipolar DC power supply. The measurements are carried out via two probe method and the electrical contacts were made on a disk shaped pellet using conducting silver epoxy in a capacitor configuration. The complex dielectric permittivity is calculated from the measured impedance via expression, $\varepsilon^* = \frac{Z^*}{\omega c_0(Z'^2+Z''^2)}$; where $C_0 = \frac{\varepsilon_0 A}{d}$, 'A' is the cross-section area and 'd' is the thickness of the sample.

References

1. E. M. Levin, R. S. Roth, *J. Res. Natl. Bur. Stand.*, **68** 197 (1964)
2. M. Valant, A. K. Axelsson, N. Alford, *Chem. mater.*, **19** 543 (2007)
3. R. Palai, R. S. Katiyar, H. Schmid, P. Tissot, S. J. Clark, J. Robertson, S. A. T. Redfern, G. Catalan, J. F. Scott, *Phys. Rev. B*, **77** 014110 (2008)
4. M. Mahesh Kumar, V.R. Palkar, K. Srinivas, S.V. Suryanarayana, *Appl. Phys. Lett.* **76** (2000) 2764
5. J. Lu, A. Gunther, F, Schrettle, F. Mayr, S. Krohns, P. lunkenheimer, A. Pimenov, V. D. Travkin, A. A. Mukhin and A. loidl, *Eur. Phys. J. B*, **75** 451 (2010)
6. V. V. Shvartsman, W. Kleemanna, R. Haumont and J. Kreisel, *Appl. Phys. Lett.*, **90** 172115 (2007)
7. R. Haumont, I. A. Kornev, S. Lisenkov, L. Bellaiche, J. Kreisel and B. Dkhil, *Phys. Rev. B*, **78** 134108 (2008)
8. D. Kothari, V. R. Reddy, V.G. Sathe, A. Gupta, A. Banerjee, A.M. Awasthi, *J. Magn. Magn. Mater.*, **320** 548 (2008)
9. Q. H. Jiang, C. W. Nan, Y. Wang, Y. H. Liu and Z. J. Shen, *J. Electroceram.*, **21** 690 (2008)
10. M. Hongyan, Z. Qiong, T. Guoqiang, Z. Gangqiang, *Journal of Wuhan University of Technology-Mater. Sci.* Ed., **23** 507(2008)
11. B. Ramachandran and M. S. Ramachandra Rao. *Appl. Phys. Lett.* **95** 142505 (2009)
12. J. Wei, D. Xue, *Mater. Res. Bull.*, **43** 3368 (2008)
13. S. Ghosh, S. Dasgupta, A. Sen, *J. Am. Ceram. Soc.*, **88** 1349 (2005)
14. S. Banerjee and P. Sujatha Devi, *J. Nanopart. Res.*, **9** 1097 (2007)
15. R. Mazumder, P. Sujatha Devi, D. Bhattacharya, P. Choudhury, A. Sen and M. Raja *Appl. Phys. Lett.*, **91** 062510 (2007)

16. D. C. Craig and N. C. Stephenson, *J. Solid State Chem.*, **15** 1 (1975)
17. R. V. K. Mangalam, R. Ranjith, A. Iyo, A. Sundaresan, S. B. Krupanidhi and C. N. R. Rao, *Solid State Comm.*, **140** 42 (2006)
18. M. Mahesh Kumar, A. Srinivas, S. V. Suryanarayana, G. S. Kumar, and T. Bhimasankaram, *Bull. Matter. Sci.*, **21** 251 (1998)
19. G. V. Duong, R. Groessinger, M. Schoenhart and D. Bueno-Basques, *J. Magn. Magn. Mater.*, **316** 390 (2007)
20. P. N. Vishwakarma, *Solid State Comm.*, **149** 115 (2009)

Chapter 3

Magnetic properties of cobalt substituted $BiFeO_3$ ($BiFe_{1-x}Co_xO_3$: x = 0, 0.01, 0.02)

This chapter describes the effect on the magnetic properties of $BiFeO_3$ on substituting Co at Fe - site. Here the dilute concentration of Co substituted $BiFeO_3$ i.e. $BiFe_{1-x}Co_xO_3$ (x= 0, 0.01, 0.02) is the focal point of the discussion. To get the magnetic properties of the phase pure $BiFe_{1-x}Co_xO_3$ samples, the higher concentration of Cobalt i.e. for x = 0.03 onwards, has not taken into consideration as they contain the secondary phases (discussed in chapter 2). The temperature dependent DC magnetization study reveals various magnetic states viz. superparamagnetic, antiferromagnetic and ferromagnetic states of parent as well as the Co substituted samples. It has been observed that Co doping greatly influences the magnetic properties of $BiFeO_3$ due to various magnetic states acquired by Co^{3+}. The signature of the spin glass transition is observed in M vs. T plots for all the three samples. A first order transition corresponds to the spin state transition in x= 0.01 and 0.02, has also been seen.

3.1 Introduction

Since its discovery, Bismuth ferrite, $BiFeO_3$ (BFO) has been investigated by a large number of researchers due to its multiferroicity above room temperature. G-type antiferromagnetism (T_N = 643K)[1] superimposed with incommensurate cycloid spin structure with a periodicity of 62nm, has been of importance in particular[2]. The antiferromagnetic ordering hinders it for the practical applications as the net magnetization is cancelled out due to the above peculiar magnetic arrangement. There are various ways reported via which the magnetic properties of $BiFeO_3$ may be enhanced (described in chapter 1). Various researches have been carried out to study the cycloidal spin arrangement via some suitable substitution at Bi or Fe - site or via inducing lattice distortion. For example, the enhancement in magnetic moment by the structural changes[3], suppression of spiral spin structure is observed when rare earth elements viz. Dy^{3+} [4], La^{3+} [5, 6], Nd^{3+} [7], Eu^{3+} [8], Gd^{3+} [9], Pr^{3+} [10], Sm^{+3} [11] and divalent ions, e.g. Ca^{2+}, Sr^{2+}, Pb^{2+}, Ba^{2+} [12] is partially substituted. Besides the Bi-site substitution, many literatures are based on Fe-site substitution in $BiFeO_3$ to obtain a collinear magnetic ordering. In $BiFe_{1-x}Mn_xO_3$, the magnetization does not improve sufficiently on Mn substition[13–15]. Recently cluster glass behavior for partial substitution of Fe with Co ($Bi(Fe_{0.95}Co_{0.05})O_3$)[16, 17] is observed by Xu et.al which is supported by few other literatures[18, 19]. Thus, it is clear that the chemical substitution has a pronounced effect on the magnetic properties of $BiFeO_3$ as it interrupts the cycloidal spin and improves the magnetization. But one of the drawbacks of this type of substitution is the presence of secondary phases. So the synthesis of pure $BiFeO_3$ without disturbing its other inherent properties is a great challenge.

Co^{3+} in ABO_3 type oxides is known for thermally stimulated spin state transitions from low spin (LS; $T < 100$ K) to high spin (HS; $T > 500$ K) via an intermediate spin (IS; $100K < T < 300$ K)[20]. This behavior is attributed to the comparable energy of crystal field splitting of Co-d states (Δ_{CF}) and Hund's exchange energy (Δ_H) which results a small separation between t_{2g} and e_g levels, of the order of k_BT[21]. Hence a variety of interesting physics may be witnessed for partial substitution of Co^{3+} for Fe^{3+} in $BiFeO_3$ due to various magnetic states acquired by Co^{3+} and its interaction with neighbouring Fe^{3+} in the cycloidal arrangement. Through this report, we are extending the works initiated by Xu et. al. [16, 17], who reported a glassy behavior of cobalt doped $BiFeO_3$. For the present study, a very dilute substitution of Co at the Fe site is chosen for this work, so that any lattice distortion due to ionic radius mismatch may be minimized.

3.2 Magnetization Study

3.2.1 Magnetization vs. Temperature (M vs. T) Measurement

The temperature dependence of DC magnetization (M) following zero field cooled (ZFC) and field cooled warming (FCW) magnetization under a magnetic field of 0.1T and 1T for all the three samples is shown in figs. 3.1 and 3.2, respectively. As the temperature is lowered, the ZFC magnetization of $BiFeO_3$ increases continuously till 120K and starts decreasing thereafter. The FCW magnetization also shows a similar increase at lower temperatures, but with slight bifurcation with ZFC and below 120K this bifurcation grows significantly. For 1T magnetic field, the maxima position (which was at 120K) in ZFC, shifts to ~50K, where FCW still holds previous behaviour, with bifurcation in ZFC and FCW for $T < 50K$. Such behavior of $BiFeO_3$ (BFO) nanoparticles is reminiscent of superparamagnetic behavior due to their nano size[22]. For $x = 0.01$ (BFCO1) and 0.02 (BFCO2), the ZFC and FCW curves are very different: absence of peak at ~ 120 K, ZFC and FCW meeting directly at ~300 K and large bifurcation in ZFC and FCW data for $T < 300K$. The ZFC curve for both the samples decreases continuously with lowering of temperature, whereas FCW data increases with lowering of temperature. Such behavior has been identified to be cluster glass behavior [17, 23–26].

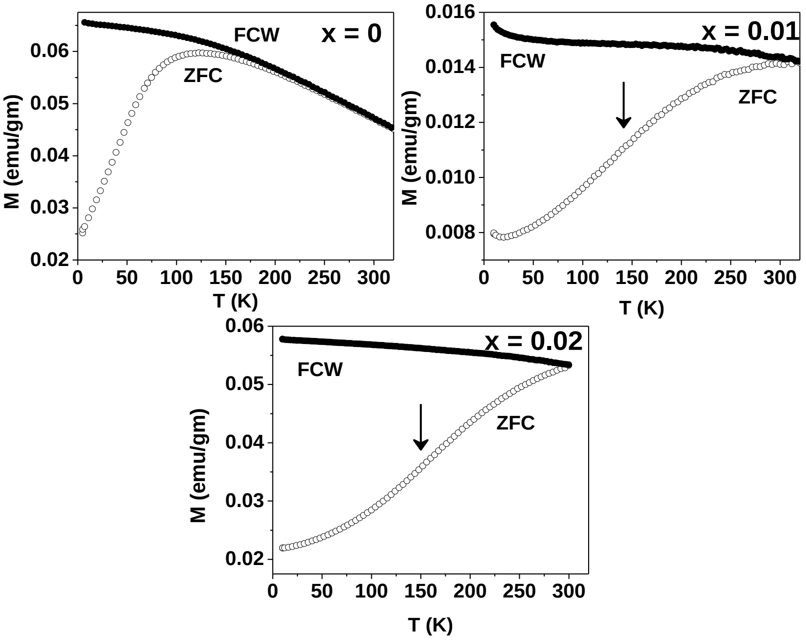

Fig. 3.1 Zero field cooled, ZFC (open symbols) and field cooled warming, FCW (solid symbols) magnetization curves of BiFe$_{1-x}$Co$_x$O$_3$(x= 0, 0.01, 0.02) as a function of temperature is measured under a magnetic field of 0.1T. Here the arrow in x = 0.01 and x = 0.02 indicates the inflection point.

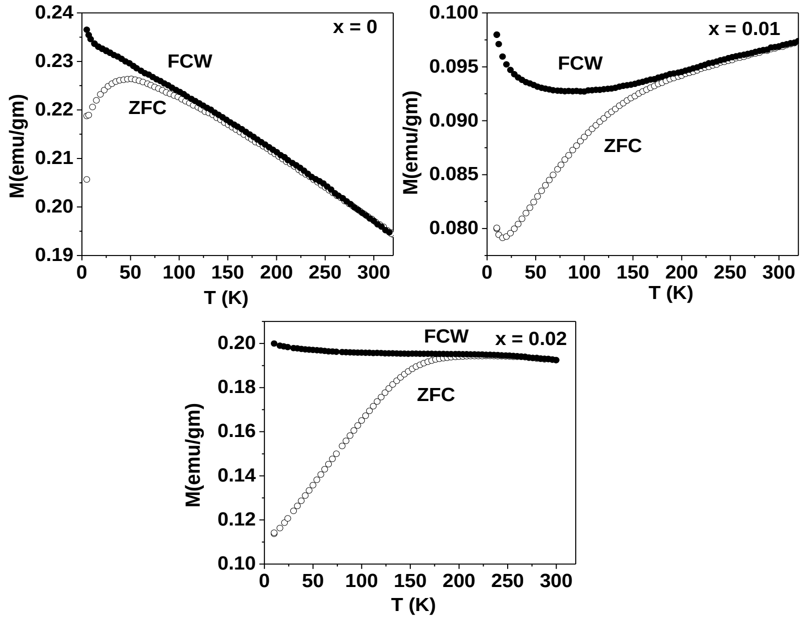

Fig. 3.2 Zero field cooled, ZFC (open symbols) and field cooled warming, FCW (solid symbols) magnetization curves of BiFe$_{1-x}$Co$_x$O$_3$(x= 0, 0.01, 0.02) as a function of temperature, is measured under a magnetic field of 1T.

3.2.2 Magnetic relaxation Measurement

The magnetic relaxation measurements are carried out at various temperatures (temperature range over which zero-field cooled (ZFC) and field-cooled (FC) curves bifurcate) using the following protocol for x= 0 and x= 0.02. The samples are cooled from 350K to the target temperature in ZFC mode and allowed enough time for the temperature to stabilize. Then a 6 Tesla magnetic field is applied at the rate of 100 Oe/sec and the field is held constant for one hour. Subsequently the field is reduced to zero (at 100 Oe/sec) and the magnetization is measured continuously as a function of time for 14400 secs (4 hours). Fig.3.3 shows the normalized M(t)/M(t=0) versus time at T = 50K and 125K for BFO and BFCO2 respectively. It can be seen that the magnetization is continuously decreasing with time and it has not stabilized even after 4 hours. The exponential decay of magnetization with time is fitted to a stretched exponential eq. 3.1.

$$M(t) = M_0 + M_r \exp\left[-\left(\frac{t}{\tau}\right)^{1-n}\right] \quad \text{----------------- (Eq. 3.1)}$$

Here, M_0 and M_r represent the intrinsic magnetic moment and glassy component mainly contributing to relaxation effect, respectively. Similar fitting of the magnetic relaxation data taken at other temperatures are attempted. The fitting parameters M_0, τ and n are plotted as a function of the measured temperature (fig 3.4). Coming to the BFO first, M_0 increases with the decreasing temperature and at T = 125K it starts decreasing. At the same time, the relaxation time τ increases from 467s (300K) to 21000s (175K) and again falls to 450s at lower temperatures. Also the parameter 'n' measure of stretched potential also approaches n = 1, for lower temperatures, thus signifying no time dependence of magnetization i.e., fast dynamics. These are indications of strengthening of cycloidal spin arrangement at lower temperatures, which is discussed in later chapters. For BFCO2, M_0 gradually increases with the decrease in temperature. As the cooperative ordering of magnetic moments have already taken place at Neel temperature, which is quite high compared to these temperatures, such rise in M_0 cannot be merely explained on the basis of ordering of magnetic moments. Correlating this to the behavior of 'τ' (increase at lower temperatures) and 'n' (fluctuates between 0.6 and 0.7), shows highly intermingled and slow relaxation of magnetization. This is also supported by the M vs T data where large bifurcation is seen in ZFC and FCW data. Hence, from these data, it is very clear that the two process are responsible for the glassy behavior of BFO: a non-cooperative spin dynamics as seen from the value of 'n' and rate of spin dynamics (may be due to spin frustration), evident from the value of 'τ'.

At 5K, the value of n is 0.75 indicating a fractal-exponential decrease and hence showing slight glassiness of the sample. With increase in temperature this value decreases to 0.68, indicating improvement in the exponential decrease.

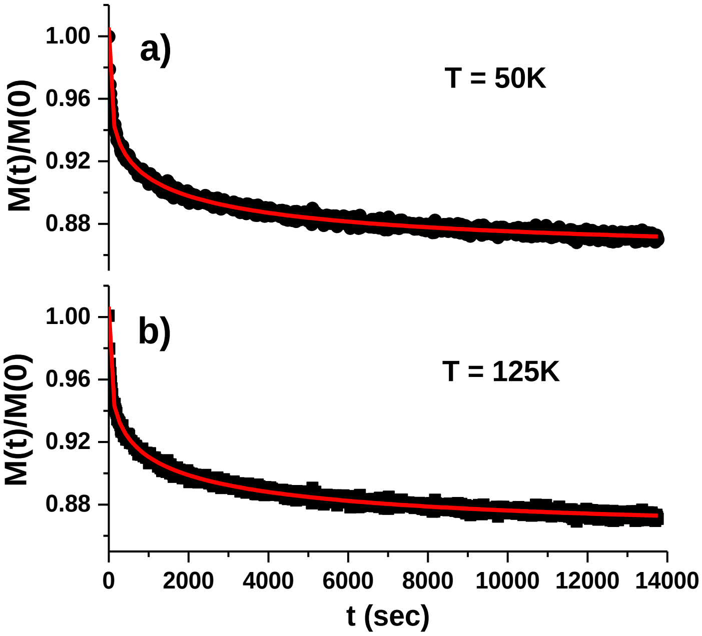

Fig. 3.3 Normalized ZFC magnetization of a) BFO and b) BFCO2 measured as a function of time at T = 125K. The solid red line represents the non linear fitting of the observed data with equation 3.1.

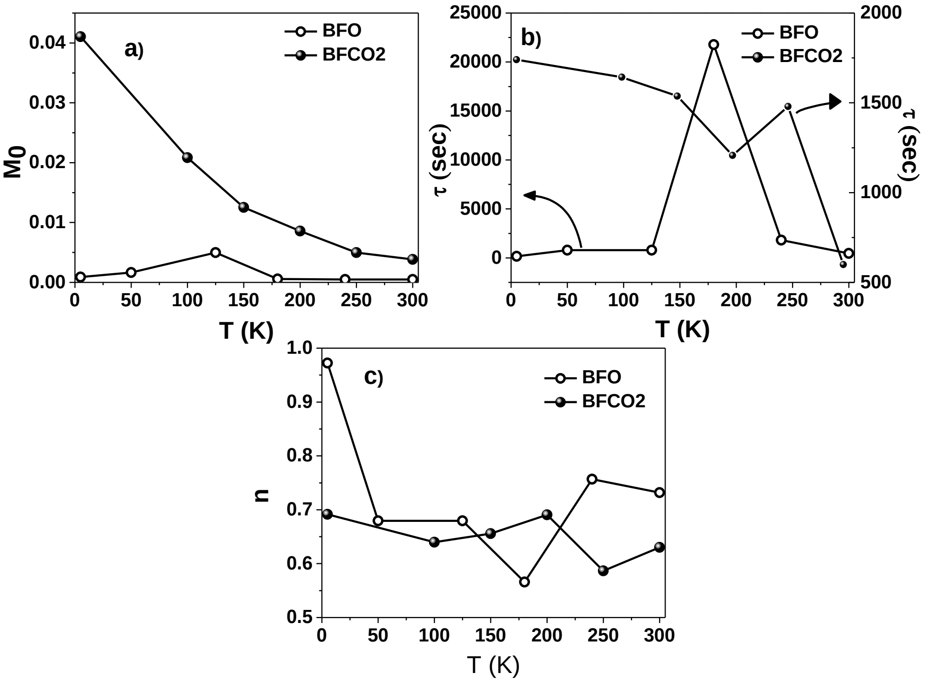

Fig. 3.4 shows the plot of temperature variation of a) intrinsic magnetic moment, b) relaxation time and c) relaxation component of $BiFe_{1-x}Co_xO_3$(x= 0, 0.02).

A careful observation of ZFC data of both the cobalt doped BFO at 0.1T shows an inflection point near T ~ 150 K. Such inflection points are not seen in the magnetization data of either parent BFO or Co-doped BFO under 1T magnetic field. This inflection point is seen better, in the derivative of ZFC data, which shows maxima at ~ 150 K. Apparently no shift in maxima position with respect to cobalt concentration is observed, rather the peak became more pronounced for higher concentration of Co. This may be an onset of possible magnetic transition depending mainly on concentration of Co^{3+}. Under 1T of magnetic field, the ZFC and FCW data for x = 0.01 decreases simultaneously with lowering of temperature till T ~ 180 K and then the bifurcation in ZFC and FCW starts which grows continuously with lowering of temperature. Such behavior indicates, strengthening of antiferromagnetic behavior with some glassy behavior below 180 K [18]. For x = 0.02, the nature of the curve is different from the other two samples. ZFC and FCW are almost flat with temperature till 180K, below which the bifurcation starts such that FCW remains almost unchanged whereas ZFC decreases almost linearly with temperature. This behavior is reminiscent of ferrimagnetic type behavior with significant glassiness below 180K [17].

3.2.3 Magnetization vs. Magnetic field (M vs. H) Measurement

The M-H measurements done at two temperatures, namely 10 K and 300K for all the three samples are shown in fig. 3.5. Here the magnetization of parent compound (x = 0) at 10K increases in consistent with Brillouin function, initially [27], and then linearly with magnetic field. Small hysteresis (reminiscent of ferromagnetic interaction) at low fields (~ 1 T) is also seen in the 10K data. Similar ferromagnetism has also been observed in BFO nanoparticles, which is ascribed to uncompensated spins of spinoidal structure due to the small size of particle [26]. The M~H plot for x = 0.01 displays linear behavior at 10K with slight nonlinearity at 300K for lower fields (<1T). No hysteresis is observed in this case. This resembles an antiferromagnetic behavior [28] which is also supported by M-T data. For x = 0.02, again a linear behavior at high field and Brillouin function like nonlinearity at lower field is present in 300K data. At 10K, the high field data is linear, whereas nonlinearity with hysteresis is present at low field (< 2.5 T). However the nature of non-linearity is different from Brillouin like and resembles more like glassy behavior (S-shape). This is an indication of ferrimagnetism in the sample[18], and is also seen in M-T data. One important observation which is also noticed for both the Co-doped BFO: the high field magnetization value at 300K is higher than that at 10 K, an observation contrary to traditional magnetic materials. This indicates a relatively higher magnetic moment for high temperature phase than low temperature phase.

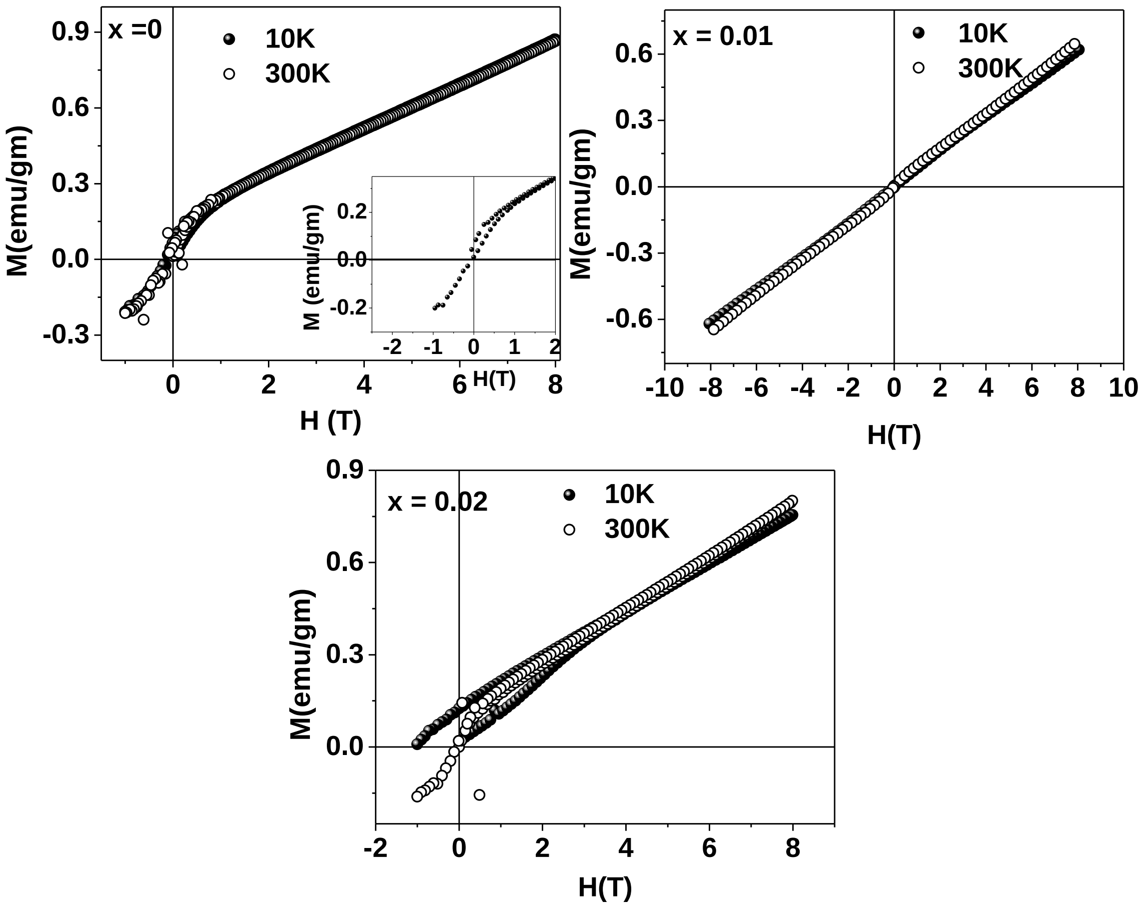

Fig. 3.5 The M vs. H plots of $BiFe_{1-x}Co_xO_3$(x= 0, 0.01, 0.02) measured at 10K (solid symbol) and 300K (open symbol). The inset in first figure shows the magnified view of hysteresis in the 10K data for field below 2.5T.

3.3 Discussions

Surprising results obtained when the magnetization data are plotted as Arrott plot (M^2 vs. H/M), shown in fig. 3.6. A consistent nonlinear increase for parent BFO is observed at both 10K and 300K. The doped sample exhibited a discontinuous change in the slope (positive to negative) at magnetic field ~ 1- 2.5T when measured at 10K whereas no such sharp change is seen in 300K data. The negative slope in the 10K curve in both1% and 2% Co doped $BiFeO_3$ correspond to a first order phase transition [29].

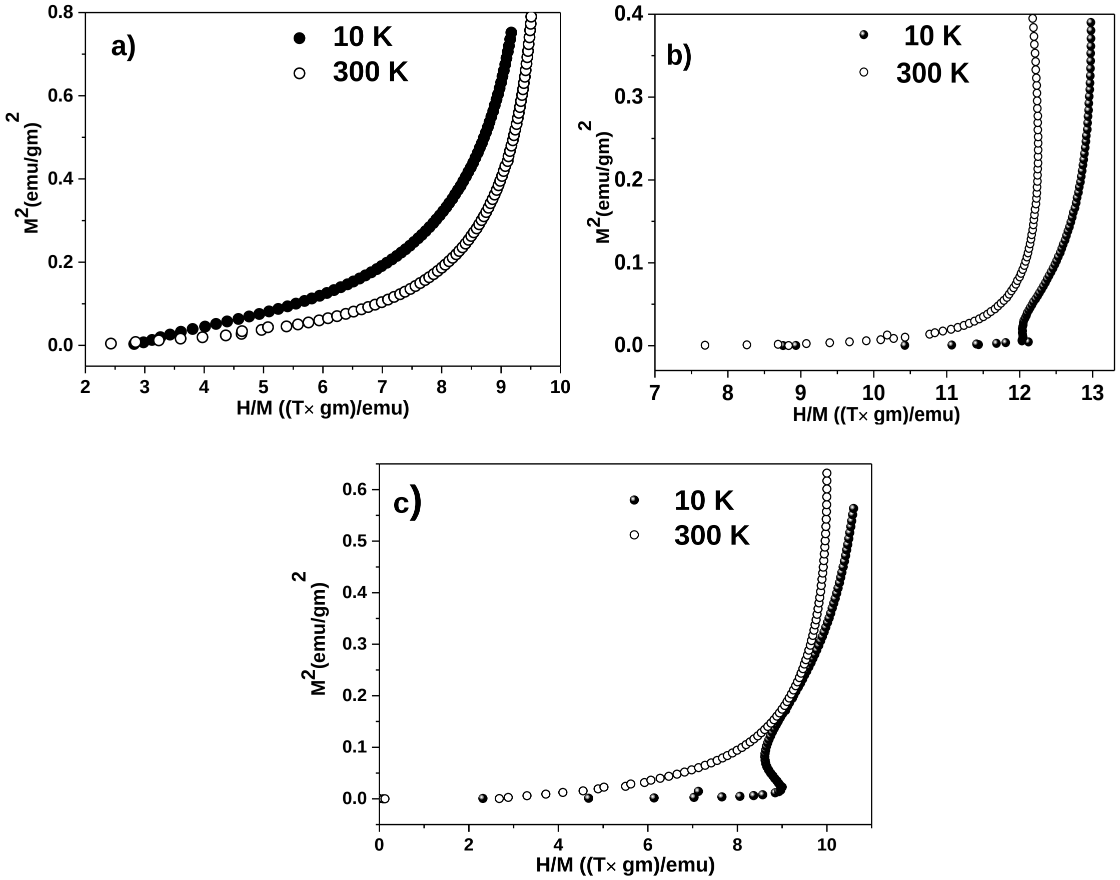

Fig. 3.6 Arrot plot of $BiFe_{1-x}Co_xO_3$(x= 0, 0.01, 0.02) measured at 10K (solid symbol) and 300K (open symbol). The signature of negative slope, which indicates a first order transition (LS- IS) is observed at 10K in case of x = 0.01 and x = 0.02.

It is known that BFO has an incommensurate cycloidal spin structure with periodicity of 64nm along $[110]_h$ direction, such that two Fe^{3+} are separated by 0.585nm. Then the number of Fe^{3+} participating in one complete cycloid is 64/0.585= 109. Hence the substitution of 1% and 2% Co at Fe sites will cause nearly one or two Co^{3+} ions per cycloid, respectively (see fig. 3.7). The DM interaction $D_{ij}(S_i \times S_j)$ which is mainly responsible for the cycloidal spin structure in BFO [30] may be disrupted locally if the jth spin at Fe site, is made different from the rest of the spins. It is known that Co^{3+} ions undergoes a variety of magnetic states LS (0.29 μ_B), IS (1.64 μ_B) and HS (2.16 μ_B) while going from low temperature to high temperature [31] (fig. 3.8). As the moments of Co^{3+} ions differ significantly from Fe^{3+} ions (5.92 μ_B in HS), substitution of Co^{3+} for Fe^{3+} may disrupt the exchange interaction locally (at the Co^{3+} site) and the cycloidal spin on either side of Co^{3+}

will have no (weak) correlation to the LS (HS) state of Co^{3+}. In $LaCoO_3$, the low temperature LS state makes a transition to IS state at ~ 100K and from IS to HS at 500K. Hence, in the temperature range of the present study, we may expect LS to IS transition ~ 100K. One such transition ~150K in the ZFC data under 0.1T has already been witnessed, and becomes more prominent for higher concentration of Co^{3+}, hence may be linked to the LS–IS transition. This is confirmed further from the M-H data, where 300K state is having more magnetization than 10K state. Now we can say that the Co^{3+} in the spin cycloidal is in the LS state at low temperature and makes a transition to IS state at 150 K. However, nothing yet said about the magnetic field induced transition, seen in the Arrot plot and 1T M-T data. Till now the magnetic field induced LS–IS transition of Co^{3+} is not seen in similar compounds like $LaCoO_3$. This is because, the magnetic field needed for this will be too high to be achieved in a laboratory, $B = \frac{k_{BT}}{(\mu_{IS} - \mu_{LS})} \approx 100T$.

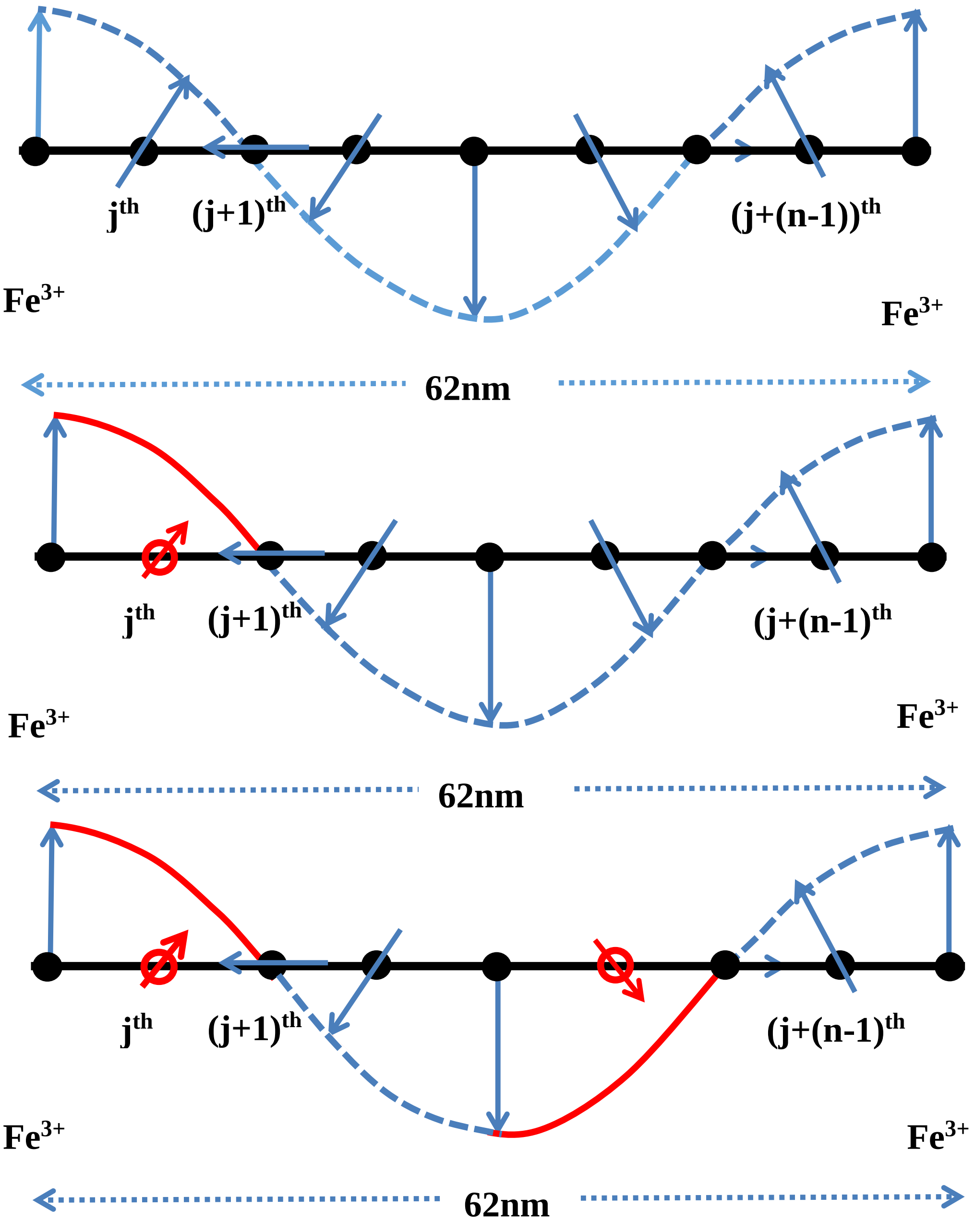

Fig. 3.7 **A schematic model showing the status of cycloidal spin arrangement of $BiFe_{1-x}Co_xO_3$(x= 0, 0.01, 0.02). Here the Fe^{3+} and Co^{3+} is represented by solid black and hollow red spheres respectively. The arrows stand for the magnetic moment of iron (big) and cobalt (small). The solid portion of curve represents the region of weak link formed by Co^{3+} in the cycloidal spin structure.**

However, it should be mentioned that in $LaCoO_3$, each LS-Co^{3+} is surrounded by other LS-Co^{3+} (μ = 0.29 μ_B). In the present case, each LS Co^{3+} is surrounded by other HS-Fe^{3+}, whose magnetic moment is 20 times higher than that of LS-Co^{3+} in a similar environment. Thus the conditions for attaining IS state magnetically, in this case is 20 times more favorable. Hence a transition is expected for 150/20 ≈ 7K and magnetic field 100/20 ≈ 5 T for LS–IS transition. The temperature and magnetic field for LS–IS transition which we observed is of the same order, i.e.,10K and 1T.Hence the first order transition observed in the Arrot plot, may be linked to LS–IS transition.

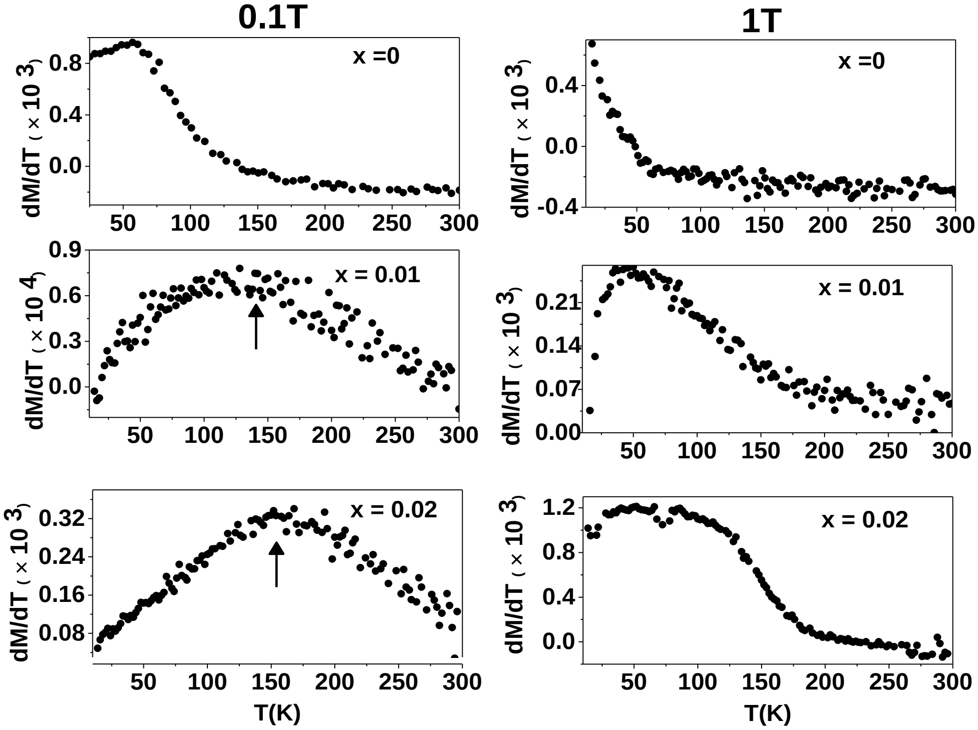

Fig. 3.8 The dM/dT plot for $BiFe_{1-x}Co_xO_3$(x= 0, 0.01, 0.02) at 0.1T (left) and 1t (right). The peak position (shown by arrow) has been associated with the onset of magnetic transition of Co^{3+}, as per proposed model.

Now let us discuss the experimental results on the basis of the above-mentioned model. The large bifurcation between ZFC and FCW in Co doped BFO is an indication of the spin glassy nature in the compound [16]. Similar observations with x =0.05 were reported in [15,16], where the authors concluded the presence of cluster spin glass phase in the compound. As per our model, the spin glass or the cluster glass state appears due to spin upset in the cycloidal structure at Co site. This effect is more pronounced when Co is in LS state and less pronounced when Co is in IS state. Therefore the large bifurcation, seen for x = 0.01 in the 0.1T data, is due to LS state of Co. On the application of 1T magnetic field, the Co attains IS state and the long range spin cycloidal structure is stabilized partially (because even in IS state, Co^{3+} differs from its counter Fe^{3+} by 4 μ_B), so that the net moment in the spin cycloid between two Co^{3+} is almost zero, resulting an antiferromagnetic behavior. It can be seen in fig. 3.1 that the magnetization value of x =0.01 sample is much lower than that of x = 0 and x = 0.02. For x = 0.02, the full spin cycloid is divided in three parts and in each part the magnetic moments are non-zero, so that on the application of magnetic field, they may reorient further in the direction of the magnetic field, and hence a ferromagnetic behavior may be expected. The cluster glass behavior reported earlier can also be explained by this model. When cobalt goes in the spinoidal arrangement, it weakens the interaction between the two Fe on either side of Co. Because of this, a weak link is created at the Co site. Hence, the region between the two Co acts like a cluster, as it is weakly connected at the Co site. Under an external magnetic field, these clusters reorient about the Co site, as per magnetic field direction.

3.4 Conclusions

In conclusion, we have made a systematic study on the effect of Co doping on the magnetic properties of $BiFeO_3$ via DC magnetization measurements. It is found that Co doping greatly influences the magnetic properties of $BiFeO_3$ due to various magnetic states acquired by Co^{3+}. A model is proposed to explain the observed magnetization data. The cobalt doped $BiFeO_3$ undergoes a first order transition induced both thermally and magnetically. Based on the arguments mentioned above, this transition is believed to be due to LS–IS states of Co^{3+}. The Co^{3+} is in LS state when [$T<150K$; $H < 0.1T$] and [$T<10 K$; $H<1T$] and Co^{3+} is in IS state for [$T >150K$; $H > 0.1T$] and [$T>10K$; $H>1T$]. The cluster glass behavior reported earlier may also be explained on the basis of present model. The spinoidal lattice is divided (magnetically) into smaller components due to LS state of Co^{3+} and the region surrounded by LS-Co^{3+} behaves like one cluster. Through this work, a very small concentration of cobalt is found sufficient to bring significant changes in the magnetic state of $BiFeO_3$. Hence $BiFeO_3$ may be tailored for various magnetic applications when appropriately doped by cobalt. Though the observed glassiness and various magnetic states have been ascribed to several spin states of Co^{3+} in the spin cycloid model, a high resolution neutron diffraction may be needed to confirm the proposition.

References

1. G. A. Smolenskii, I. E. Chupis, *Soviet Physics–Uspekhi* ,**25** 475 (1982)
2. I. Sosnowska, M. Loewenhaupt, W. I. F. David, & R. M. Ibberson, *Physica B*, **180 & 181** 117 (1992)
3. W. M. Zhu, H. Y. Guo, Z. G. Ye, *Phys. Rev. B*, **78** 014401 (2008).
4. P. Uniyal, K. L. Yadav, *J. Phys.: Condens Matter*, **21** 012205 (2009).
5. S. T. Zhang, Y. Zhang, M. H. Lu, C. L. Du, Y. F. Chen, Z.G. Liu, Y. Y. Zhu, and N. B. Ming, *Appl. Phys. Lett.*, **88** 162901 (2006)
6. G. Le Bras, D. Colson, A. Forget, N. Genand-Riondet, R. Tourbot and P. Bonville, *Phys. Rev. B*, **80** 134417 (2009)
7. G. L. Yuan, Siu Wing Or, J. M. Liu and Z. G. Liu, *Appl. Phys. Lett.*, **89** 052905 (2006)
8. K. Chakrabarti, K. Das, B. Sarkar and S. K. De, *J. Appl. Phys.*, **110** 103905 (2011)
9. V. A. Khomchenko, D. A. Kiselev, I. K. Bdikin, V. V. Shvartsman, P. Borisov, W. Kleemann,J. M. Vieira, A. L. Kholkin, *App. Phys. Lett.*, **93** 262905 (2008)
10. B. Yu, M. Li, Z. Hu, L. Pei, D. Guo, X. Zhao and S. Dong, *App. Phys. Lett.,* **93** 182909 (2008)
11. S. K. Singh, C. V. Tomy, T. Era, M. Itoh and H. Ishiwara, *J. Appl. Phys.*, **111** 102801 (2012)
12. V. A. Khomchenko, D. A. Kiselev, J. M. Vieira, Li Jian, A. L. Kholkin, A. M. L. Lopes, Y. G. Pogorelov, J. P. Araujo, and M. Maglione, *J. Appl. Phys.*, **103** 024105 (2008)
13. I. Sosnowska, W. Schafer, W. Kockelmann, K. H. Andersen, I. O. Troyanchuk, *App. Phys. A*, **74** S1040 (2002)
14. D. Kothari, V. Raghavendra Reddy, A. Gupta, D. M. Phase, N. Lakshmi, S. K. Deshpande, A. M. Awasthi, *J. Phys.:Condens. Matt.*, **19** 136202 (2007)
15. M. Azuma, H. Kanda, A. A. Belik, Y. Shimakawa, M. Takano, *J. Phys.: Condens. Matt.*, **310** 1177 (2007)

16. Q. Xu, H. Zai, D. Wu, T. Qiu, M. X. Xu, *Appl. Phys. Lett.*, **95** 112510 (2009).
17. Q. Xu, S. Zhou, D. Wu, M. Uhlarz, Y. K. Tang, K. Potzger, M. X. Xu, H. Schmidt, *J. Appl. Phys.*, **107** 093920 (2010).
18. M. K. Singh, R. S. Katiyar, W. Prellier, J. F. Scott, *J. Phys.: Condens. Matt.*, **21** 042202 (2009).
19. M. K. Singh, W. Prellier, M. P. Singh, R. S. Katiyar, J. F. Scott, *Phys. Rev. B*, **77** 144403 (2008).
20. M. Imada, A. Fujimori, Y. Tokura, *Rev. Mod. Phys.*, **70**1039 (1998).
21. M. Abbate, J. C. Fuggle, *Phys. Rev. B*, **47** 16124 (1993).
22. T. Park, G. C. Papaefthymiou, A. J. Viescas, A. R. Moodenbaugh, S. S. Wong, *Nano Lett.*, **7** 766 (2007).
23. R. S. Freitas, L. Ghivelder, F. Damay, F. Dias, L. F. Cohen, *Phys. Rev. B*, **64** 144404 (2001).
24. M. Vasundhara, V. Srinivas, V. V. Rao, *Phys. Rev. B*, **78** 064401 (2008).
25. K. Vijayanandhini, Ch. Simon, V. Pralong, V. Caignaret, B. Raveau, *Phys. Rev. B*, **79** 224407 (2009).
26. O. F. deLima, J. A. H. Coaquira, R. L. deAlmeida, S. K. Mallik, *J. Appl. Phys.*, **107** 09E107 (2010).
27. C. Kittel, *Introduction to Solid State Physics*, vol.**7**, John Wiley & Sons.
28. D. Lebeugle, D. Colson, A. Forget, M. Viret, P. Bonville, J. F. Marucco and S. Fusil, *Phys. Rev. B*, **76** 024116 (2007).
29. W. Dunhui, T. Shaolong, H. Songling, Z. Jianrong and D. youwei, *J. Magn. Magn. Mater.*, **268** 70 (2004).
30. C. Ederer and N. A. Spladin, *Phys. Rev. B*, **71** 060401R (2005).
31. T. Jia, H. Wu, G. Zhang, X. Zhang, Y. Guo, Z. Zeng and H. Q. Lin, *Phys. Rev. B*, **82** 205107 (2010).

Chapter 4

Neutron diffraction study on Co substituted $BiFeO_3$ ($BiFe_{1-x}Co_xO_3$: x = 0, 0.01, 0.02)

Nano particles of $BiFeO_3$ and $BiFe_{0.98}Co_{0.02}O_3$ are studied via neutron diffraction technique. At room temperature, the Co^{3+} are found to be in an intermediate spin state corresponding to magnetic moment 2.828 μ_B, whereas that of Fe^{3+} as 3.848μ_B. The decrease in temperature reveals the signature of spin state transition from an intermediate spin (S = 1) to low spin (S = 0) of Co^{3+} ion, hence satisfying our previous assumption (see chapter 3). Analysis of purely magnetic peak near d ~ 4.56Å, reveals large spin canting and anharmonic cycloidal magnetic structure, i.e., bunching of the magnetic moment along c-axis at 300K. This is in contrary to that observed in bulk, where the spins are restricted to a-b plane only. The substitution of Co^{3+} is found to be inducing more spin canting. On decreasing the temperature, magnetic anharmonicity decreases and the magnetic cycloidal structure revives.

4.1 Introduction

Since its discovery, $BiFeO_3$ (BFO) has been the only prototype among all the multiferroics, and it exhibits G-type antiferromagnetism (T_N = 643 K) superimposed with an incommensurate cycloidal spin arrangement of Fe^{3+} ions with a periodicity of 62 nm resulting in zero net magnetization[1,2]. Multiferroicity above room temperature makes $BiFeO_3$ (BFO) an ideal candidate for investigation. The multiferroicity in BFO is attributed to the peculiar arrangement of mutually perpendicular magnetic and electric dipoles. The magnetic moments of Fe^{3+} are coupled ferromagnetically within the $(001)_h$ planes and antiferromagnetically between the adjacent planes, hence results G-type antiferromagnetism.

Since its conceptualization and independent investigations by several groups, the modulated magnetic structure of BFO, below room temperature (RT) is still an area needs to be investigated [3-9]. The neutron diffraction measurements by Przenioslo et.al.[5], on polycrystalline BFO, concluded that the modulated cyclic ordering does not change on cooling from 300K to 4K. Measurements on single crystal BFO by Ramazanoglu et.al.[6], observed a slow and gradual change of cycloid periodicity, for T < 300K. Using the low temperature NMR technique, Zalesskii et.al.[7], reported that the degree of anharmonicity in BFO increases with decrease in temperature. Using the same NMR studies, Pokatilov et.al.[8], contradicted the conclusion of Zalesskii and pointed that BFO at 4.2K has a spatial spin modulated cycloid magnetic structure rather than an anharmonic spin modulated cycloid structure. In their report of neutron diffraction, Sosnowska et.al.[9], discarded any possibility of anharmonicity in the temperature range of 4K to 300K on polycrystalline $BiFeO_3$ powder sample. Recently, Sosnowska et.al. observed the cycloidal to collinear magnetic ordering below RT in $BiFe_{0.8}Co_{0.2}O_3$. Here, the weak ferromagnetism is found to be coexistent with the collinear magnetic ordering[10].

While studying the magnetic cycloidal structure, sometimes a perturbation (in the form of atomic substitution) to the magnetic cycloid structure of BFO is very helpful,[11-14] hence in this regard, we have substituted Co^{3+} at the Fe^{3+} sites. The magnetic property of nano-BFO differs from bulk and shows ferromagnetic loop in M-H plot indicating non-vanishing spontaneous magnetization. The non-vanishing spontaneous magnetization has been attributed to the unsaturated spins in the magnetic cycloidal structure[15]. Still a detailed knowledge about the spin orientations leading to unsaturation/spontaneous magnetization in the nano-BFO is lacking. Hence, neutron diffraction studies are carried out to gain an insight of the impact created by substituted Co^{3+}, on the local magnetic moments. Neutron diffraction (ND) is well suited to investigate the local magnetic arrangements at atomic levels. Moreover, due to the large neutron absorption cross-section for cobalt, ND is an ideal tool for low cobalt concentration. Hence, by the neutron diffraction measurement, it is aimed to reveal (i) the spin cycloid in nano BFO (ii) the effect of Co^{3+} substitution on the magnetic cycloid of BFO (iii) the evolution of Co^{3+} substituted BFO with decrease in temperature.

4.2 Results and Discussions

As higher substitution of cobalt (e.g., x = 0.03, BFCO3) in $BiFeO_3$ lead to emergence of secondary phases (as discussed in previous context), hence not considered for magnetization measurements. Magnetization studies of $BiFe_{1-x}Co_xO_3$; x=0, 0.01 and 0.02 show various magnetic states (superparamagnetic, antiferromagnetic and weakly ferromagnetic, respectively) along with an indication of magnetic field induced first order transition in the Arrot plot (details in chapter 3). The above mentioned first order transitions strengthens on increasing Co content in the sample. Considering the various spin states exhibited by Co^{3+} as a function of temperature, a cycloidal spin model is proposed to explain these induced magnetic states and the above mentioned spin state transitions in Co doped $BiFeO_3$.

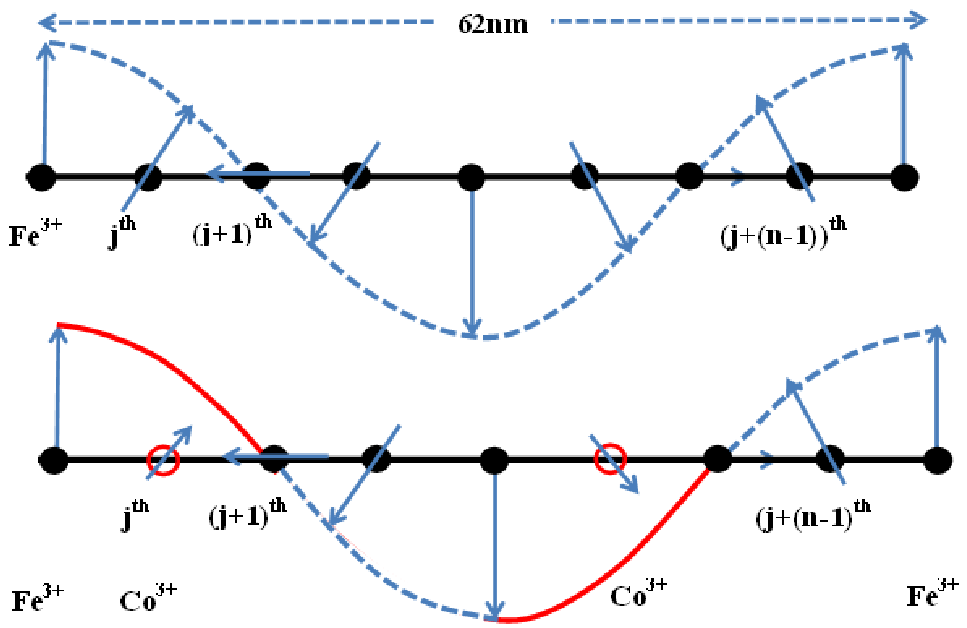

Fig. 4.1. A schematic model showing the status of a cycloidal spin arrangement of $BiFe_{1-x}Co_xO_3$ (x= 0, 0.02). Here the Fe^{3+} and Co^{3+} are represented by solid black and hollow red spheres respectively. The arrow stands for the magnetic moments of iron (big) and cobalt (small). The solid portion of the curve represents the region of weak link formed by Co^{3+} in the cycloidal spin structure.

In this model, it is considered that substitution of Co^{3+} ion at the Fe site leads to the creation of a weak link between two neighboring HS Fe^{3+} ions in the cycloid (see fig 4.1). This weak link is more pronounced when Co^{3+} goes to LS state on lowering the temperature. Hence, because of these weak links, the long cycloidal structure virtually splits in various smaller segments, which upon application of magnetic field may reorient accordingly. Though the present model successfully explains the observed magnetic phenomenon, a direct evidence of various spin states acquired by Co^{3+} on lowering the temperature is very much needed. Hence, in order to confirm our proposition and strengthen the proposed model, ND measurements were carried out for x = 0 and 0.02 samples at various temperatures.

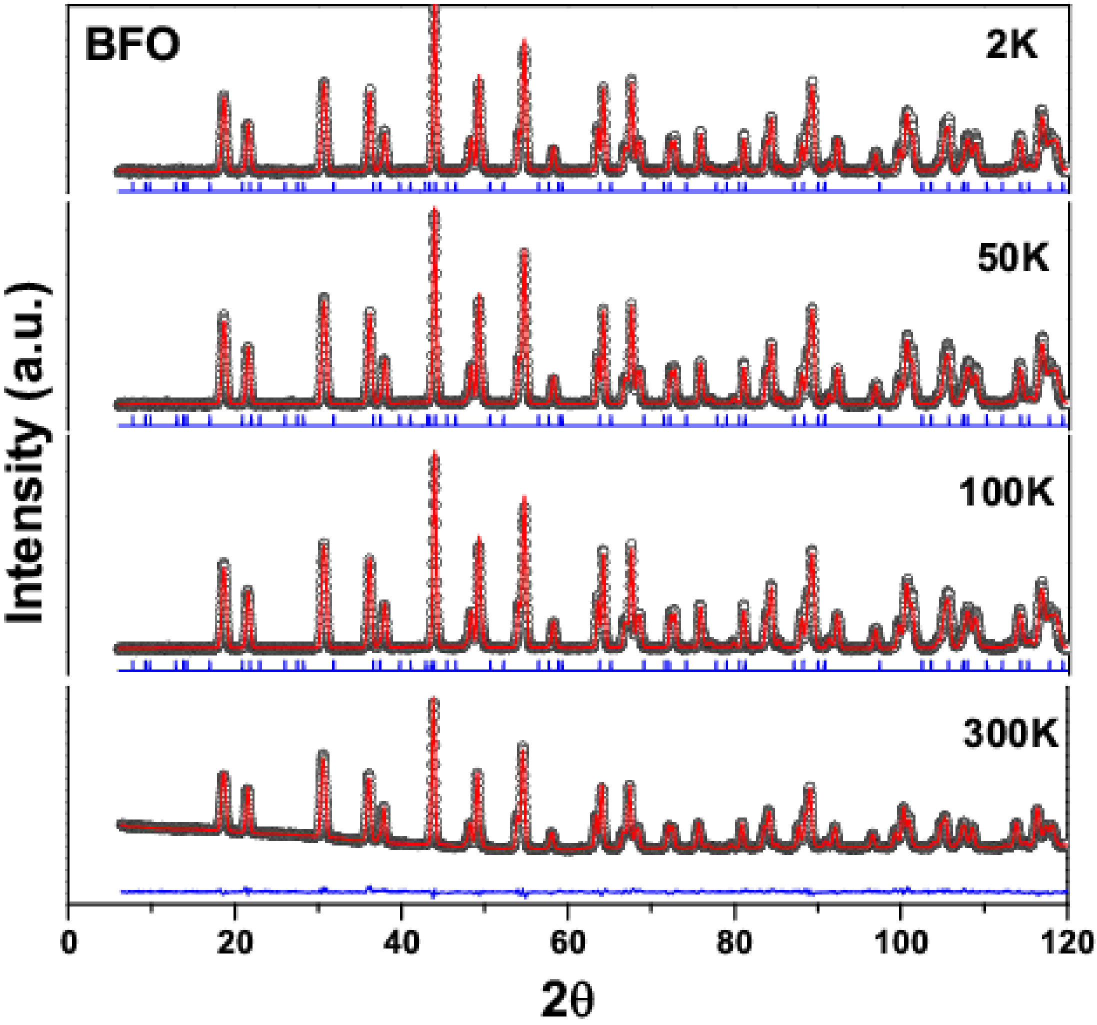

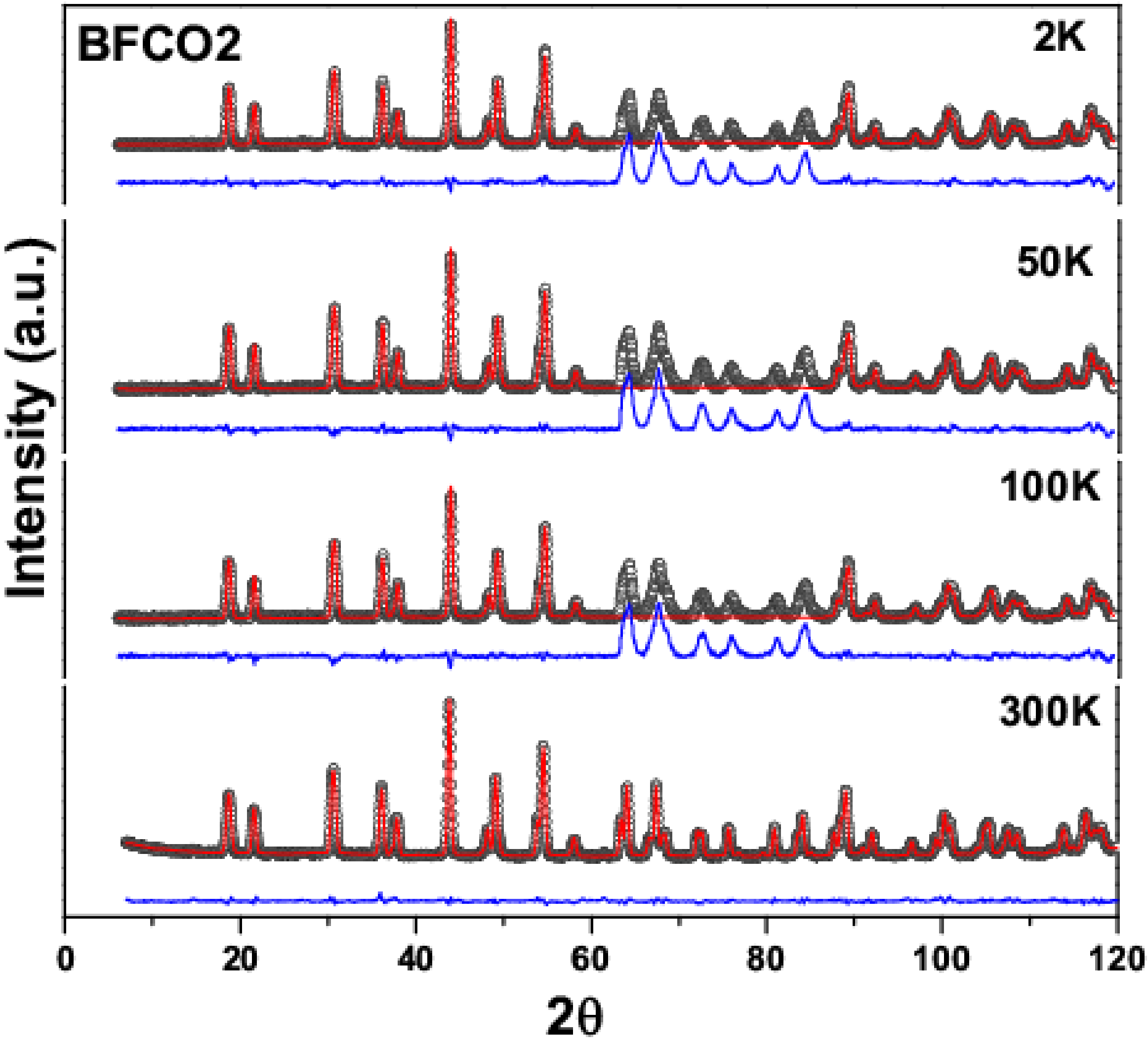

Fig. 4.2. Reitveld refined neutron powder diffraction plot of BFO and BFCO2 at 2K, 50K, 100K and 300K.

The temperature dependent ND not only provides the crystal structure, but also the magnetic aspect of the sample. The Reitveld refined ND data for BFO and BFCO2 at 300K, 100K, 50K and 2K are shown in fig. 4.2. The nuclear structure is found to be crystallized in rhombohedral structure with the space group *R3c*, (No. 161) having Wyckoff positions

Bi: {0, 0, 0}; Fe: {0, 0, z} and O: {x, y, z}[16]. All the samples are found to be phase pure and no extra peaks could be detected. The lattice parameter so obtained from the neutron diffraction is slightly different from the XRD. This discrepancy can be explained on the basis of atomic scattering amplitude. Since neutron scattering amplitude does not depend on the atomic weight, hence it can thoroughly probe the lighter elements like oxygen present in the sample. To obtain the exact magnetic structure, the magnetic contribution is fitted by considering the least symmetry with space group *P-1* throughout the temperature range, so that any possibilities of either structural or magnetic transition in both the systems are ruled out. Conical model[17] is used for the refinement of the G-type antiferromagnetic structure with a superimposed long cycloidal modulation. This time the refinement is done only for the magnetic parameters (magnetic moments, propagation vectors, etc.). Due to some technical fault in one of the monochromator, data in the 2theta range 60^0- 86^0 for BFCO2 is not taken into consideration while refining.

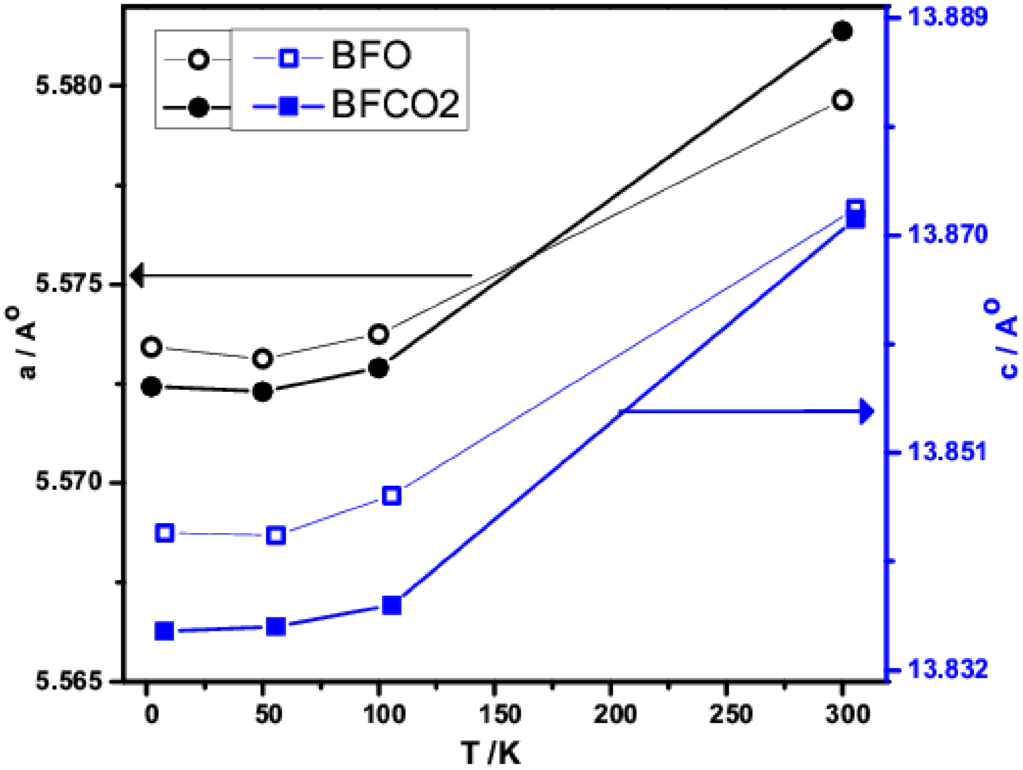

Fig. 4.3. Temperature dependent variations in the lattice parameters of BFO and BFCO2.

Temperature variation of lattice parameters for BFO and BFCO2 obtained from the ND data at their respective measurement temperatures are shown in fig. 4.3. Co^{3+} substitution in BFO results slight decrease in the 'c' value (13.8723(2) to 13.8714(1) Å), whereas the 'a' value increases slightly (5.580(6) to 5.581(2) Å) at 300K. So the cell volume remains almost unchanged: 374.03Å^3 (BFO) and 374.18 Å^3 (BFCO2). On cooling, both the lattice parameters decrease and saturate at low temperatures: similar to earlier reports of BFO[11,16, 18]. The cell parameters of BFCO2 also follow the similar decrease as that of BFO. This is quite expected for the similar ionic size of Fe^{3+} and Co^{3+}. Hence the cobalt doping in BFO does not induce any crystal structure change due to size mismatch. The magnetic refinement results a spatially modulated spin structure. The periodicity of the modulated spin structure (fig 4.4) is having the propagation vector (k_x, k_x, 0), with k_x ~ 0.01025 (see table 4.1 for respective values) and found to be incommensurate with the crystallographic lattice parameters.

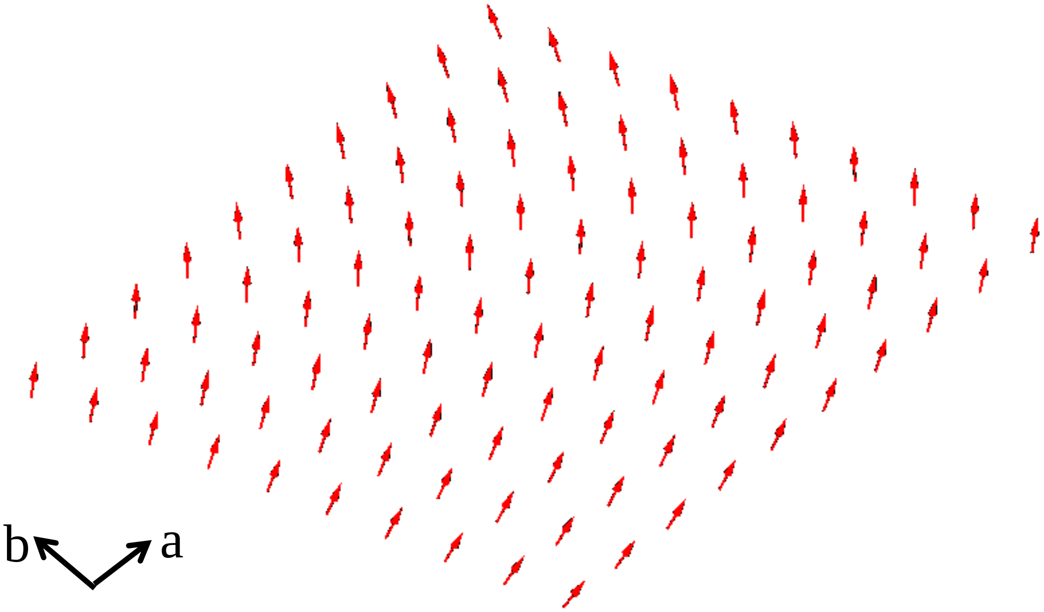

Fig. 4.4 Cycloidal spin arrangement modulated along [110] direction generated from the magnetic refinement of BFO using Fullprof software.

Table 4.1. Comparison of various parameters obtained from the Reitveld refinement of room temperature neutron diffraction data.

Sample	**Lattice parameters (Å)**	**Wyckoff positions**	**Fe-O bond length (Å)**	**k_x**	**φ (degree)**
BFO	5.5796(2) 13.8723(1)	Fe (z): 0.2209 O(x): 0.4460 (y): 0.0165 (z): 0.9524	I: 1.9457(9) II: 2.1124(6)	0.01025	47
BFCO2	5.5809(6) 13.8714(2)	Fe(z): 0.2211 O(x): 0.4471 (y): 0.0175 (z): 0.9527	I: 1.9505(11) II: 2.1071(8)	0.01049	40

Table 4.2.Variation of lattice parameters of both BFO and BFCO2 as a function of temperature obtained from the Reitveld refinement of neutron diffraction data.

Sample	Lattice parameters (Å)			
	300K	100K	50K	2K
BFO	5.5796(2) 13.8723(1)	5.57375(3) 13.84728(4)	5.57313(5) 13.84377(1)	5.57342(1) 13.84402(2)
BFCO2	5.5809(6) 13.8714(2)	5.5729(7) 13.83769(3)	5.5723(2) 13.83584(4)	5.57243(3) 13.8354(1)

The magnetization direction in the bulk $BiFeO_3$ is perpendicular to the electric-polarization direction, i.e., in the $(110)_h$ plane. So, the deviation of the magnetization direction from $(110)_h$ plane, is an indication of deviation in corresponding polarization direction. Hence, purely magnetic peak in the neutron diffraction data, i.e., the peak near d ~ 4.56Å (corresponding 2θ ~ 18.4°) is investigated in detail. Fig. 4.5 shows the magnetic peak corresponding to d ~ 4.56Å[9]. The cycloidal spin structure of BFO having periodicity 62 nm with magnetization direction in the $(110)_h$ plane, should result four distinct peaks at d ~ 4.53Å, 4.55Å, 4.58Å & d ~ 4.62Å corresponding to left (L): (1+δ, δ, 1), central (C): (-1+δ, 1+δ, 1), right (R): (1-δ, -δ, 1) triplet and (δ, δ, 3) respectively[9]. Instead, in our samples, we found only one broad peak at d ~ 4.56Å as shown in fig. 4.6. According to the spiral model, a slight rotation of the spins out of $(110)_h$ plane would result in smearing of the satellite peaks giving rise to (101) triplet and the central peak will be wider than the side peaks[3].

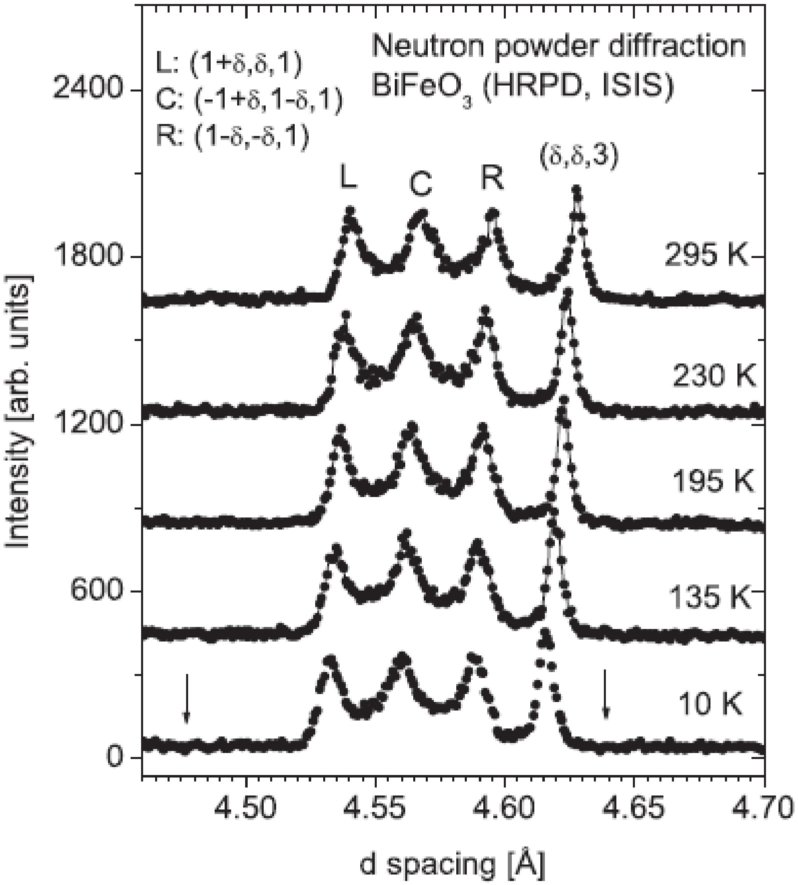

Fig. 4.5 Neutron powder diffraction pattern of $BiFeO_3$ measured at several temperatures between 10 and 295 K. The symbols L, C, R correspond to the labelling given in ref 9. Vertical arrows show the positions of the third-order satellites $(1 - 3\delta, -3\delta, 1)_{hex}$ and $(1 + 3\delta, +3\delta, 1)_{hex}$ expected for the anharmonic model at low temperature[9].

Hence, to study the magnetic structure, the magnetic peak is deconvoluted in four peaks (for first order satellites) or six peaks (including the 3rd order satellites contribution) as shown in fig. 4.6. Appearance of 3rd order satellite peaks at L3q: d ~ 4.50Å: (1-3δ, -3δ, 1) and R3q: d ~ 4.64Å: (1+3δ, +3δ, 1) is an indication of anharmonicity in the commensurate magnetic structure i.e., bunching of magnetic moments along c-axis. For the BFO data, even the best possible deconvolution gave four peaks corresponding to the (101) triplet & (003). The third order peaks couldn’t be deconvoluted. Whereas for BFCO2, we got a very good deconvolution with six peaks. This is a very good sign of anharmonitcity in BFCO2.

For the low temperature data, we found difficult to proceed this way because, the 3rd harmonics are generally very weak and particularly in this case, where the individual peaks are not very distinguishable, this may give a wrong interpretation. Hence we proceeded by estimating the intensity ratio, $A = I_{\delta\delta 3}/(I_L + I_C + I_R)$ as followed by Przenioslo et.al.[5]. The values of 'A' obtained for BFCO2 at 100K, 50K and 2K are 0.20, 0.26 and 0.32. For a harmonic cycloidal ordering (degree of anharmonicity; m = 0), the value of 'A' (maximum) has been calculated to be A = 0.232 [3,9]. The value of 'A' decreases with increasing 'm' (for m = 0.5, A = 0.208 & for m = 0.9, A = 0.157) [9]. Our low temperature values are higher than the maximum limit of 0.232. At this juncture, it is appropriate to mention that, the theoretical limit of A = 0.232 was obtained for no-canting of spins, i.e., when the spins are restricted to a-b or (110) plane.

A general expression for the reflection intensity (for any orientation of spin) after Sosnowska[3], is

$$I \,\alpha\, j\left[1 + \frac{1}{2}\sin^2\eta + \cos^2\gamma\,\left(\cos^2\eta - \frac{1}{2}\sin^2\eta\right)\right] \text{---------- (Eq. 4.1)}$$

where j: multiplicity factor, η: angle between normal to diffraction plane and c*, γ: angle between normal to spin rotation plane and c*. If the spin rotation plane is perpendicular to the spin modulation direction, $\gamma = 90^0$. For (101) triplet, j = 3, $\eta = 70.8^0$ and for (003) plane, j = 1 & $\eta = 0^0$. Then the theoretical value of intensity ratio when spins are in the a-b plane is,

$$\frac{I_{003}}{I_{101}} = \frac{1}{3}\left[\frac{1}{1+\frac{1}{2}\sin^2 70.8^0}\right] = 0.23 \text{ ------------------- (Eq. 4.2)}$$

However, if there is canting of spins out of a-b plane, then $\gamma < 90^0$ and a finite contribution will arise from the third term in eq. 4.1. This contribution will be more pronounced for (003) plane than (101) triplet: hence the intensity ratio I_{003}/I_{101} will be slightly higher than 0.23. According to eq. 4.2, the observed intensity ratio $I_{003}/I_{101} = 0.32$ corresponds to $\gamma = 60^0$ i.e., 30° canting of spins out of a-b plane. In table 4.1, φ is the orientation of magnetic moment with respect to the c-axis, which is same as γ (of eq. 4.1) because c & c* are in the same direction. Hence 90-φ gives the canting angle which is 40° for BFO and

50° for BFCO2. The poor resemblance of the canting angles obtained via refinement (50°) and via intensity ratio (30°), may be due to our inability to deconvolute the poorly resolved magnetic satellite peaks. In spite of this, canting of magnetic moment out of a–b plane is very clear. Moreover, with decrease in temperature, the 'A' value increases, i.e. the magnetic ordering tends towards harmonic cycloidal.

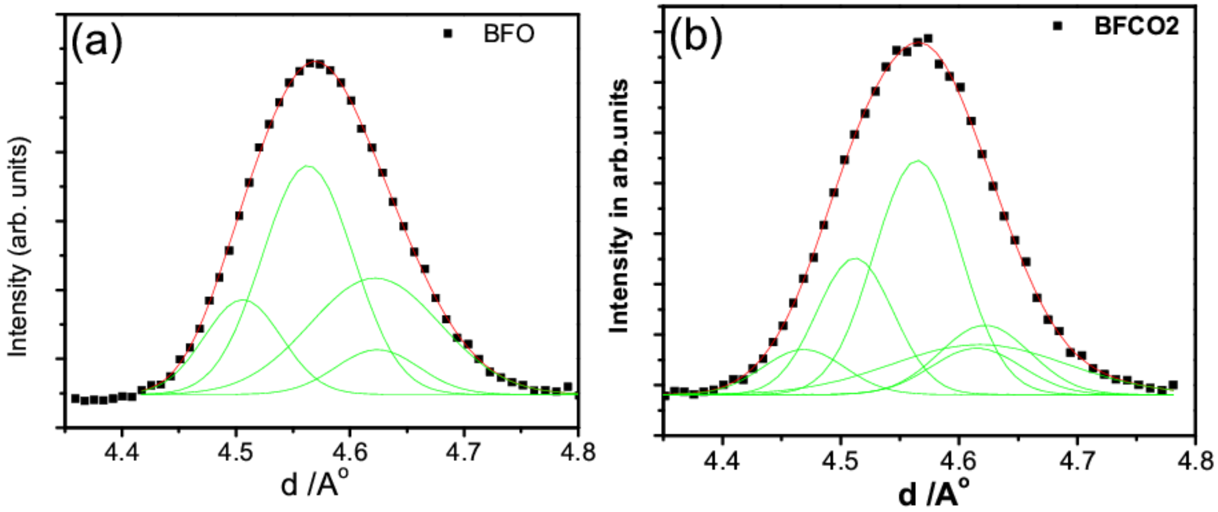

Fig. 4.6. Deconvolution of broad magnetic peak corresponding to d ~ 4.56Å for (a) BFO and (b) BFCO2.

Apart from aforementioned investigations, the neutron diffraction data are analysed for the magnetic moment of Fe^{3+} for BFO and BFCO2. The magnetic refinement shows random substitution of Co at Fe sites. At x = 0.02, nearly two Co^{3+} ions substitute the Fe^{3+} ions in one complete cycloid (described in chapter 3). At RT, the Co^{3+} ions are supposed to be in IS state[19] (S=1;$\mu = 2\sqrt{S(S+1)} = 2.828\mu_B$). The magnetic moment of Fe^{3+} in x = 0 is found to be 3.848 μ_B and in x = 0.02, it is found to be 3.828 μ_B. Since this value is the net effect due to both Fe^{3+} and Co^{3+}, the magnetic moment of Co^{3+} is obtained using the relation,

$$\mu_T = 0.98(\mu_{Fe(III)}) + 0.02(\mu_{Co(III)}) \quad \text{----------------- (Eq. 4.3)}$$

which is found to be 2.85 μ_B. This result is in agreement with one of our proposition that Co^{3+} is in IS state at RT. ND measurements are in progress to confirm the IS to LS transition of Co^{3+} at low temperature. Using these values, the value of μ so obtained is, $\mu_{Fe} = 3.827\mu_B$, which is in good agreement with the experimentally observed value of $3.828\mu_B$, for BFCO2 (see table 4.3). This confirms the IS state of Co^{3+} at RT.

Table 4.3. Magnetic moment of BFCO2 at various temperatures

	Magnetic moment (μ_B)		
Temperature (K)	Observed	Calculated based on LS state	Calculated based on IS state
2	4.018	4.0180*	4.0745
50	3.940	3.9396*	3.9961
100	3.903	3.9029*	3.9595
300	**3.828**	**3.7710**	**3.8276***

**represents the close proximity of magnetic moment with the observed one.*

A plot of the magnetic moment obtained via refinement of ND data for both the samples (BFO and BFCO2) are shown in fig. 4.7. For the reference purpose, the values reported by Jacobson et.al.,[20] is also shown along with our data. Our data for BFO are in close proximity with that of Jacobson et.al.[20] With a decrease in temperature the magnetic moment for both BFO and BFCO2 increases: a result similar to BFO and other BFO based materials[20,21]. With reference to our earlier report, if any spin state transition of Co^{3+} to LS state is occurring for T < 100K, then according to eq. 4.3 the observed ground state magnetic moment of BFCO2 should be, $4.018\mu_B$, with reference to the ground state value for the magnetic moment of Fe^{3+} as $\mu_{Fe} = 4.1\mu_B$. The observed value of $\mu_{Fe} = 4.018\mu_B$ is in good agreement with our earlier proposition of the LS state of Co^{3+} at 2K: hence a spin state transition of Co^{3+} from IS (at RT) to LS (<100K)[19] is confirmed.

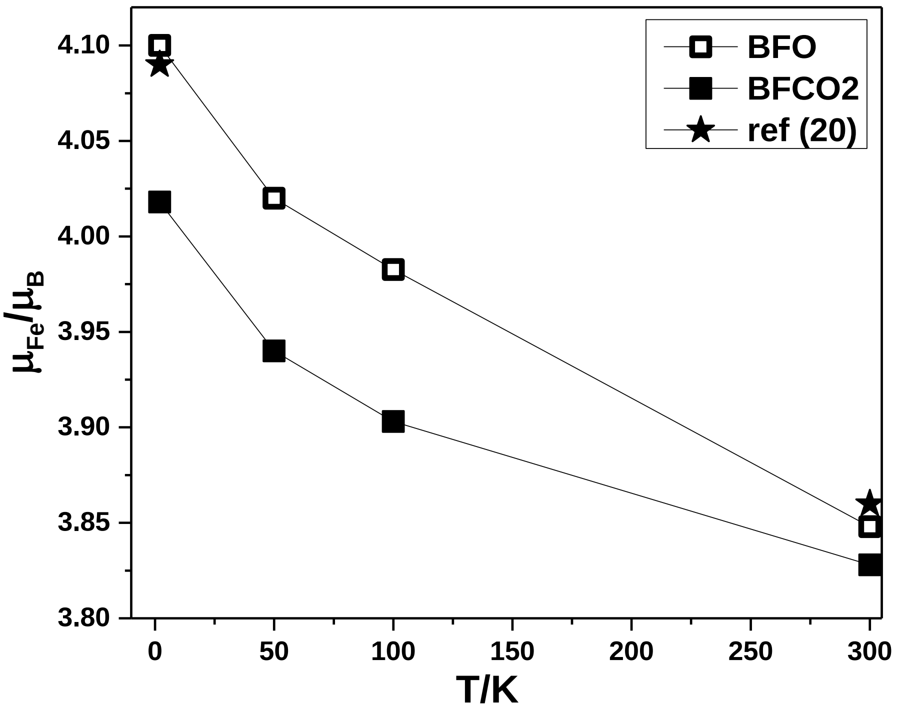

Fig. 4.7. Observed magnetic moment of Fe-site ions in BFO and BFCO2 at various temperatures. For reference, the value in ref 20 is also shown as star. The lines are only a guide to eye.

4.3 Conclusions

The cycloidal spin structure along [110] propagating direction is found in BFO (x=0) sample, with IS spin state of Co^{3+} at room temperature. The calculation of magnetic moment for both the samples shows 3.848 μ_B for Fe^{3+} and 2.85 μ_B for Co^{3+}. Effect of partial substitution of Co^{3+} in $BiFeO_3$ at RT as well as at various low temperatures is studied. The intermediate spin state of Co^{3+} at RT have been confirmed. The refinement suggests that, Co^{3+} undergoes a spin state transition from an intermediate spin (S=1) to low spin (S=0), at low temperatures. The neutron diffraction measurement shows that, cobalt doping in $BiFeO_3$ transforms the modulated G-type antiferromagnetic order towards G-type collinear antiferromagnetic structure (bunching of magnetic moments along c-axis) with an increase in canting angle out of [110] plane. With decrease in temperature, the magnetic structure becomes harmonic cycloidal.

References

1. M. Fiebig, *J. Phys. D,* **38** R123 (2005).
2. W. Eerenstein, N. D. Mathur, and J. F. Scott, *Nature,* **442** 759 (2006).
3. I. Sosnowska, T. Peterlin-Neumaier and E. Steichele *J. Phys. C: Solid State Phys.*, **15** 4835 (1982)
4. S. V. Kiselev, R. P. Ozerov and G. S. Zhdanov, *Sov. Phys. –Dokl*, **7** 742 (1963)
5. R. Przenioslo, A. Palewicz, M. Regulski, I. Sosnowska, R. M. Ibberson and K. S. Knight, *J. Phys:. Condens. Matter*, **18** 2069 (2006)
6. M. Ramazanoglu, W. Ratcliff II, Y. J. Choi, S. Lee, S. W. Cheong and V. Kiryukhin, *Phys. Rev. B*, **83** 174434 (2011)
7. A. Zalesskii, A. Frolov, T. Khimich, A. Bush, V. Pokatilov and A. Zvezdin, *Euro Phys. Lett.*, **50** 547 (2000)
8. V. S. Pokatilov and A. S. Sigov, *JETP*, **110** 440 (2010)
9. I. Sosnowska and R. Przenioslo, *Phys. Rev. B*,**84** 144404 (2011)
10. I. Sosnowska, M. Azuma, R. Przeniosło, D. Wardecki, W. T. Chen, K. Oka and Y. Shimakawa, *Inorg. Chem.*, **52** 13269 (2013)
11. I. Sosnowska, W. Schäfer, W. Kockelmann, K. H. Andersen and I. O. Troyanchuk *Appl Phys. A*, **74** S1040 (2002).
12. M. Azuma, H. Kanda, A. A. Belik, Y. Shimakawa and M. Takano, *J. Phys: Condens: Matter*, **310** 1177 (2007)
13. Q. Xu, H. Zai, D. Wu, T. Qiu and M. X. Xu, *Appl. Phys. Lett.*, **95** 112510 (2009).
14. Z. X. Cheng, X. L. Wang, Y. Du and S. X. Dou, *J. Phys. D: Appl. Phys.*, **43** 242001 (2010).
15. T. J. Park, G. C. Papaefthymiou, A. J. Viescas, A. R. Moodenbaugh, and S. S. Wong, *Nano Lett.*, **7** 766 (2007)
16. F. Kubel and H. Schmid, *Acta Cryst.*, **B 46** 698 (1990).
17. J. M. Hastings and L. M. Corliss, *Phys. Rev. B,* **126** 556 (1962).
18. I. Sonowska, R. Przenioslo, P. Fischer, and V. A. Murasov, *J. Magn. Magn. Mater*, **160** 384 (1996)
19. J. C. Burley, J. F. Mitchell, and S. Short, *Phys. Rev. B,* **69** 054401 (2004)

20. A. J. Jacobson and B. E. F. Fender, *J. Phys. C: Solid State Phys.*, **8** 844 (1975)
21. P. Fischer, M. Polomska, I. Sosnowska and M. Szymanski, *J. Phys. C: Solid State Phys.*, **13** 1931 (1980)

Chapter 5

Magnetoelectric study on $BiFe_{1-x}Co_xO_3$: x= 0, 0.01, 0.02

This chapter describes room temperature magnetoelectric (ME) measurements on phase pure $BiFe_{1-x}Co_xO_3$ (x = 0, 0.01, 0.02). The longitudinal ME coupling coefficient (α) for $BiFeO_3$, $BiFe_{0.99}Co_{0.01}O_3$, $BiFe_{0.98}Co_{0.02}O_3$ is found to be α = 20.935, 12.465 and 17.375 at zero field. The α decreases on application of magnetic field and displays hysteresis in magnetic field (H) for the increasing and decreasing cycle of H. This hysteresis disappears for $BiFe_{0.98}Co_{0.02}O_3$ and α becomes linear in H which is good enough for device applications, especially where α must follow the applied magnetic field linearly, e.g., transistors, transducers, etc. Neutron diffraction studies show lattice stiffening due to cobalt substitution in $BiFeO_3$ and likely to be the cause of the disappearance of hysteresis in α. Room temperature magnetodielectricity of 5% and 3.2% is observed for $BiFeO_3$ and $BiFe_{0.98}Co_{0.02}O_3$ respectively. Interestingly similar to α, ε' also shows hysteresis in magnetic field for $BiFeO_3$ and the hysteresis disappears for $BiFe_{0.08}Co_{0.02}O_3$. The DC electrical resistivity measurements, suggests variable range hopping (VRH) with an average hopping range $50.038/T^{0.25}$ and $40.058/T^{0.25}$ in $BiFeO_3$ and $BiFe_{0.98}Co_{0.02}O_3$ respectively, as the conduction mechanism.

5.1 Introduction

Magnetoelectric multiferroics have widely been studied and earned a considerable research interest due to their potential in the creation of various multifunctional devices[1]. $BiFeO_3$, in particular, brings a special attention for its rich physics and possible application in novel magnetoelectric (ME) based devices. Due to the coupling of various order parameters such as ferroelectric and (anti)ferromagnetic, the change in one order parameter induces the other and enables for the development of a wide range of innovative devices such as memories for spintronics, sensors, actuators and tunable microwave filters [1, 3-7]. A good understanding of the coupling between these order parameters renders it for other applications as well [3, 8 and 9]. Applications based on memory device require strong ME coupling [10, 11]. Composite of $BiFeO_3$ with other compounds such as $BaTiO_3$[12-14], $CoFe_2O_4$[15], $PbTiO_3$[16], $CaTiO_3$[17] has been found to enhance the ME coupling significantly. Conversely, for the applications where linear dependence of multiferroicity on control parameter is required, approach other than the composite materials may be needed. Chemical substitution at Bi and Fe sites of $BiFeO_3$ has been tried so that magnetoelectric coupling may be tuned at the microscopic level. Various rare earth elements such as La^{3+}[18], Gd^{3+}[19], Dy^{3+}[20], diamagnetic ions, e.g. Ca^{2+}, Sr^{2+}, Pb^{3+}, Ba^{2+}[21] are substituted at Bi site and Mn^{3+}[22], Cr^{3+}[23], Nb^{3+}[24] at Fe site. Using first principle studies, it has been shown that the lone pair of Bi^{3+} plays important role in establishing the electric polarization in $BiFeO_3$[25]. Since Bi substitution may hamper the ferroelectricity of the sample, so it won't be a good idea to replace Bi by other elements and thus we restricted ourselves to the Fe site only.

5.2 Results and Discussions

Magnetoelectric property is sensitive to the sample purity; hence the sample quality is examined beforehand. Neutron diffraction (ND) measurement is preferred over typical x-ray diffraction because, ND not only provides the crystal structure, but may also detect the minute secondary phases (if any) due to cobalt doping (e.g., cobalt ferrite). It is found that both BFO and BFCO2 are phase pure and the secondary phases appear only from 3% onwards (See chapter 2). Being assured of sample purity and crystal structure intactness, we proceeded for magnetoelectric measurements.

The linear longitudinal magnetoelectric coupling coefficient (α) is measured via dynamic method. In the dynamic method, the V_{out} is measured against a small AC magnetic field $h = h_0 \cos \omega t$ with $h_0 = 2.3\ Oe$, superimposed on the DC magnetic field (H) to avoid the accumulation of charges at the grain boundaries[26].

According to Landau free energy, the contribution to total polarization 'P' in a magnetoelectric material may be written as,

$$P_i\,(E,H) = -\frac{\partial F}{\partial E_i} = P^s{}_i + \varepsilon_0 \varepsilon_{ij} E_j + \alpha_{ij} H_j + \frac{1}{2}\beta_{ijk} H_j H_k + \gamma_{ijk} H_i H_j - \text{--------} \text{ (Eq. 5.1)}$$

so that the linear ME coefficient 'α' may be expressed as

$$\alpha = \frac{\partial P}{\partial H} = \frac{1}{d}\frac{dV}{dH} = \frac{V_{out}}{h_0 d} \text{ -- (Eq. 5.2)}$$

where V_{out} is the output ME voltage measured across the sample and d is the thickness of the sample.

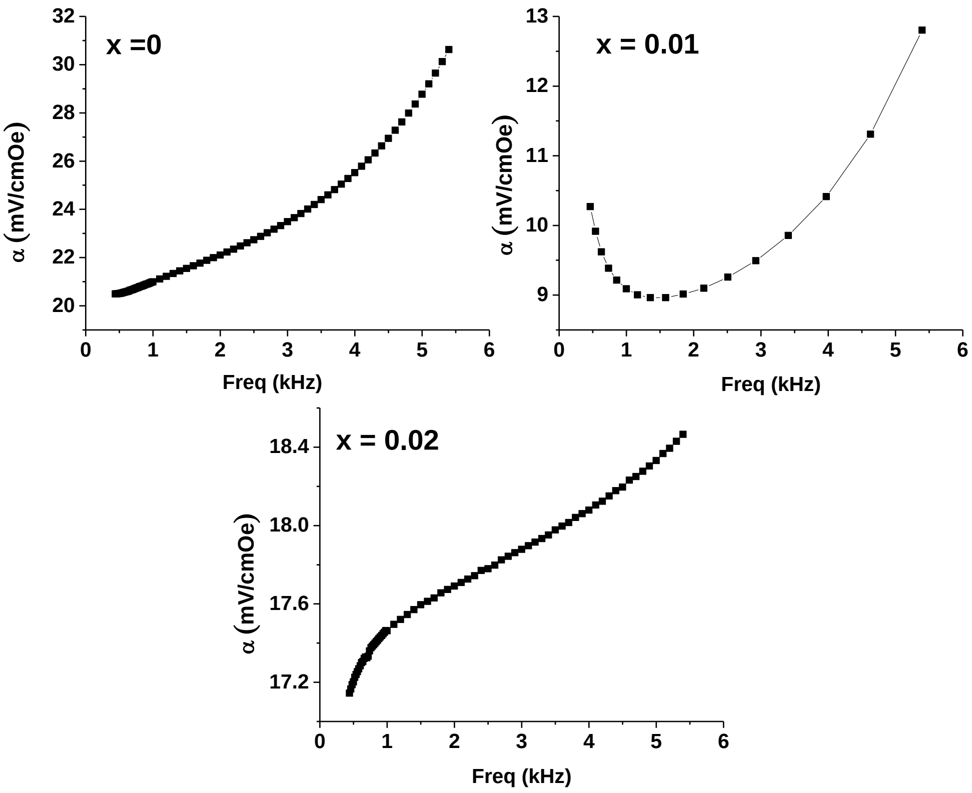

Fig. 5.1. Linear longitudinal magnetoelectric coupling coefficient 'α' vs. frequency of the ac magnetic field for BFO, BFCO1 and BFCO2 at room temperature without dc bias magnetic field.

Fig. 5.1 shows the frequency dependence of linear longitudinal magnetoelectric coupling coefficient 'α' for x= 0, x = 0.01 and x = 0.02 at zero DC magnetic field. For all the samples, a monotonic increase in 'α' with frequency is observed, with slight differences. The value of 'α' in case of BFO rises almost linearly at low frequencies, but the rise becomes steeper as high frequencies are approached. An earlier report of magnetoelectric measurement on BFO shows similar behaviour where 'α' peaks ~ 10kHz and decreases thereafter [27]. The peak is generally called electromechanical resonance [28]. The variation of 'α' in BFCO1 is different from BFO as it first decreases sharply and then increases at ~ 1kHz. However, the variation of 'α' in BFCO2 is almost similar to BFO except the steepness in rise appears at slightly higher values of frequency. This shifting of the frequency towards higher value in x = 0.01 and x = 0.02 is an indication of higher value of the resonance frequency. Blue-shift in resonance frequency is an indication of an increase in lattice stiffness.

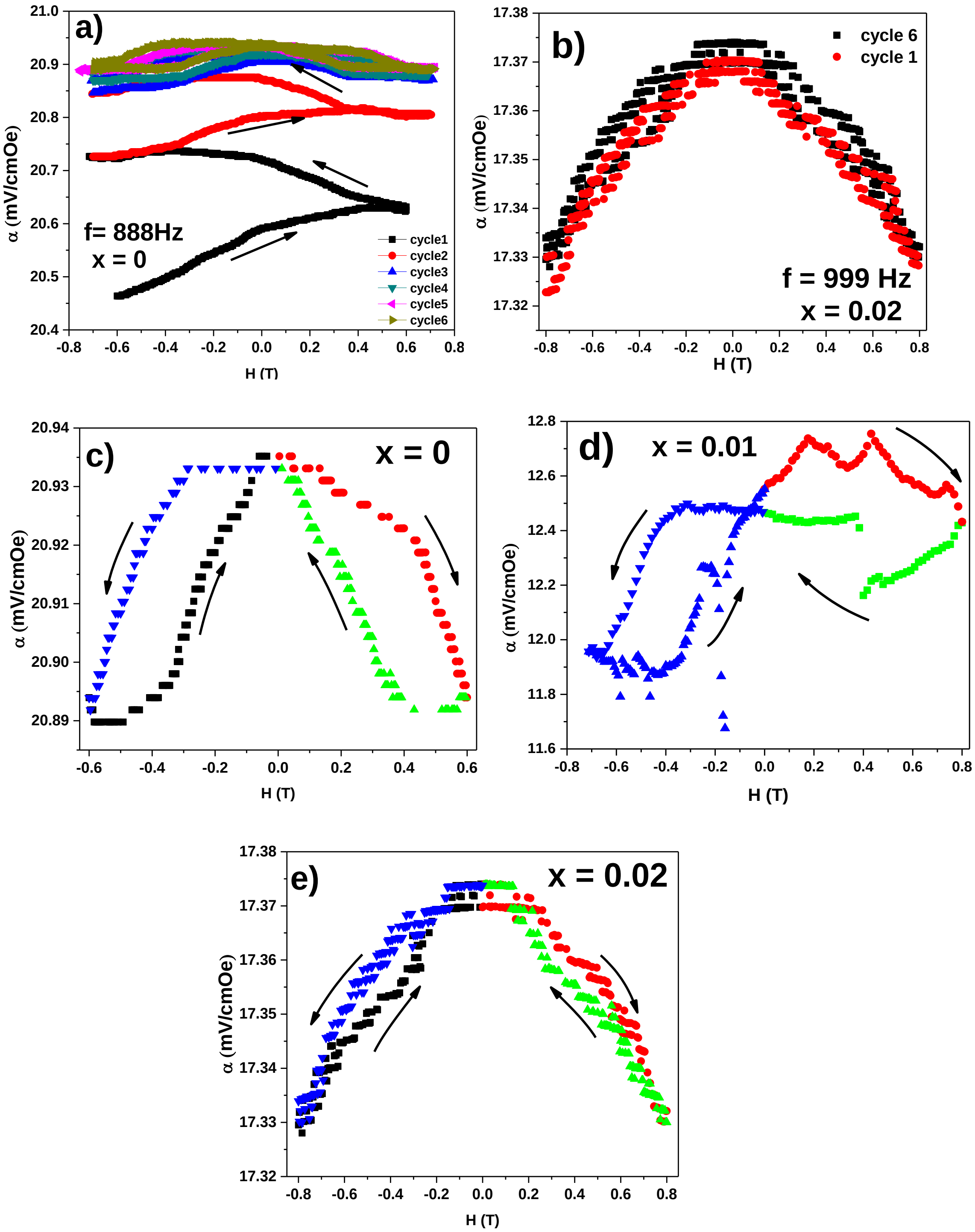

Fig. 5.2. Variation of linear magnetoelectric coupling coefficient ‘α’ with magnetic field for (a) x =0 for six continuous cycles at 888Hz (b) x =0.02 for first & sixth cycle at 999 Hz (c) 6th cycle of x = 0 at 888Hz (d) 6thcycle of x = 0.01 and (e) 6thcycle of x = 0.02 at 999 Hz.

The DC bias magnetic field dependence of α for x = 0, x = 0.01 and x = 0.02 are measured at AC frequencies of 888 and 999 Hz respectively. In case of x = 0, initial measurement of 'α' for one complete magnetic cycle did not result closed loops, see fig. 5.2 (a), hence we proceeded for more cycles until the loop is closed. It is only in sixth cycle when the loop is closed. During these six cycles, the magnitude of 'α' kept on increasing with every cycle. A similar behaviour has been observed for the magnetization as a function of DC bias voltage in epitaxially grown FeRh over $BaTiO_3$ crystals, where the authors consider two factors to be responsible for such asymmetric behaviour: (1) mismatch in magnetic and electrostatic ordering length scale (2) structural strain[29].

The BFO is known to be structurally strained which is also responsible for the multiferroicity in it. Considering the bismuth to be at the corner positions, any asymmetry in Fe-O bonding will reflect the strain in the lattice. From the refinement of neutron diffraction data of BFO, we found that the bonding of Fe^{3+} to six O^{2-} is via two bond lengths (see inset of fig 5.4) viz., $[Fe–O]_I$ ~1.9 and $[Fe–O]_{II}$ ~ 2.1 Å, which otherwise should have been only one value ~2.0 Å for an ideal symmetric perovskite structure. Because of the difference in two Fe–O bond lengths, the net negative charge of six O^{2-} ions in the octahedra do not coincide with the positive charge of Fe^{3+}, resulting in a non-zero dipole moment. Hence the asymmetricity in the lattice is reflected in the difference between the two Fe–O bonds, $\Delta Fe–O = [Fe–O_{II}] – [Fe–O_I]$. A plot of ΔFe–O for BFO and BFCO2 for various temperatures are shown in fig 5.3. From the plot, it is evident that the Co^{3+} doping in BFO leads to decrease in ΔFe–O, thereby homogenizing the Fe – O bonds in the octahedral. Hence a more symmetric α vs. H plot is expected for BFCO1 and BFCO2.

Similar to BFO, measurement on BFCO1 also did not result a closed loop in the first cycle itself. After several cycles the loop got closed, but still the loop is asymmetric for the positive and negative cycle of magnetic field. The plot of α as a function of magnetic field for BFCO2 is shown in fig. 5.2(b). Here a closed loop is obtained in the first cycle itself and not much shift is observed in consequent cycles. To avoid complexity due to overlapping of data of various cycles, only first and sixth cycles are shown.

For comparison, the magnetic field dependence of 'α' (of 6th cycle) for BFO, BFCO1 and BFCO2 are shown in figure 5.2 (c), (d) & (e). The behaviour of BFO sample exhibits hysteresis for the increasing and decreasing H in both positive and negative field directions, with maximum $\alpha = 20.935$ at $H = 0$. This behaviour is reminiscent to the earlier reports[28]; with the exception in the shape of the loop, which is not butterfly in the present case. In the case of BFCO1, though the hysteresis behaviour is almost similar to BFO in the negative cycle, but it is not found to be symmetric. Here, the maximum value of α decreases in comparison to BFO with 40% drop and the value is obtained as $\alpha = 12.465$ at $H = 0$. In BFCO2, the hysteresis behaviour is suppressed by large and almost linear behaviour of α with the magnetic field, is observed. A 17 % decrease in α ($H = 0$) to $\alpha = 17.375$ for BFCO2 sample is observed. The decrease of α is an indication of lattice stiffening (opposite to lattice softening which leads to increase in α [30]) for cobalt doped BFO. This is further supported by the fact that the measurement frequency has shifted from 888Hz to 999Hz, and blue-shift of resonance frequency, on doping BFO with cobalt.

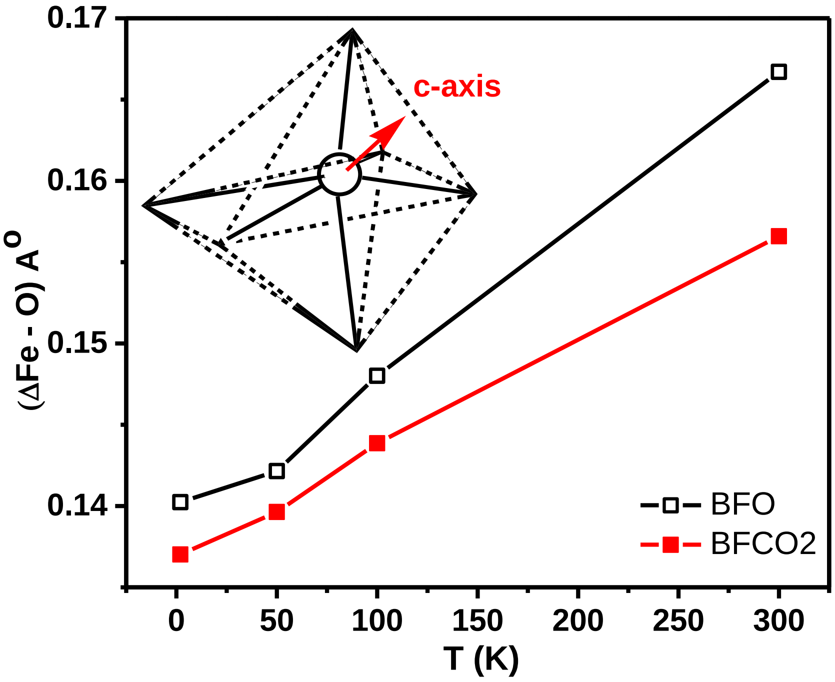

Fig. 5.3. Plot of ΔFe–O = [Fe–O_{II}] – [Fe–O_I] as a function of temperature for BFO (open symbol) and BFCO2 (solid symbol). The line is just a guide to eye. The inset shows schematic of shifting of the central metal ion (Fe/Co) along the $[001]_h$ direction (shown by arrow), producing two sets of asymmetric Fe–O bonds.

Another aspect of decrease in ΔFe–O is that cobalt doped BFO should be less polar in nature. Hence, to confirm this aspect, room temperature polarization vs. electric field (P – E) loop measurement is done for both BFO and the maximum Co substituted BFO (BFCO2) samples (shown in fig 5.4). The P – E plot of BFO sample shows a well-defined ferroic loop, signifying the ferroelectric nature of the sample. On the other hand, the same measurement on BFCO2 sample shows a nearly circular loop, indicating large leakage current and decrease in ferroelectricity of the sample. Surprisingly, the magnitude of the observed polarization even in BFO, is found too low compared to the expected theoretical value of 48.4 μC/cm^2 and 39.3 μC/cm^2 for BFO and BFCO2 respectively, obtained via simple ionic model expression[31],

$$P = \sum_i m_i r_i q_i / V \quad \text{---} \quad \text{(Eq. 5.3)}$$

Here m_i is the site multiplicity, r_i is the atomic position in the unit cell (obtained from the reitveld refinement of neutron data) and q_i is the nominal charge of the ith atom and the sum runs over all the atom of the unit cell. The low magnitude of the polarization may be due to the nanoparticles. Coincidently the decrease in theoretical value by 19% (from 48.4 to 39.3 μC/cm^2) is very close to the decrease in α (by 17%), which is the implication of a close correlation of magnetoelectricity to the lattice strain and important role played by the latter. Values of ‘P’ smaller than theoretical value have been obtained by other workers as well. It is a general belief that lower values of polarization are associated with poor quality of the sample. However, this belief may not be applicable to the present case as it is very clear from the neutron diffraction data that the sample is in phase pure form. Some contribution from the speromagnetic[32] grain boundaries may be expected as it constitutes a good fraction of the total volume owing to the nano-nature of the sample. This possibility seems more plausible, as it may be seen from the P-E loop, that the polarization has not reached its saturation. In a theoretical approach by Ravindran et. al.[25], they found that in BFO, the natural direction of polarization is $[001]_h$ or $[111]_c$ and large polarization is observed only if the sample is polarized along $[001]_h$ direction. If the polarization direction is not $[001]_h$, smaller values of polarization are possible.

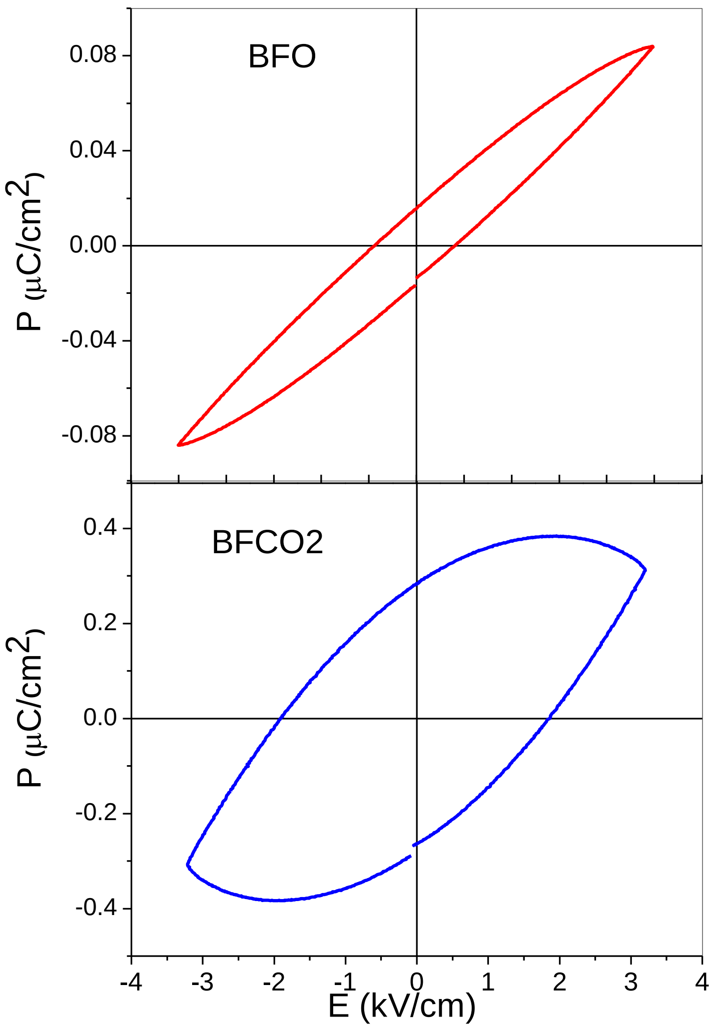

Fig. 5.4. Polarization vs. Electric field, P – E, hysteresis loop of BFO (top) and BFCO2 (bottom) at room temperature.

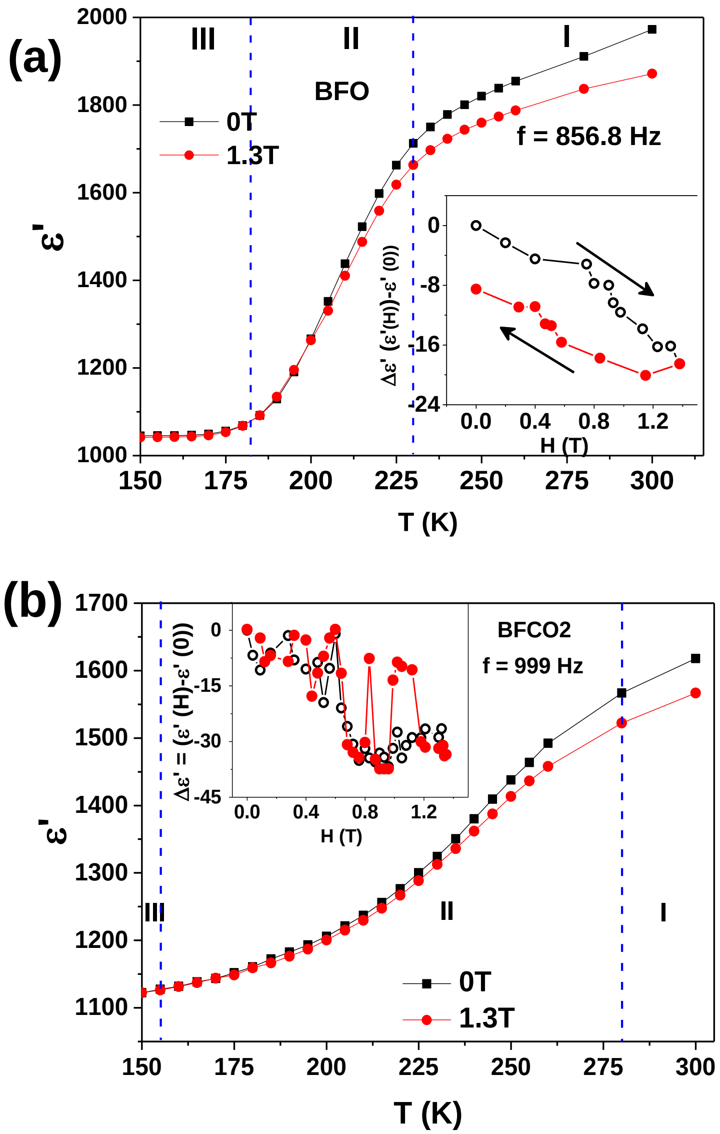

Fig. 5.5. Temperature dependence of dielectric permittivity measured at zero field and 1.3T for (a) BFO and (b) BFCO2 at frequencies f = 857Hz and 999Hz respectively. Inset shows the magnetic field variation of $\Delta\varepsilon'$ for the same. The hollow and solid symbols of the inset stand for the increasing and decreasing magnetic field. The lines are only guide to eyes.

As the magnetoelectric coupling is well reflected in magnetodielectricity[33, 34], temperature dependence (300 K to 150K) of the real part of dielectric permittivity (ε') measurement at zero and 1.3T magnetic field is carried out and is shown in fig 5.5 (a) and (b). For keeping a better correlation of magnetodielectric (MD) to magnetoelectric, the frequency of dielectric measurement is kept close to that of magnetoelectric measurement.

From the behaviour of ε', the plot may be divided into three regions: I, II and III. For BFO, region III is T < 180K, region I is T > 230K and region II is 180 < T < 230K. For BFCO2, the region II has broadened (170 – 280K) and the other two regions are beyond the temperature window. An increase in the width of region II reflects an increase in dielectric disorder or distribution of relaxation times[35]. The substitution induced dielectric disorder has been observed in many materials which many a times are ascribed to the formation of nano-polar regions whose dielectric relaxation differs from the rest of host[36]. But here the most interesting point to be noted is the amount of substitution which is only 2%, which is sufficient to disturb electrostatic long range ordering and increasing the non-cooperative relaxations. The room temperature dielectric for BFO is found to be $\varepsilon'(0) = 1972$ and decreases to $\varepsilon'(0) = 1618$ in BFCO2. Due to cobalt substitution, a 18% decrease in $\varepsilon'(0)$ is observed, which is in agreement with the drop in magnetoelectric coefficient α (17%) and polarization P (19%), and hence confirms their intrinsic origin.

On applying the magnetic field, ε' decreases and a clear bifurcation in the dielectric response is seen. At room temperature (region I), bifurcation in $\varepsilon'(0)$ and $\varepsilon'(H)$ leads to ~ 5% MD and this difference gradually reduce for lower temperature and becomes zero in the region III. A similar behaviour is observed in BFCO2, except slightly lower value of room temperature MD ~ 3.2%. This decrease in magnetodielectricity might be due to the lattice stiffening discussed earlier. In order to check the reproducibility of data, another batch of samples of same compositions is prepared and the magnetic field dependence of dielectricity is measured on them (see the inset of fig. 5.5). The magnetic field dependence of $\Delta\varepsilon' = (\varepsilon'(H) - \varepsilon'(0))$ for increasing and decreasing cycle of magnetic field is shown in the inset of fig. 5.5. For BFO, the $\Delta\varepsilon'$ decreases on increasing the magnetic field, but the path is not retraced back while decreasing magnetic field, so that a clear hysteresis is seen. Similar measurement on BFCO2, also results a decrease in $\Delta\varepsilon'$ with increasing magnetic field, but this time no hysteresis is seen. A significant hysteresis in BFO and the disappearance of hysteresis in BFCO2 is in agreement with magnetoelectric coefficient α dependence on the magnetic field, discussed earlier.

As any device based application of BFO and its derivative, requires a beforehand knowledge of its electrical conduction, the two samples are subjected to investigation of electrical conduction. The behaviour of DC resistivity ‘ρ’ with respect to temperature is shown in fig. 5.6. As the temperature is lowered, the resistivity first rises slowly and near T ~ 225K, it rises steeply till T ~ 150K and then shows saturation. One remarkable feature seen in the resistivity data is broad maxima near T ~ 170K for BFO and it is ascribed to the signature of pyroelectric effect[37] whereas this maxima is absent for BFCO2. The saturation at low temperatures is attributed to spin dependent scattering mechanism[38]. Hence, the region before saturation (T > 170K) is the best part to investigate for the conduction mechanism. This region is found to obey the polaronic Mott variable range hopping (VRH) conduction model[39],

$$\rho(T) = \rho_0 \exp\left(T_M / T\right)^{1/4} \text{ -------------------------------------- (Eq. 5.4)}$$

where T_M is the parameter called Mott temperature. The linearity of $\ln \rho(T)$ vs. $T^{-1/4}$ plot (inset of figure 5.6) shows a good fit of the experimental data to Mott VRH. From the fitting we obtained $T_M = (473)^4 K \,\&\, (376)^4 K$ corresponding to BFO & BFCO2 respectively. The hopping range of polarons (R) under VRH mechanism is[40, 41]

$$R = \xi^{1/4} / 8\pi k_\beta N(E_F) T^{1/4} \text{ --------------------------------- (Eq. 5.5)}$$

where ξ and $N(E_F)$ are the decay length of localized wave function and the localized density of states at the Fermi level respectively. Here the average distance between neighbouring Fe-Fe and/ or Fe-Co ions is considered as the decay length.

Using the relation, $T_M = 24/\left[\pi k_\beta N(E_F) \xi^3\right]$---------------------- (Eq. 5.6)

We obtained $N(E_F) = 2.842 \times 10^{16} \mathrm{eV}^{-1}\mathrm{cm}^{-3}$ for BFO and $7.115 \times 10^{16} \mathrm{eV}^{-1}\mathrm{cm}^{-3}$ for BFCO2 respectively. So, the value of R so obtained using eq. 5.5 is $50.038/T^{0.25}$ for BFO and $40.058/T^{0.25}$ for BFCO2 in the temperature range obeying Mott VRH (shown by the solid line in the inset of fig. 5.6). A more homogeneous Fe-O bond lengths in $BiFe_{0.98}Co_{0.02}O_3$ offers symmetric hopping, thereby increases the hoping probability and thus leading to a smaller hopping range. Thus a decrease in the hopping range, on cobalt doping, explains the more conducting nature of BFCO2 compared to BFO. From the inset of fig. 5.6, it may be noticed that, the temperature range, obeying Mott VRH (eq. 5.4) decreases for BFCO2, compared to BFO. This is an indication of weakening of polaron based VRH, on doping BFO with cobalt. Homogenization of bonds results less lattice distortion and hence decreases the polaron strength in BFCO2.

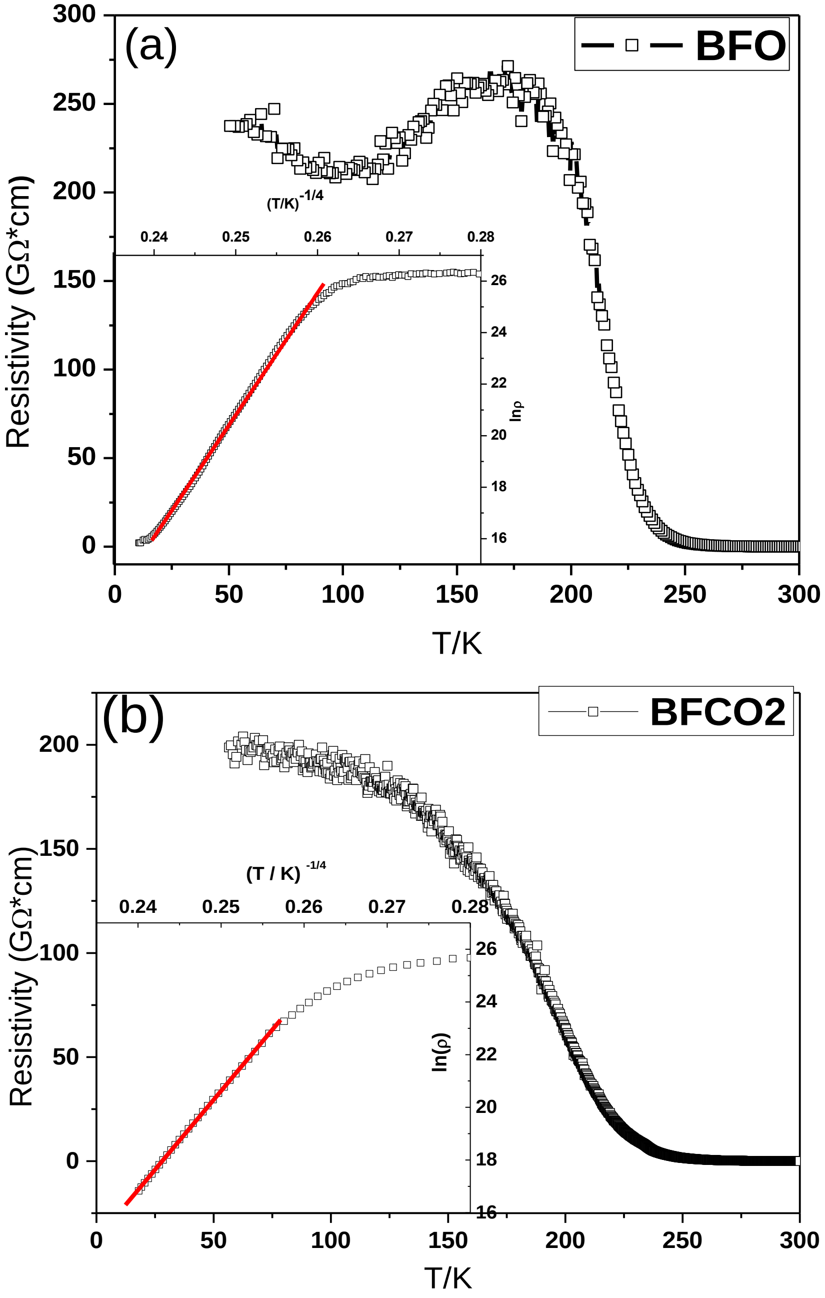

Fig. 5.6. Temperature dependence of resistivity for (a) BFO and (b) BFCO2. The inset shows the plot of $\ln\rho$ vs. $1/T^{1/4}$. The solid line in the inset is the linear fit in the temperature range obeying Mott VRH hopping model.

5.3 Conclusions

Effect of cobalt substitution on the magnetoelectricity of bismuth ferrite is investigated. Hysteresis behaviour is seen in the magnetic field variation of the magnetoelectric coefficient (α) for $BiFeO_3$. The hysteresis is not affected much in BFCO1 and only the magnitude decreases by 40% in comparison to BFO. To see the best effect of Co substitution, the highest concentration of cobalt is analysed further. This hysteresis behaviour becomes linear for$BiFe_{0.98}Co_{0.02}O_3$ with 17% drop in the magnitude of α. In spite of a 17% drop, magnitude of α is sufficient enough for device applications, especially where α must follow the applied magnetic field linearly, e.g., transistors, transducers, etc. Frequency dependence of α indicates lattice stiffening due to cobalt substitution. This is supported by neutron diffraction analysis, which also explains the drop in electric polarization observed in P – E measurement. Temperature dependence of dielectric measurement shows 18% drop in dielectric constant for $BiFe_{0.98}Co_{0.02}O_3$. On application of 1.3 Tesla magnetic field, 5% and 3.2% magnetodielectricity at room temperature is seen for $BiFeO_3$ and $BiFe_{0.98}Co_{0.02}O_3$ respectively. Maximum magnetodielectricity near room temperature and the value decreases with lowering of temperature and becomes zero in the region III. Similar to magnetoelectric behaviour, the magnetodielectric dependence on magnetic field also shows hysteresis for BFO and no hysteresis for BFCO2, for increasing and decreasing magnetic field. This shows a close correlation of magnetoelectricity to magnetodielectricity. Low temperature DC conductivity measurements on the two samples suggest Mott's variable range hopping between the $Fe^{3+}$to be the conduction mechanism. The calculated average hopping range also is in agreement with the increase in conductivity of $BiFeO_3$ on cobalt doping.

References

1. R. Ramesh and N. Spaldin, *Nature Mater.*, **6** 21 (2007)
2. G. A. Smolenskii, I. E. Chupis *Soviet Physics – Uspekhi*, **25** 475 (1982)
3. H. Schmid, *Ferroelectrics*, **162** 19 (1994)
4. T. Kimura, T. Goto, H. Shintani, K. Ishizaka, T. Arima nad Y. Tokura, *Nature*, **426** 55 (2003)
5. M. Fiebig, *J. Phys. D*, **38** R123 (2005)
6. W. Eerenstein, N. D. Mathur, and J. F. Scott, *Nature*, **442** 759 (2006)
7. C. W. Nan, M. I. Bichurin, S. Dong, D. Viehland, and G. Srinivasan, *J. Appl. Phys.*, **103** 031101 (2008)
8. S. Y. Yang, L. W. Martin, S. J. Byrnes, T. E. Conry, S. R. Basu, D. Paran, L. Reichertz, J. Ihlefeld, C. Adamo, A. Melville, Y.-H. Chu, C.-H. Yang, J. L. Musfeldt, D. G. Schlom, J. W. Ager III, and R. Ramesh,Appl. Phys. Lett., **95** 062909 (2009)
9. G. Catalan and J. F. Scott, *Adv. Mater. Weinheim, Ger.*, **21** 2463 (2009)
10. C. Elderer and N. A. Spladin, *Phys. Rev. B*, **71** 060401 (2005)
11. Yu. F. Popov, A. K. Zvezdin, G. P. Vorob'ev, A. M. Kadomtseva, V. A. Murashev, and D. N. Rakov, *JETP Lett.*, **57** 69 (1993)
12. S. C. Yang, A. Kumar, V. Petkov, and S. Priya, *J. Appl. Phys.* **113** 144101 (2013)
13. A Singh, A. Senyshyn, H. Fuess, T. Chatterji and D. Pandey, *Phys. Rev. B*, **83** 054406 (2011)
14. A Singh, V. Pandey, R. K. Kotnala and D. Pandey, *Phys. Rev. Lett.*, **101** 247602 (2008)
15. F.Yan, G. Chen, L. Lu, P. Finkel and J. E. Spanier, *Appl. Phys. Lett.*, **103** 042906 (2013)
16. W. M. Zhu, H. Y. Guo and Z. G. Ye, *Phys. Rev. B*, **78** 014401 (2008)
17. Q. Q. Wang, Z. Wang, X. Q. Liu and X. M. Chen, *J. Am. Ceram. Soc.*, **95** 670 (2012)
18. S. R. Das, R. N. P. Choudhary, P. Bhattacharya, and R. S. Katiyar, P. Dutta, A. Manivannan, and M. S. Seehra, *J. Appl. Phys.*, **101** 034104 (2007)
19. V. A. Khomchenko, D. A. Kiselev, I. K. Bdikin, V. V. Shvartsman, P. Borisov, W. Keeman, J. M. Vieira and A. L. Kholkin, *Appl. Phys. Lett.*, **93** 262905 (2008)
20. P. Uniyal, K. L. Yadav, *J. Phys.: Condens. Mater*, **21** 012205 (2009)

21. V. A. Khomchenko, D. A. Kiselev, J. M. Vieira, Li Jian, A. L. Kholkin, A. M. L. Lopes, Y. G. Pogorelov, J. P. Araujo, and M. Maglione, *J. Appl. Phys.*, **103** 024105 (2008)
22. V. R. Palkar, D. C. Kundaliya, and S. K. Malik, *J. Appl. Phys.*, **93** 4337 (2003)
23. F. Chang, N. Zhang, F. Yang, S. Wang and G. Song, *J. Phys. D: Appl. Phys.*, **40** 7799 (2007)
24. Y. K. Jun and S. H. Hong, *Solid State Commun.*, **144** 329 (2007)
25. P. Ravindran, R. Vidya, A. Kjekshus, H. Fjellvag, *Phys. Rev. B*, **74** 224412 (2006)
26. G. V. Duong, R. Groessinger, M. Schoenhart and D. Bueno-Basques, *J. Magn. Magn. Mater.*, **316** 390 (2007)
27. J. M. Caicedo, J. A. Zapata, M. E. Gomez, and P. Prieto, *J. Appl. Phys.*, **103** 07E306 (2008)
28. R. Grossinger, G. V. Duong, and R. Sato- Turtelli, *J. Magn. Magn. Matt.*, **320** 1972 (2008)
29. R.O. Cherifi, V. Ivanovskaya, L. C. Philips, A. Zobelli, I. C. Infante, E. Jacquet, V. Garcia, S. Fusil, P. R. Briddon, N. Guiblin, A. Mougin, A. A. Unal, F. Kronast, S. Valencia, B. Dkhil, A. Barthelemy and M. Bibes, *Nat. Mater.*, **13** 345 (2014)
30. J. C. Wojdet and J. Iniguez, *Phys. Rev. Lett.*, **105** 037208 (2010)
31. V. A. Khomchenko, D. V. Karpinsky, L. C. J. Pereira, A. L. Kholkin and J. A. Paixao, *J. Appl. Phys.*, **113** 214112 (2013)
32. S. Nakamura, S. Soeya, N. Ikeda, and M. Tanaka, *J. Appl. Phys.*, **74** 5652 (1993)
33. H. M. Jang, J. H. Park, S. Ryu and S. R. Shannigrahi, *Appl. Phys. Lett.*, **93** 252904 (2008)
34. S. N. Tripathy, K. K. Mishra, S. Sen, B. G. Mishra, D. K. Pradhan, R. Pallai and D. K. Pradhan, *J. Appl. Phys.*, **114** 144104 (2013)
35. N. Setter and L. Cross, *J. Appl. Phys.*, **51** 4356 (1980)
36. D. Viehland, X. H. Dai and Z. Xu, *J. Appl. Phys.*, **84** 458 (1998)
37. R. Jarrier, X. Marti, J. Herrero-Albillos, P. Ferrer, R. Haumont, P. Gemeiner, G. Geneste, P. Berthet, T. Schulli, P. Cevc, R. Blinc, S. S. Wong, Tae-Jin Park, M. Alxe, M. A. Carpenter, J. F. Scott, G. Catalan, and B. Dkhil *Phys. Rev. B*, **85** 184104 (2012)

38. Q. He, C. –H. Yeh, J. –C. Yang, G. Singh-Bhalla, C. –W. Liang, P. –W. Chiu, G. Catalan, L.W. Martin, Y. –H. Chu, J. F. Scott and R. Ramesh, *Phys. Rev. Lett.*, **108** 067203 (2012)
39. N. F. Mott *J. Non-Cryst. Solids*, **1** 1 (1968)
40. A. Karmakar, S. Majumdar and S. Giri, *Phys. Rev. B*,**79** 094406 (2009)
41. S. Deshpane, S. N. Achary, R. Mani, J. Gopalakrishnan and A. K. Tyagi, *Phys. Rev. B*, **84** 064301 (2011)

Chapter 6

Low and high temperature Dielectric and Magnetodielectric study on $BiFe_{1-x}Co_xO_3$: x = 0, 0.01, 0.02

In this chapter, dielectric and magnetodielectric measurements on $BiFe_{1-x}Co_xO_3$: x = 0, 0.01 & 0.02 in the temperature range 70 – 300K and up to magnetic field 1.3T are discussed. The dielectric data are well described by Haverliak – Negami (HN) expression plus an additional term for the Maxwell Wagner (MW) type relaxations, whose contribution is dominant near room temperature. The dielectric relaxations found to be obeyed by polaronic variable range hopping model. The magnetodielectric measurement is also carried out for all the three samples. The effect of Co substitution on $BiFeO_3$ above room temperature is also studied. A signature of relaxor type behavior is observed in $BiFe_{0.98}Co_{0.02}O_3$ above the room temperature.

6.1 Introduction

Multiferroic $BiFeO_3$ (BFO) captivates the scientific community till date for its underlying physics as well as for potential applications. BFO offers a number of device applications which includes spintronics, sensors, actuators and tunable microwave filters, spin valves, data storage, etc.[1-6]. Physical phenomena such as ferroelectricity, spiral magnetic ordering[7], multiple magnetic transitions[8], magnetodielectricity (MD)[9] and magnetoelectric coupling[10] are some of the interesting features associated with this compound. The MD is one of the upcoming trends of investigation, which has drawn attention of various research groups.

Other than BFO, the MD effect has been observed in various oxides such as in CuO [11], spin spiral system, e.g. $TbMnO_3$[3], colossal magnetodielectricity in double perovskites e.g. La_2NiMnO_6[12], La_2CoMnO_6[13] and Bi based oxides e.g. $LaBiMn_{4/3}Co_{2/3}O_6$[14]. However, in BFO, strong ferroelectricity originates from the stereochemistry of $6s^2$ lone pair of Bi, whereas the magnetism arises due to B-site Fe^{3+} ion. This makes the material different from others and at the same time, offers to study its various aspects via substitution at Bi-site as well as Fe-site [15--21].

Due to possession of dual ordering parameters (electric at 1140K and magnetic at 643K [22]) and a strong coupling between them, a variety of magnetic-electric transitions have been witnessed at temperatures much below the ordering temperatures. From the Raman scattering and dielectric measurements on single crystal and polycrystalline BFO, phase transitions at 50K, 140K, 200K and 230K have been inferred [8, 23, and 24]. These phase transitions have also been observed as the dielectric anomalies and are inferred as: 50 K, (magnetic, but glassy and with magnetoelectric coupling), 140 K (dominantly magnetic), 200 K (magnetoelastic with small coupling to polarization) and 230 K (magnetic; glassy and also weakly coupled to polarization) [8]. In reduced dimensions, for instance thin film, “one magnon” scattering is observed at 90K and also a kink in magnon intensity at 150 K and a strong anomaly near 210 K as a representation of spin reorientation transition [25]. For samples prepared under vacuum annealed condition, additional two dielectric anomalies has been reported at 25 and 281K. The anomaly at 25K has been found to be due to structural distortion, which affects charge, spin, and structural degrees of freedom and that at 281K is due to the antiferromagnetic to spin glass transition [26]. For A-site substituted BFO via Ca, two dielectric anomalies at 66K and 260K are observed. The anomaly at 66K exhibits relaxor like ferroelectric properties involving strongly interacting relaxing clusters and the anomaly at 260K is ascribed as Maxwell Wagner (MW) effect [27]. Indications of dominant MW and magnetoresistance effects have also been observed in the magnetodielectric data of BFO ceramics [9, 28 and 29].

In general, the dielectric relaxations in a material may be ascribed to two contributions: (i) intrinsic (ii) extrinsic. The intrinsic contribution as the name suggests, is an inherent contribution and results from the off-centering of positive and negative ions in a crystal. This contribution leads to permanent dipole moment and is very essential for data storage applications. Contributions other than intrinsic are termed extrinsic and they originate from various factors such as finite conductivity, defect dipoles, accumulation of charge carriers, interfaces between electrode and sample, grain boundaries in crystalline materials, twin boundaries in single crystals [30-32] etc. Though these extrinsic contributions do not find much of technological applications, but their study is highly desirable in order to separate out the intrinsic contribution from the rest. In the event of several above mentioned dielectric transitions in BFO, it becomes very essential to understand the nature of these, so that appropriate technological applications may be materialized.

Now a days, Relaxor ferroelectrics have gained a lot of attention as they are widely used in multilayer capacitors, microelectronic components, etc. They possess certain peculiar characteristics such as a) diffuse phase transition b) temperature dependent strong frequency dispersion, c) the maximum dielectric peak temperature must follow Vogel-Fulcher relaxation[33,34], d) microscopic compositional fluctuations, e) coupling of electric and magnetic order parameters, f) merging of micro/nanopolar region into molecular region[35]. In the vicinity of the diffuse dielectric anomaly the relaxor material shows superparaelectric behavior and these superparaelectric clusters freezes at the nanopolar region at so called freezing temperature (T_f)[34].

Here we have focused our attention on low temperature dielectric and magnetodielectric response of BFO as well as its Co substituted compounds. Moreover the dilute substitution of Co in $BiFeO_3$ may act as nanometer scale chemical defects which may be the source of random electric fields and controls the dynamics of the polar clusters[34]. So, the effect of cobalt substitution on the dielectric properties is studied in the low temperature as well in the high temperature range.

6.2 Low temperature dielectric and magnetodielectric study

The frequency dependent dielectric measurements are carried out for all the three samples, i.e. $BiFeO_3$ (BFO), $BiFe_{0.99}Co_{0.01}O_3$ (BFCO1) and $BiFe_{0.98}Co_{0.02}O_3$ (BFCO2) at various static low temperatures. The temperature dependent real and imaginary part (ε'& ε'') of permittivity are extracted from the frequency dependence of dielectric measurement at static temperatures. Fig. 6.1 (a) – (f) shows the temperature dependent real and imaginary parts (ε'& ε'') of permittivity for BFO, BFCO1 and BFCO2 at various frequencies. Fig. 6.1a displays the temperature dependence of real part of permittivity (ε') of BFO at selected frequencies. The ε' shows a step like transition from room temperature value ~ 1600 to intrinsic value ~ 500 at low temperatures. This transition is seen as peak in ε'' plot so that the maxima position coincides with the transition temperature. This maxima position moves to higher temperatures for elevated frequencies, thus hints at the involvement of the activation process in the relaxation. The low temperature dispersionless plateau region is called intrinsic region, whereas the high temperature plateau region (with some dispersion) is extrinsic region. A similar behavior is seen for BFCO1 and BFCO2, with an addition that the entire plot moves towards right (higher temperature) in the temperature window. For BFCO1 (fig 6.1c&d), the beginning of the extrinsic plateau region is just seen, whereas for BFCO2 (fig 6.1e&f) even the beginning is not seen properly and the transition can only be estimated from the peak in ε'' plot. An additional relaxation of unknown origin in the form of shoulder is seen for BFCO1 at ~180K (shows as black arrow in fig. 6.1c& d). This relaxation is also seen in BFCO2 but at a lower temperature (~140K) and weaker than former.

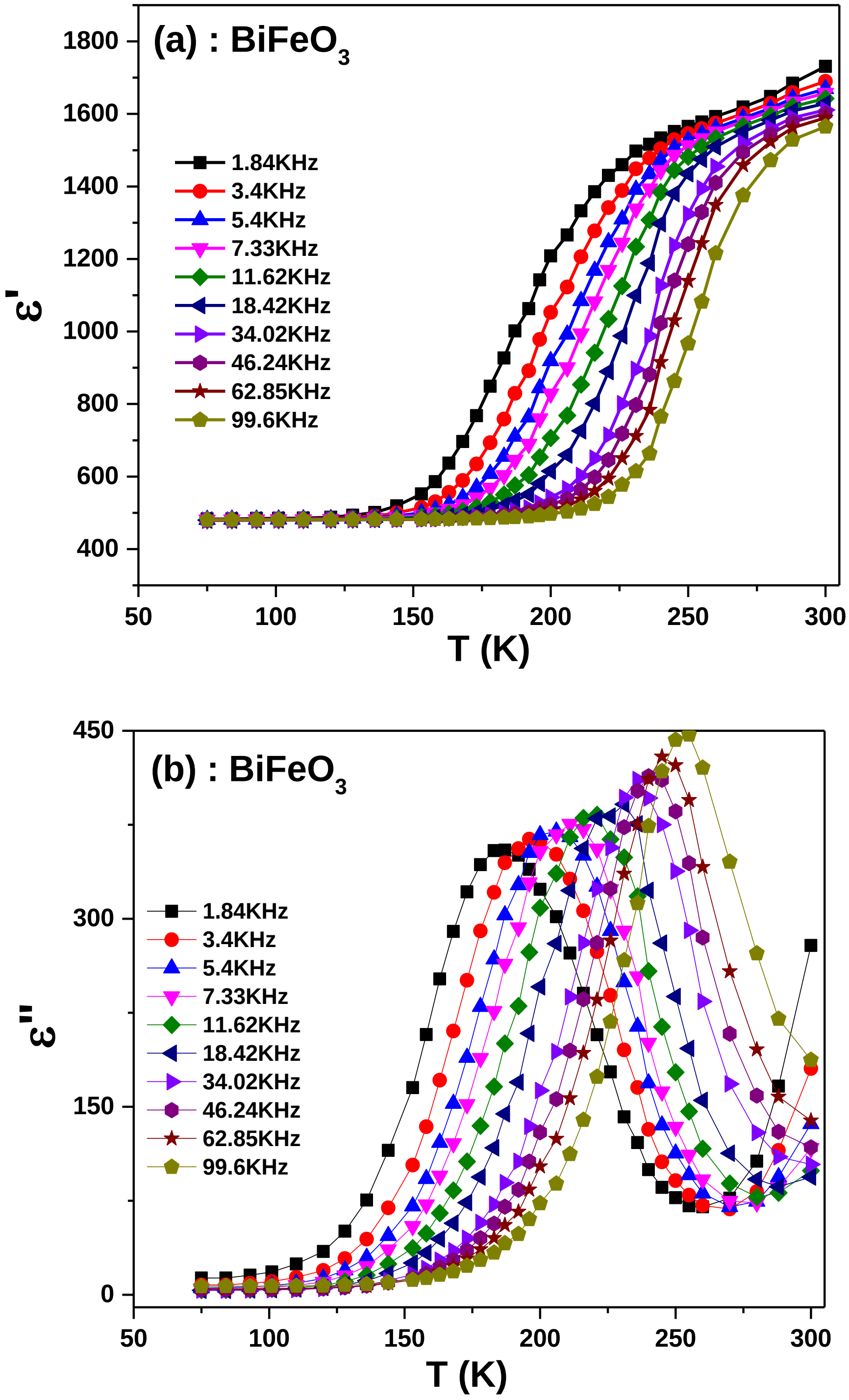

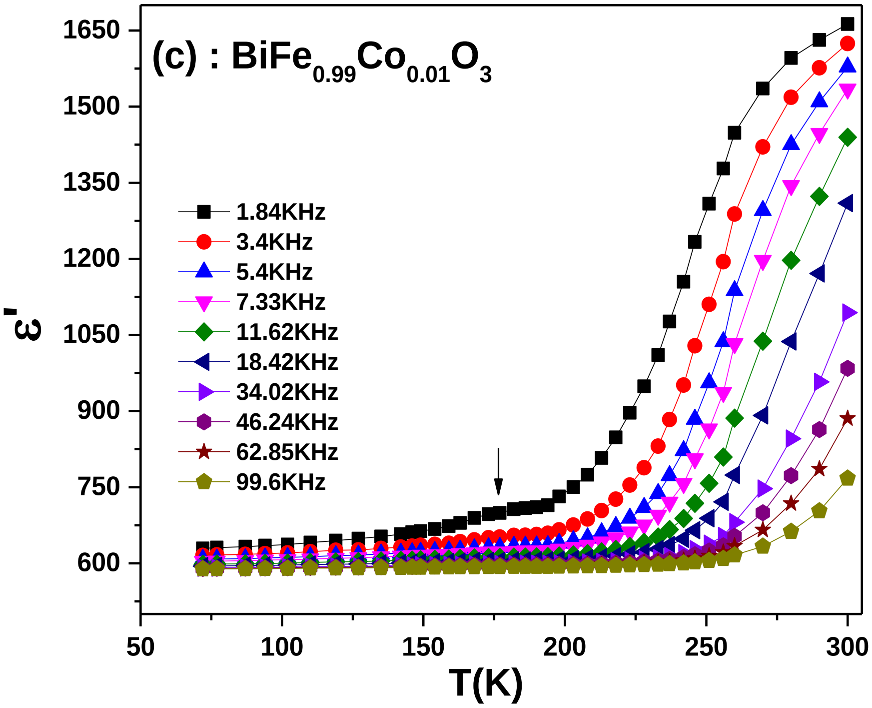
(c) : BiFe$_{0.99}$Co$_{0.01}$O$_3$
1650
1500
1350
1200
1050
900
750
600
ε'
1.84KHz
3.4KHz
5.4KHz
7.33KHz
11.62KHz
18.42KHz
34.02KHz
46.24KHz
62.85KHz
99.6KHz
50
100
150
200
250
300
T(K)

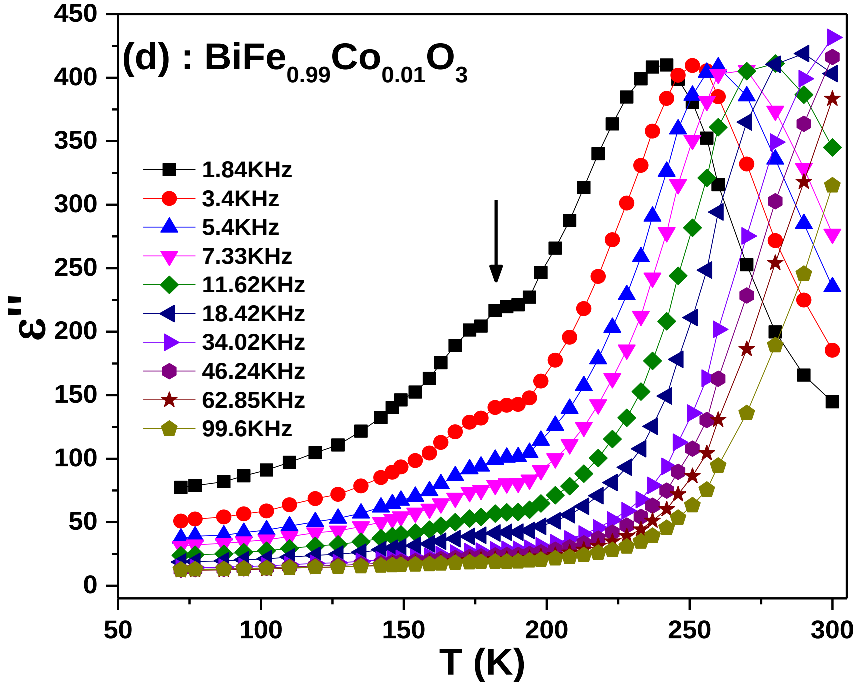
(d) : BiFe$_{0.99}$Co$_{0.01}$O$_3$
450
400
350
300
250
200
150
100
50
0
ε''
1.84KHz
3.4KHz
5.4KHz
7.33KHz
11.62KHz
18.42KHz
34.02KHz
46.24KHz
62.85KHz
99.6KHz
50
100
150
200
250
300
T (K)

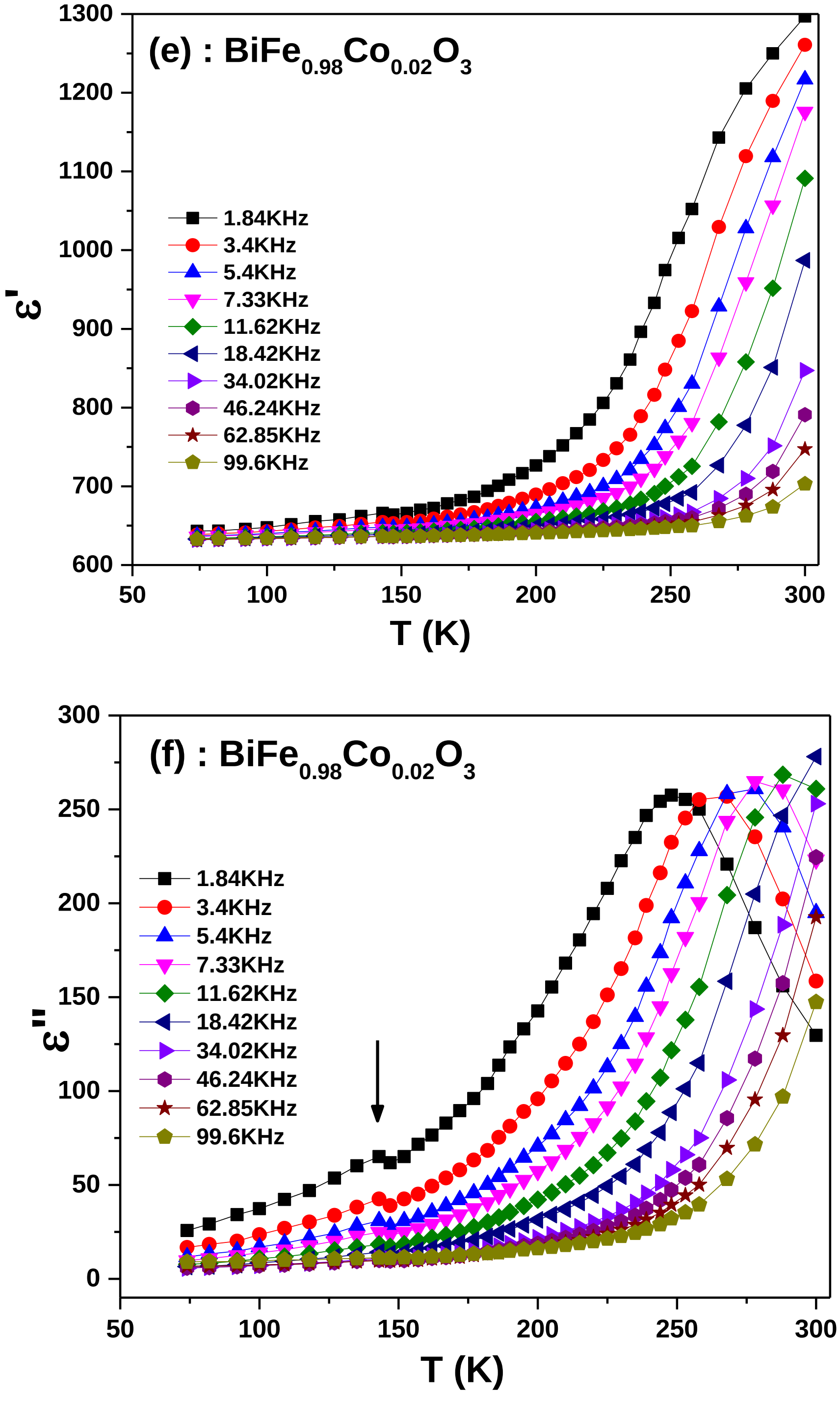

Fig. 6.1. Temperature dependent real part (ε') and imaginary part (ε'') of dielectric permittivity at several frequencies for BFO (a) & (b), BFCO1 (c) & (d), BFCO2 (e) & (f). The lines are only guide to eyes.

In order to get an insight into the step transition, the imaginary part of dielectric data (ε'') is plotted as Bode plot. The ε'' relaxation peak in the Bode plot is found to be asymmetrically broadened along with a rise at lower frequencies, thus hints at non-Debye type contribution of the form $(1/\omega)^n$ to dielectric permittivity. A widely used non-Debye contribution of similar nature to the dielectric permittivity found to dominate in many materials is the Maxwell Wagner (MW) type polarization and Warburg tunneling. For an intrinsic Debye type polarization, the Bode plot of ε'' is expected to display a symmetric peak at some non-zero ω and $\varepsilon'' \rightarrow 0$ as $\omega \rightarrow 0$, while in MW type polarization ε'' diverges at low frequencies[36]. Thus the data in fig. 6.2, is representation of mixed nature where the low frequency rise is due to extrinsic effect (such as MW) and the peak is due to Debye type relaxation. Initially the dielectric peak is not seen in the frequency window until the temperature is lowered below 260K (for BFO). On further lowering of temperature this peak position continues its shifting towards lower frequency (left side of the window) and for temperature below 145K (for BFO) it goes out of the frequency window from the left side. For BFCO1 and BFCO2, the respective temperature ranges of peak display in ε'' plot are 260 - 163K and 260K - 182K. In an event of finite contribution from non-Debye type relaxation to the dielectric, the data in Bode formalism are fitted to a generalized Haverliak-Negami (HN) relaxation expression. In addition to a HN relaxation a finite conductivity contribution of $(1/\omega)^n$ type is also found necessary while fitting. The expression of the equation used to fit the data is given in eq. 6.1 [37], where the first term represents the polar nature of relaxation (such as Debye) and the second term is due to the contribution from finite conductivity.

$$\varepsilon^*(\omega) - \varepsilon_\infty = \frac{(\varepsilon_s - \varepsilon_\infty)}{[1+(i\omega\tau)^\alpha]^\beta} - i\left[\frac{\sigma_{dc}}{(\varepsilon_0\omega)}\right]^n \text{-------------------------- (Eq. 6.1)}$$

where $\sigma_{dc} = 1/\rho$, $\omega = 2\pi f$ is the angular frequency and the exponent n lies between 0 and 1. $\varepsilon_0 - \varepsilon_\infty$ is the static dielectric constant of the relaxation present in the system and τ is the corresponding relaxation time. The parameter α and β are the broadness and asymmetry of the corresponding relaxation spectra. Values of α and β less than unity mark the deviation from Debye behavior.

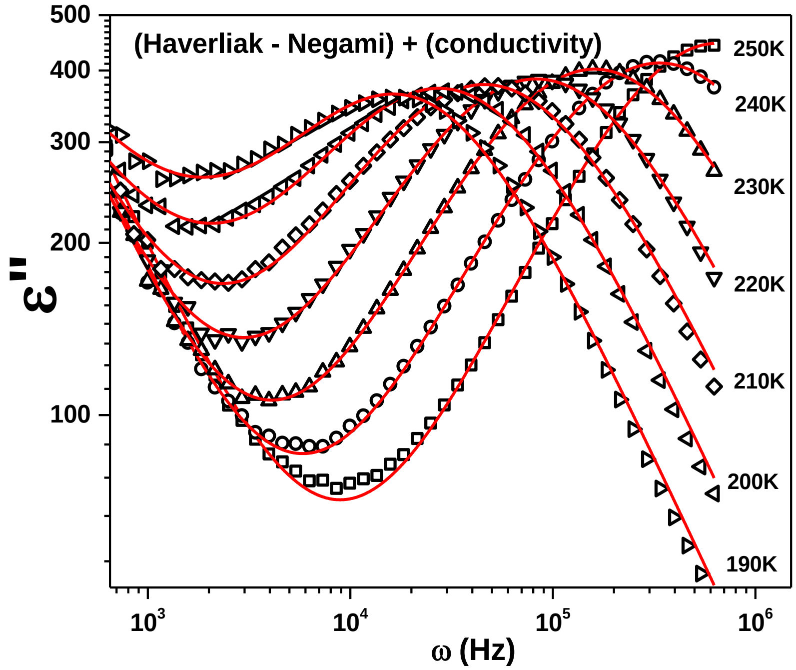

Fig. 6.2. Shows the variation of imaginary part of dielectric permittivity (ε'') vs. angular frequency fitted by Havriliak – Negami function along with contribution of conductivity at various temperatures of BFO.

The fitting of experimental data to eq. 6.1 is shown as solid line in fig. 6.2. The fitting is found to be very good and the fitting parameters so obtained for BFO, BFCO1 and BFCO2 respectively are shown in fig. 6.3, 6.4 & 6.5. For the entire temperature range, the parameter β is found to be constant at $\beta = 1$, hence not shown in the plot. To see the effect of magnetic field on the relaxation and conductivity properties, the measurements are repeated in the presence of 1.3T magnetic field and the parameters obtained in the similar fashion are shown as red solid data points in the plot (fig. 6.3, 6.4 & 6.5). Due to respective temperature ranges of peak display in ε'' for the three samples, the fitting parameters are obtained in those temperature ranges only.

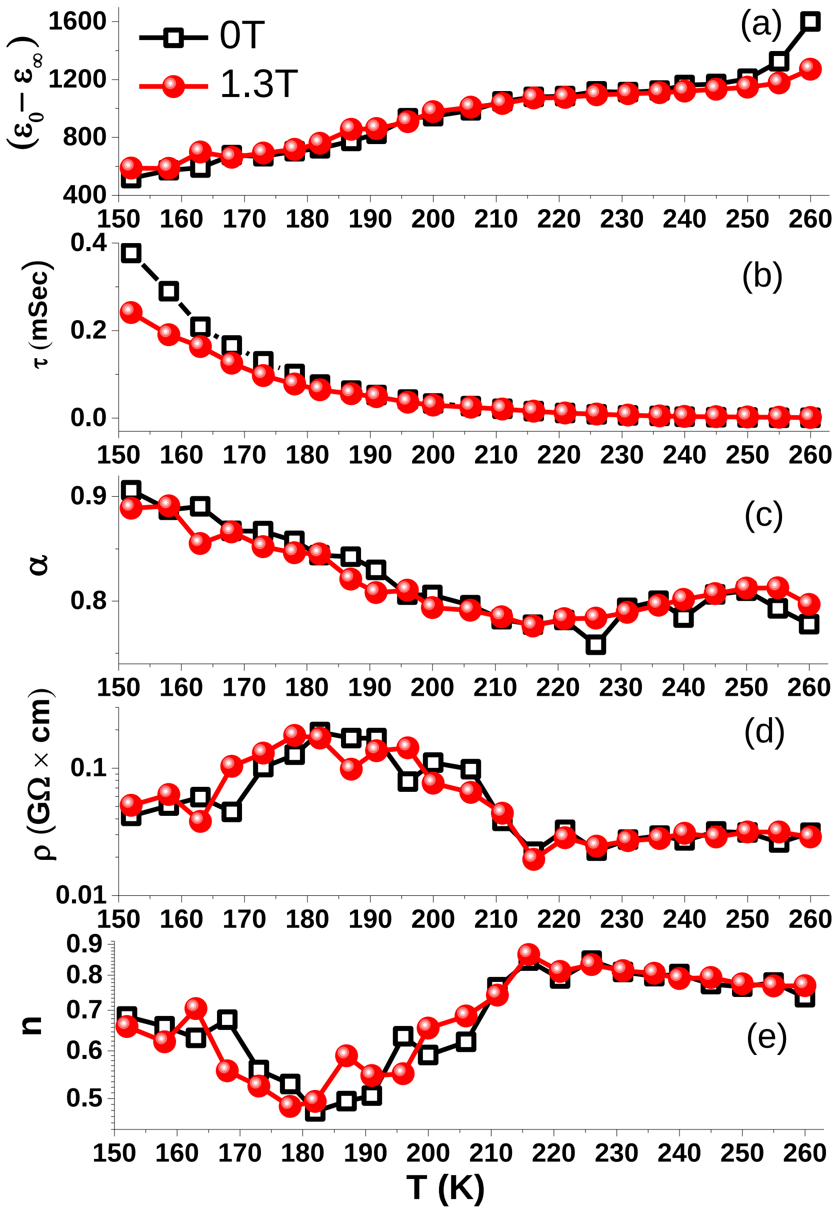

Fig. 6.3. The temperature dependence of parameters obtained from the fitting of ε'' via eq. 6.1, for BFO.

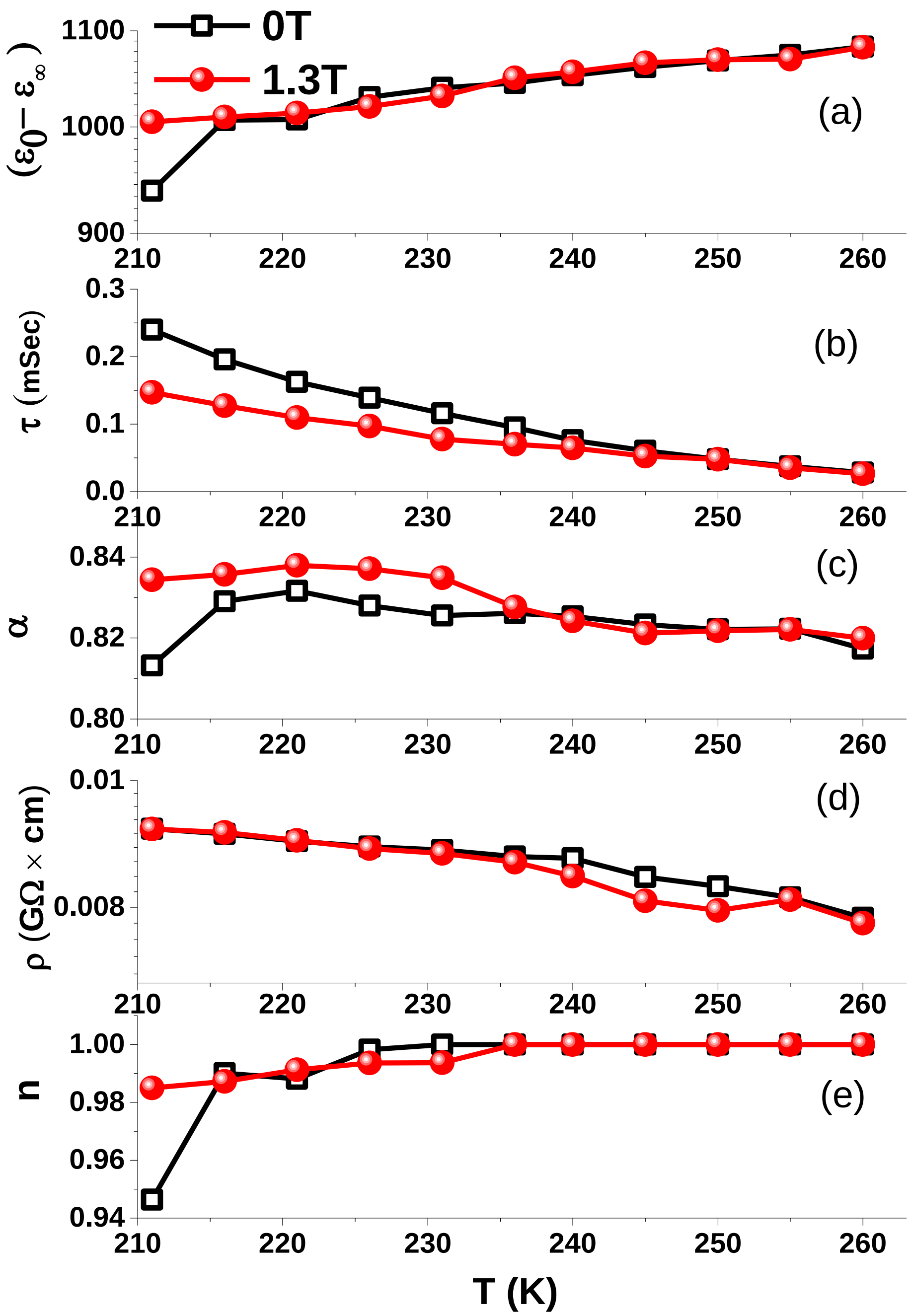

Fig 6.4. The temperature dependence of parameters obtained from the fitting of ε'' via eq. 6.1, for BFCO1.

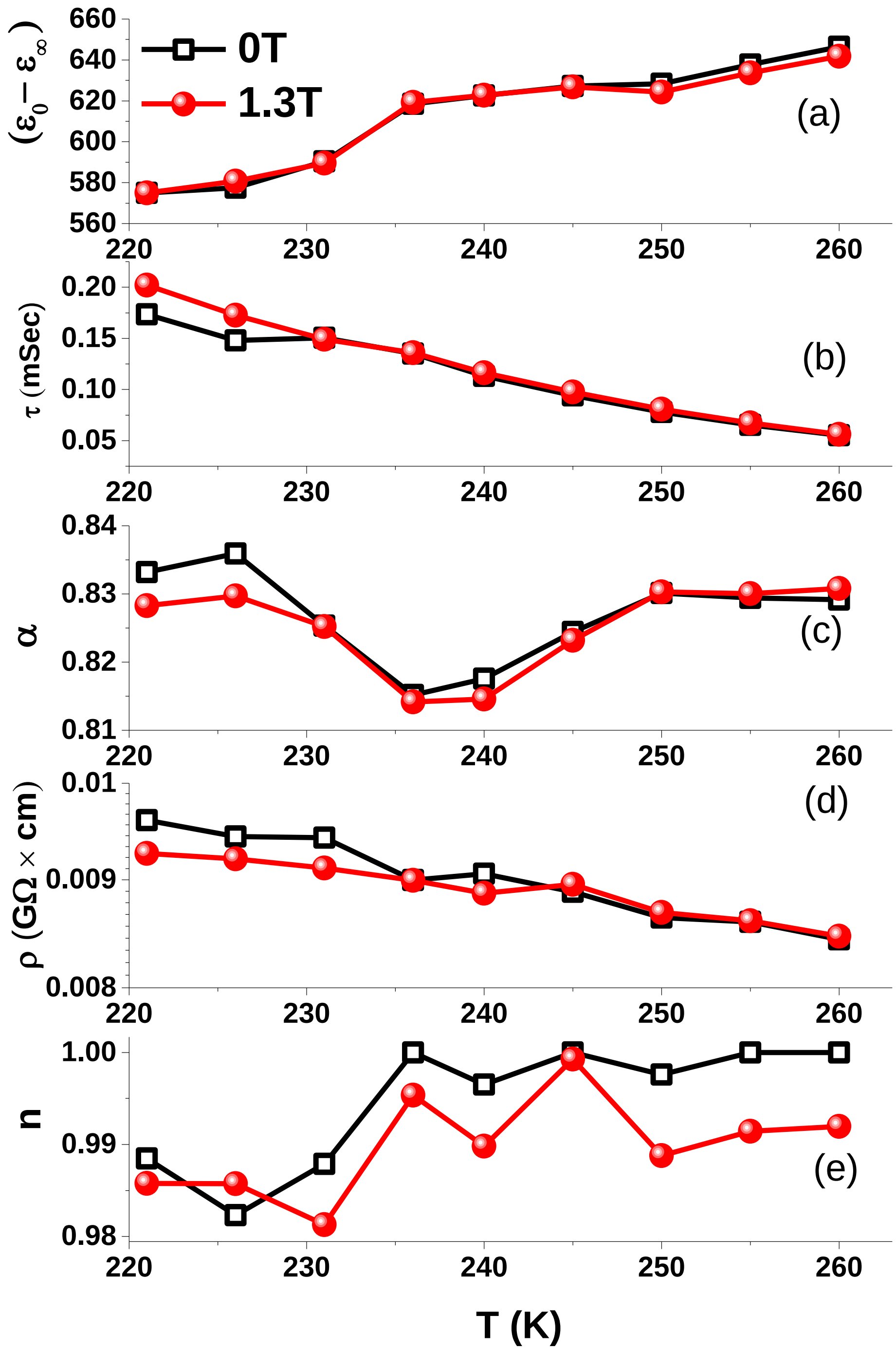

Fig 6.5. The temperature dependence of parameters obtained from the fitting of ε'' via eq. 6.1, for BFCO2.

Of the first term in eq. 6.1, let us start with the dielectric parameter $\varepsilon_0 - \varepsilon_\infty$ for BFO (fig. 6.3a), BFCO1 (fig. 6.4a) and BFCO2 (fig. 6.5a). On decreasing the temperature, $\varepsilon_0 - \varepsilon_\infty$ decreases monotonously and is in accordance with the earlier discussed variation of ε' with temperature. Application of 1.3T magnetic field marginally affects the low temperature data, but a considerable decrease is seen in the room temperature data, signifying the presence of a substantial amount of room temperature magnetodielectricity. The behavior for BFCO1 and BFCO2 are similar, except the absence of magnetodielectricity in the temperature window of fitting.

The relaxation time τ increases nonlinearly for lower temperatures along with growing bifurcation between the with- and without-field data (fig. 6.3b, 6.4b & 6.5b). The increase in relaxation time is the manifestation of slower dynamics of the relaxations as temperature decreases. Generally the magnetic field does not affect electric dipoles and only orients the magnetic moments along the direction of the magnetic field. The magnetic field induced lowering of relaxation times reflects the interdependence of the dielectric and the magnetic ordering parameters. The Co^{3+} substitution is found to increase the relaxation times: for instance at T = 220K, the respective zero field relaxation times for BFO, BFCO1 and BFCO2 are 0.012s, 0.16s and 0.2s. In an earlier report, the Co^{3+} substitution has been found to induce magnetic glassiness [38]. Thus the increase in dielectric relaxation times may be a direct consequence of the magneto-electric coupling in the system, such that slow dynamics of magnetic relaxation, leads to slower dielectric relaxation.

Fig. 6.3c, 6.4c & 6.5c shows the temperature dependence of asymmetry parameter α in 0T and 1.3T magnetic field. The room temperature value for all the samples is ~0.8 and for BFO this value increases towards unity (~0.9 at 150K). For BFCO1 and BFCO2 the respective room temperature values are ~0.82 and ~0.83 and remain unchanged with slight fluctuations, even on lowering of temperatures. The value of $\alpha \sim 0.8$, is a mark of deviation from ideal Debye type dielectric relaxations. For BFO, approach of α towards unity is an indication that the relaxation approaches towards the Debye type at lower temperatures, but for BFCO1 and BFCO2, no indication of Debye relaxation, at least in the temperature window of fit is seen. Moreover, the increase in the room temperature value α ~0.8 (BFO), ~0.82 (BFCO1) and ~0.83 (BFCO2) with Co^{3+} substitution shows, increasing participation of the non-Debye relaxations in the sample. The effect of magnetic field on this parameter is very mixed: no change is seen in BFO, slight improvement in the value by 0.007 at 220K is seen in BFCO1 whereas detoriation by 0.005 is seen in BFCO2.

After the discussion of the parameters related to polar relaxation (first term in eq. 6.1), let us now discuss the parameters of the second term (in eq. 1) related to finite conductivity. The first non-polar variable parameter is the resistivity $\rho = 1/\sigma_{dc}$. The temperature dependence of resistivity for the samples BFO, BFCO1 & BFCO2 are shown in fig. 6.3d, 6.4d & 6.5d. The resistivities of all the three samples are high (of the order of mega-ohms.cm). For BFO, a hump is seen for T < 210K. Similar humps were seen in the temperature range 140 – 200K [39], where the authors ascribed this to the pyroelectric effect. This hump was also observed in DC resistivity data of BFO in our earlier report [40]. The magnetic field of 1.3T has minimal effect on this resistivity parameter of BFO. For the other two samples, BFCO1 and BFCO2, the hump due to pyroelectric effect is absent and the parameter ‘ρ’ increases logarithmically on decreasing the temperature. The samples BFCO1 & BFCO2 shows slight negative magnetoresistivity in the respective temperature ranges 230-260K and 220-240K. We will see later that these ranges are dominated by extrinsic contributions, with magnetoresistivity as one.

Through the exponent ‘n’, we are trying to figure out the nature of conducting term: (i) Maxwell-Wagner type for n = 1 (ii) Warburg type for n = 0.5. The temperature variations of ‘n’ for the three samples are shown in fig. 6.3e, 6.4e & 6.5e. The room temperature exponent value for all the three samples are ~0.9, and this value decreases very slightly (still 0.9 in the figure) on decreasing the temperature for samples BFCO1 and BFCO2. For BFO, the value of ‘n’ decreases to ~0.5 at 180K and shows a broad minima (inverse of hump) exactly at the same temperature range of the hump. This shows that the pyroelectric effect in BFO is associated with the Warburg type diffusion. For the rest of the temperatures, the conducting term is of Maxwell-Wagner type.

The relaxation processes discussed above, are thermally activated processes and generally obeys the Arrhenius equation. However in the present case, the Arrhenius equation is found to poorly fit the observed data. Rather the polaronic variable range hopping (PVRH) [41, 42] is found to better describe the activation process. According to PVRH, the peak position in ε'' vs T plot at a fixed frequency must obey,

$$f = f_0 exp\left[-\left(\frac{T_m}{T}\right)^{1/4}\right] \text{-------------------------------- (Eq. 6.2)}$$

where f_0 is the pre-exponential factor, T_m is the Mott temperature, T is the position of the peak on the temperature axis and f is the corresponding measurement frequency. In this model, the activation energy E_a is expressed by eq. 6.3.

$$E_a = 0.25 k_B {T_m}^{1/4} T^{3/4} \text{------------------------------------} \text{(Eq. 6.3)}$$

The plot of logarithmic relaxation frequency vs. $T^{-0.25}$ at both 0T and 1.3T magnetic field for BFO, BFCO1 and BFCO2 are shown in fig. 6.6. The plot shows a good fit (solid line) to the PVRH model (eq. 6.2). From the fit, various parameters mentioned in eq. 6.2 are obtained and is shown in table 6.1. The activation energy is calculated via eq. 6.3 and is shown in table 6.2. For BFO, a distinct slope change is observed at ~215K (~0.261 on the x-axis of fig. 6.6) in both 0T and 1.3T magnetic field. Such slope change is not seen in the present temperature window of BFCO1 and BFCO2.

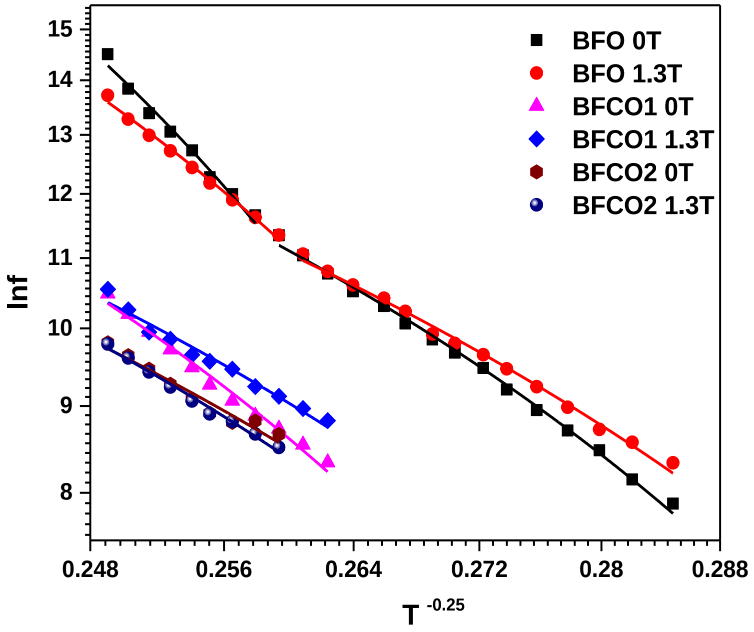

Fig. 6.6 The relaxation times obtained from the fitting is plotted in the form of lnf vs. $T^{-0.25}$ for BFO, BFCO1 & BFCO2. The solid lines are fit to the PVRH model (eq. 6.2).

Table 6.1. Fitted parameters of eq. 6.2.

	High T				Low T			
	0T		1.3T		0T		1.3T	
	f_0 (Hz)	T_m(K)	f_0 (Hz)	T_m(K)	f_0 (Hz)	T_m(K)	f_0 (Hz)	T_m(K)
BFO	5.254x10^{39}	$(309.9)^4$	1.173x10^{30}	$(223.4)^4$	9.502x10^{19}	$(134.2)^4$	5.683x 10^{17}	$(114.7)^4$
BFCO1	3.985x10^{21}	$(158.9)^4$	3.646x10^{17}	$(120.8)^4$				
BFCO2	2.696x10^{16}	$(112.8)^4$	3.897x10^{17}	$(123.5)^4$				

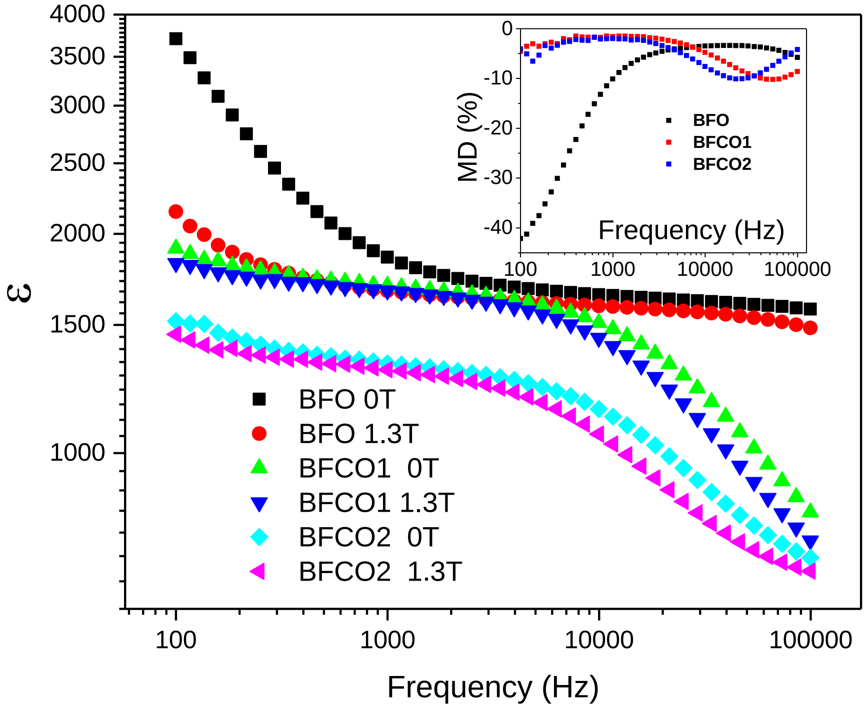

Fig. 6.7. Room temperature frequency dependent dielectric permittivity at 0T and 1.3T for BFO, BFCO1 and BFCO2. The inset shows the frequency variation of corresponding MD (%) for all the three samples.

Before we get into the actual discussion on magnetodielectric data, beforehand discussion on the origin(s) of dielectric permittivity will be helpful. The dielectric permittivity ε, is the measure of polarization created against the applied electric field. This polarization may have two origins viz, static and dynamic. The static polarization is due to the permanent separation of positive and negative charges and the materials possessing them, displays spontaneous polarization. The dynamic polarization is due to the mobile charge carriers such as electrons and holes, which creates momentarily charge imbalance for the applied electric field only. Whenever the dielectric permittivity is measured, contributions from both the factors are recorded and only after rigorous analysis, the two contributions may be separated out. Generally, these polarizations have no effect of magnetic field on them, however, if the ions/electrons responsible for the static/dynamic polarization are magnetic in nature, a magnetic field induced change in ε is expected. In BFO, the polarization created is due to off-centering of B-site Fe ions, which is magnetic and thus one may witness a variety of interesting features in ε due to external magnetic field.

Fig. 6.7 shows the room temperature, frequency dependence of dielectric permittivity ε, $(= \sqrt{((\varepsilon')^2} + (\varepsilon')^2))$ in 0T and 1.3T magnetic field. BFO displays the magnetic field induced large drop in ε at low frequencies, whereas relatively smaller drop is seen for BFCO1 and BFCO2. To highlight the magnetic field induced changes in ε, the data is plotted as magnetodielectric (MD) which is defined as the relative change in dielectric permittivity on the application of magnetic field (shown in eq. 6.4),

$$MD(\%) = \frac{\varepsilon(H)-\varepsilon(0)}{\varepsilon(0)} \times 100 \text{ -------------------------- (Eq. 6.4)}$$

The frequency variation of MD is shown in the inset of fig.6.7. A large low frequency value (~45%) is obtained in case of BFO, whereas the corresponding Co^{3+} substituted samples shows much lesser (< 10%) values of MD. Also a dip in MD is observed on the high frequency side and this dip shifts to a lower frequency for increased Co^{3+} concentration. A careful observation of fig. 6.7 reveals that this dip position coincides with the dielectric transition or the relaxation frequency position, thus indicates a possible association of the MD to the dielectric relaxation time/frequency. Hence the temperature variations of MD at various frequencies are evaluated and are shown in fig. 6.8.

In all the three samples under investigation, both positive and negative behaviors of MD are seen in respective temperature ranges. Positive and negative MD are the cases when the value of ε either increases or decreases on applying the external magnetic field. Positive MD has been observed in single phase multiferroics having coupling between ferromagnetic and ferroelectric properties, such as $DyMn_2O_5$[43] and $CaBaCo_4O_7$[44]. Whereas negative MD is seen in charge-ordered $LuFe_2O_4$, where charge frustration is reduced by the magnetic field [45, 46]. In our BFO sample, positive MD is observed for T < 215K and negative MD is seen for T > 215K. According to fig. 6.1, 215K is the temperature which separates the intrinsic (<215K) and extrinsic (>215K) dielectric response. Coincidentally, in fig. 6.6 also we find a distinct slope change at 215K, with high temperature (extrinsic region) slope being steeper than the low temperature (intrinsic region) one. The extrinsic region is found to be associated with the dielectric relaxation activation energy of $6.67T^{3/4}$ meV, which is more than twice of $2.88T^{3/4}$ meV (activation energy of intrinsic region). A similar slope change in the resistivity plot is seen for Pr_2CoMnO_6, which has been ascribed to change from charge active state to charge localized state [47].

Let's now discuss the intrinsic region and the effect of substitution on it. In the intrinsic region, BFO displays one broad positive MD peak (fig. 6.8a) which consists of three sub peaks at ~150K (say P1), ~175K (say P2) and ~190K (say P3). The P1 and P3 peak diminishes for higher frequencies with no change in their positions. Through various dielectric and spectroscopic methods, it has been established that, BFO displays a pair of spin re-orientation transitions at 140K and 200K, having possible links with magnetostriction plus piezoelectricity [24, 48]. These 140K and 200K transitions were found to be non-responsive to the applied frequencies. In our samples too, we did not find any shifting in the position of P1 & P3, due to the applied frequency, and thus may be reflecting the spin reorientation as pointed out by Scott et.al.[24]. In another study of dielectric measurement (up to 1MHz) of BFO ceramics, Kamba et.al.[9], have pointed out that 175K is the highest temperature of Maxwell-Wagner contribution to permittivity. The MW contribution is due to mobile charge carriers, which has a strong association with thermal activation. The P2 peak (~175K) of our sample also shows thermal activated behavior and thus may be ascribed to MW contribution. Its presence in our sample, but absence in the measurement of Scott et.al., might be due to nano-nature of our sample[40], which is more viable to MW contributions.

For BFCO1 (fig. 6.8b), the overall behavior is similar to that of BFO, with the plot shifted to the right (high T). Due to shifting, the new positions of peaks are at P1 ~200K, P2 ~225K and P3 ~230K. Besides similarity, there are few noticeable differences as well, such as the appearance of new humps at ~160K and at ~260K and a non-zero value of MD even in the intrinsic region (<100K). The effect of frequency is to suppress these humps, thus leads to frequency dispersion even at T < 100K, where BFO sample shows zero MD and no frequency dispersion. The frequency dispersion <100K, indicates an increase in the MW contributions, however the origin of 160K and 260K peaks are not yet known. The increased MW contribution is also reflected in the exponent 'α' which remains in the figure of 0.8 till the lowest window temperature. Such large contribution from MW may be understood from the point of activation energy of relaxations, where the E_a values for BFCO1 and BFCO2 have decreased to the level of E_a values corresponding to the extrinsic region of BFO. The behavior of BFCO2 (fig. 6.8c) is even more interesting where all the peaks have disappeared except the ~160K hump. The disappearance of these peaks is a manifestation of absence of spin re-orientation in the present temperature range (at least). One aspect of such behavior is that the spins have become more linear [49]. An experimental support to this is observed in the magnetoelectric measurement of this sample, where BFCO2 displays a linear behavior of the magnetoelectric coefficient as a function of magnetic field, whereas the parent BFO displays a hysteresis loop[40].

Coming to the extrinsic region, the BFO sample exhibits a broad minima ~250K with a small shoulder ~225K (as shown by arrow). In their report of Kamba et. al.[9], they too observed very large MD at 250K and 225K. They have ascribed this behavior to the combined effect of MW and magnetoresistance (MR). As both MW and MR are extrinsic source of dielectric contribution, considerable effect of the two in the extrinsic region is not surprising. In the DC resistivity measurement of our BFO sample too, we have found below 250K the resistivity rises drastically. For BFCO1, the entire plot has shifted to the right such that the broad minima has gone out of the temperature window. However the shoulder (earlier at 225K) is still in the temperature window and is seen at 280K. As a function of frequency, the intensity of this shoulder first increases (up to 34kHz) and then starts decreasing. This is an indication of the combined effect of MW and MR. Drop in the value of resistivity of eq. 6.1, due to the applied magnetic field also supports participation of magnetoresistance for temperatures above 230K. For BFCO2, the shift is too large to draw any conclusions. However an additional dip at ~250K and a shoulder at ~275K has appeared. The dip & shoulder disappear for higher frequencies and thus may be linked to magnetoresistance effects.

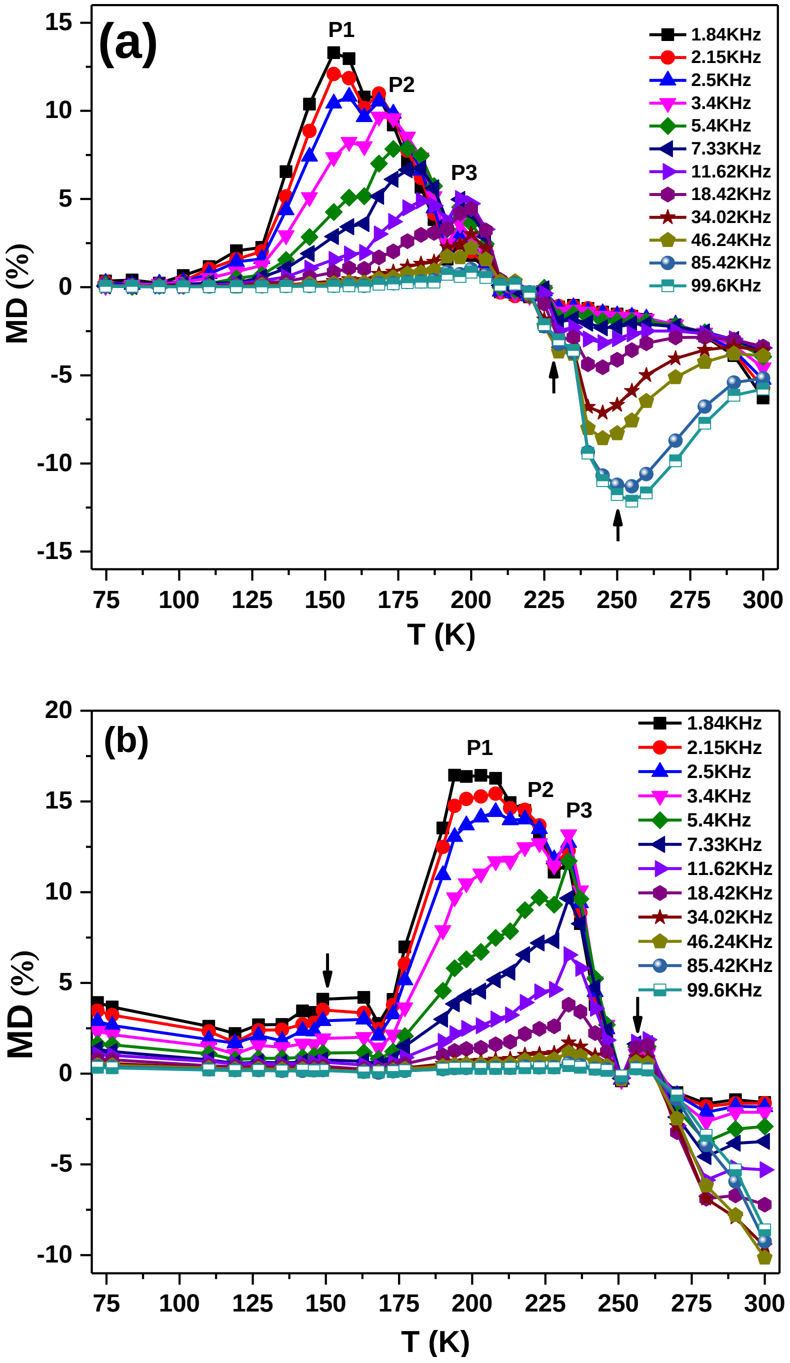

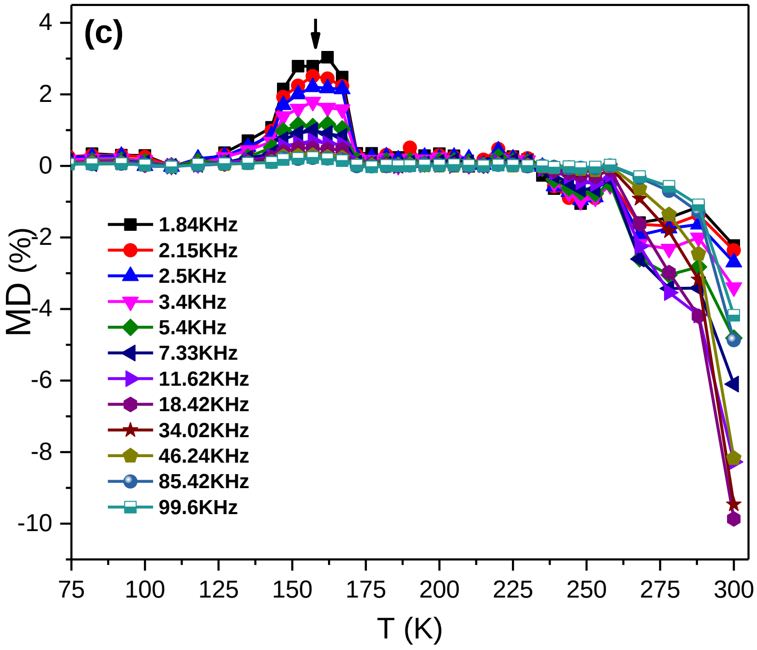

Fig. 6.8. Temperature dependent MD (%) for BFO (a), BFCO1 (b) and BFCO2 (c) at several frequencies. The solid lines are guided to eye.

Table 6.2. Activation energy calculated using eq. 6.3 at both 0T and 1.3T.

	Activation energy (E_a)x($T^{3/4}$)(meV)			
	High T		Low T	
	0T	1.3T	0T	1.3T
BFO	6.67	4.8	2.88	2.46
BFCO1	3.42	2.6		
BFCO2	2.42	2.65		

6.3 High temperature dielectric study

The $\varepsilon'$and ε'' plots of BFCO2 show two prominent relaxation peaks ~ 475K (LT peak) and ~548K (HT peak) as shown in fig. 6.9. On increasing frequency, for BFCO2, the LT peak is gradually getting suppressed and moving towards higher temperatures (shown by arrow). On the other hand the HT peak, shows a comparatively very less frequency dependence of position. Moreover, after the peak position of HT peak, there is no frequency dispersion in the data. Such behaviour has been reported to the transition temperature T_N in $BiFeO_3$ [17]. However, there are no reports of LT peak in $BiFeO_3$. In the dielectric data of our $BiFeO_3$ sample (fig. 6.9 inset), we don't see two separate LT and HT peaks. Instead a single peak ~550K along with a faint shoulder on the low temperature side is seen. On increasing frequency, the low temperature shoulder diminishes drastically: a behavior similar to BFCO2. This indicates the presence of LT peak in BFO sample as well, though of slightly weaker nature. From the fig. 6.9 (inset), it is obvious that this peak is very prominent and consistently shifting towards higher temperature with diminishing intensity. A careful observation shows frequency dispersion in LT peak is present at only on the lower temperature side and the dispersion completely goes out and all the data start merging on the high temperature side, which satisfy one of the characteristic of relaxor behaviors in ferroelectrics. Since $BiFeO_3$ is also a ferroelectric with additional magnetic ordering, it is quite possible to exhibit relaxor characteristics under special conditions. For the further evidence in the favor of relaxor material, we have plotted the temperature corresponding to maxima of LT peak (T_m) with the corresponding measurement frequency (Fig. 6.10).Plot of T_m against frequency is found to obey Vogel- Fulcher relation which is one of the other characteristics of the relaxor material.

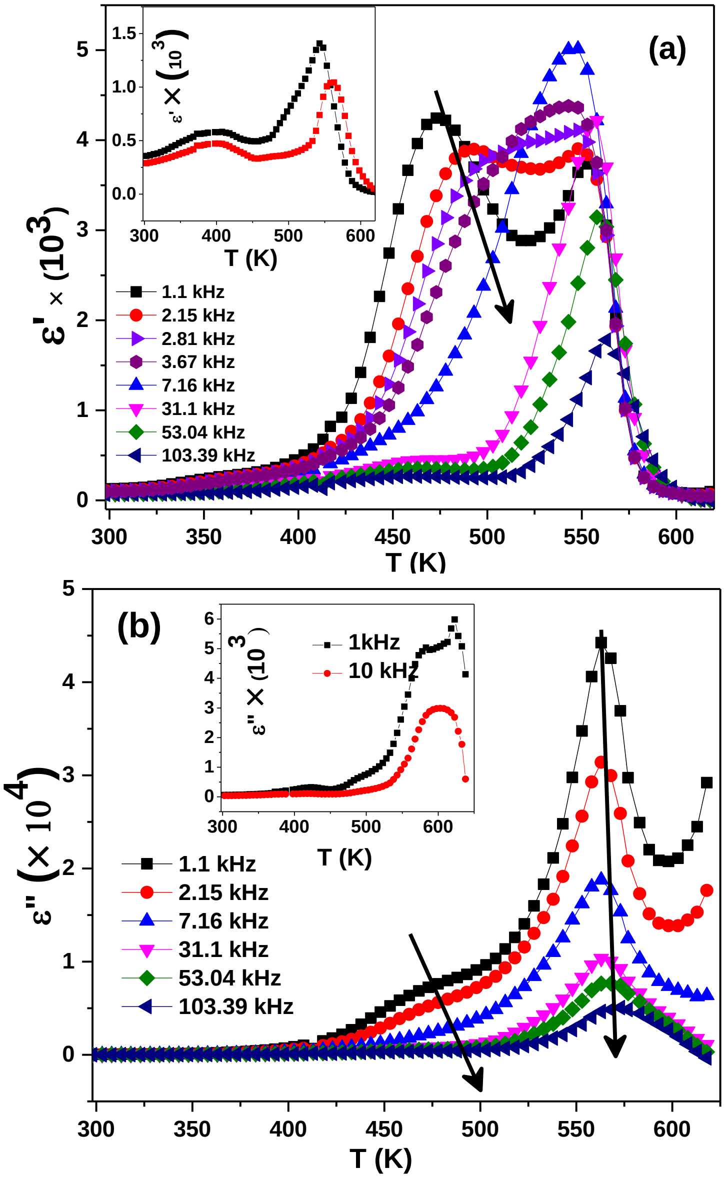

Fig. 6.9. Temperature dependent a) real b) imaginary part of dielectric permittivity of $BiFeO_3$ (inset) and $BiFe_{0.98}Co_{0.02}O_3$ at several frequencies. The lines are only guide to eye.

The activation energy (E_a) obtained is ~ 0.11eV along with the freezing temperature (T_f) = 296K. According to the literatures, the freezing state (T_f) is that temperature at which the relaxor materials freezes as nanopolar region and with the gradual increase in temperature these nanopolar regions gain energy to be mobile and coalesce to grow as micro polar region[31].

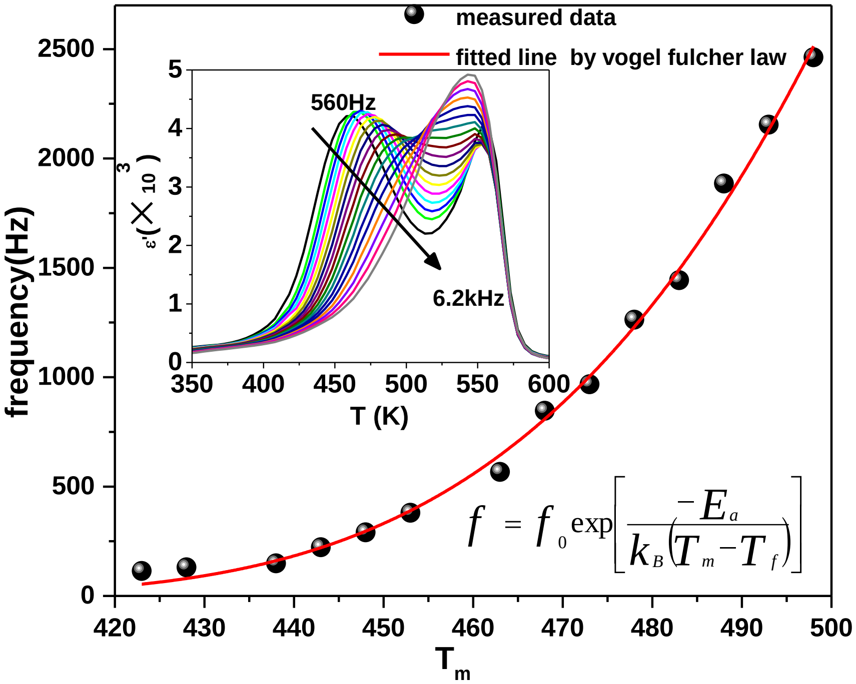

Fig. 6.10. The peak temperature T_m as a function of frequency is fitted with Vogel-Fulcher relation. Inset shows the data of fig 6.9a with close frequency intervals, so that LT peak evolution is seen clearly.

Owing to the nano-size of the polar regions, the dipoles are expected to relax quickly against external perturbation, whereas for a relatively bigger polar region of micro-size, a comparatively slower relaxation may be expected. Hence an increase in relaxation time is expected above 296K, if the nanopolar regions are growing to micro-size. In order to obtain the relaxation time(s), the dielectric data is plotted in Cole-Cole formalism. Unfortunately, the dielectric data in Cole-Cole formalism were not encouraging enough for fitting hence we switched to impedance window.

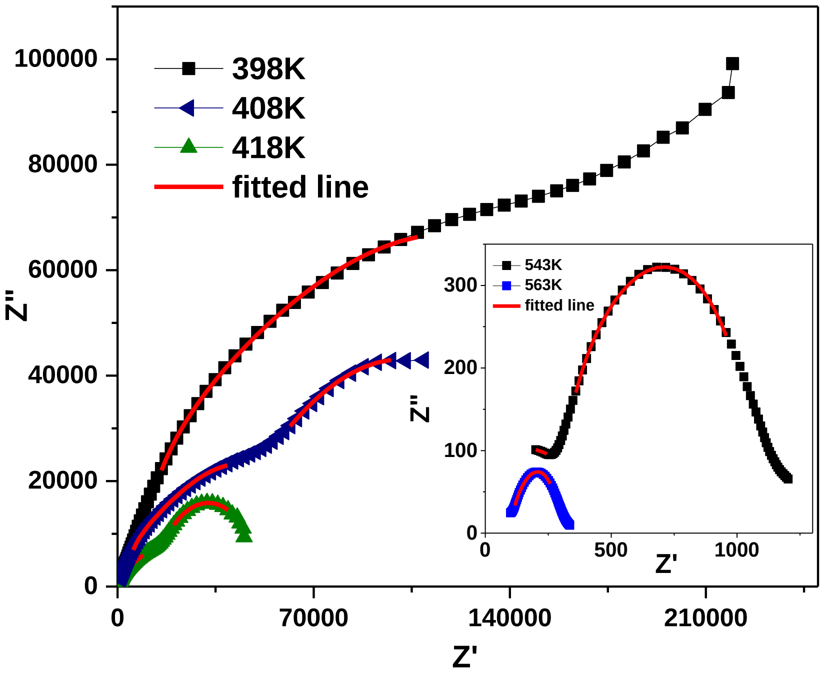

Fig. 6.11. Nyquist plot of impedance data fitted with the eq. 6.5. The solid lines represents the fitting.

The observed impedance data are fitted to the Havriliak- Negami equation equivalent for impedance [50] as given in eq. 6.5.

$$Z^*(\omega) = \frac{R}{[1+(i\omega\tau)^{\alpha}]^{\beta}} \text{------------------------------} \quad \text{(Eq. 6.5)}$$

where R, τ, α and β are the resistance, relaxation time, symmetric and asymmetric broadening parameter respectively. Nyquist plot of impedance data shows two semicircles corresponding to two relaxations. At 300K, the Cole-Cole plot for BFCO2 shows a single semicircle (hence onwards I). As temperature increases, this semicircle becomes smaller and at T ~ 398K another semicircle appears (from high Z side) first as tail and clear semicircle (hence onwards II) from 408K onwards. This combination of two semicircles continues till T ~ 543K, beyond which the semicircle I disappears and only II remains. The two semicircles are fitted to eq. 6.5 using the method described in [50]. The fitting is found to be extremely good (see fig 6.11) and the parameters so obtained are as shown in fig. 6.12.

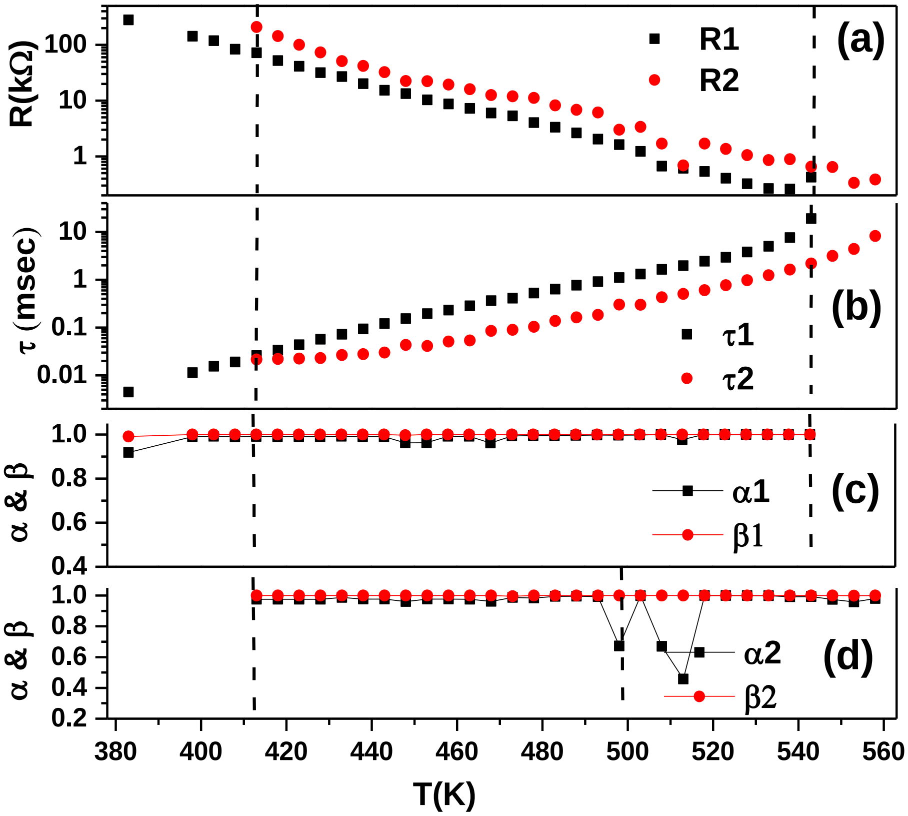

Fig. 6.12. Temperature dependent fitting parameters obtained from the Nyquist plot of $BiFe_{0.98}Co_{0.02}O_3$. The lines are only guide to eye.

The temperature dependence of the parameters R, τ, α and β obtained from semicircle I and II (hence suffix 1 & 2 in the parameters) are shown in fig. 6.12a, b, c and d respectively. Both R1 and R2 show a linear behavior in log scale. Arrhenius fitting (as shown in fig. 6.13a) of R1 results activated behavior with activation energy ~1.02eV. Similarly the activation energy of R2 is 1.09eV and 1.15 eV at low and high temperatures respectively.

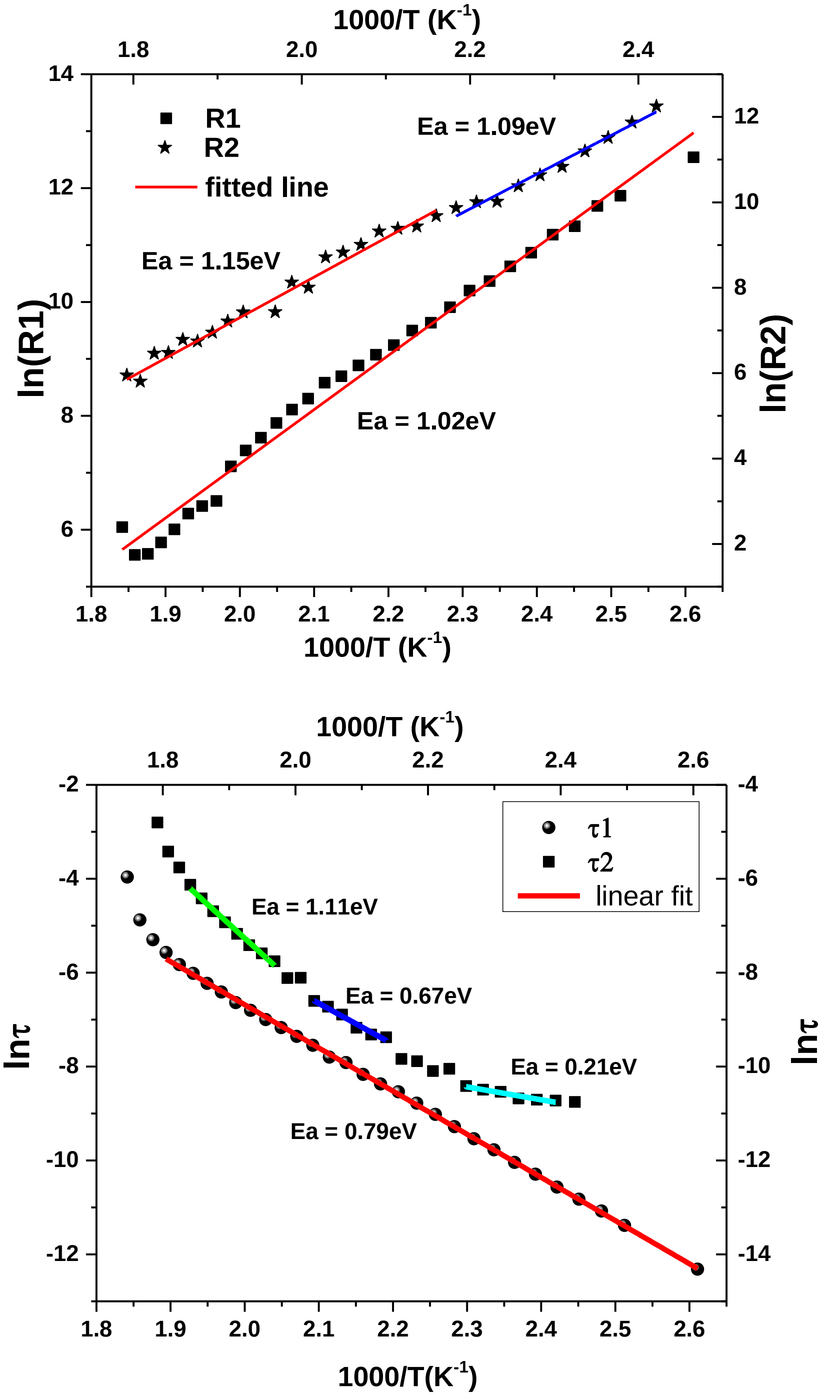

Fig. 6.13. Activated behavior of the two resistances (lnR1& lnR2) and relaxation times (lnτ1 & lnτ2) vs. 1000/T. The numerals beside the fit represent the activation energy.

The relaxation times τ1 & τ2 (fig 6.13b) increases with temperature. Such increase in relaxation time is a manifestation of slower dynamics of relaxation at elevated temperatures. This result is in accordance the growth of the polar regions from nano to micro order at elevated temperatures. Thus the behaviour of relaxation times also supports the relaxor picture of domain growth.

In eq.6.5, the deviation of α and β from unity mark the deviation from Debye relaxation. From the fitting, the respective values are found to be close to unity, except for α2 at 500 – 520K, where it deviates and fluctuates by large from unity. Similar behavior was observed near the magnetic phase transition of La_2NiMnO_6, where the authors have ascribed it to magnetic phase transition[50]. As the observed fluctuation temperature range is close to the T_N seen in ε'& ε'' plot, we too believe this strong deviation from Debye behavior might be associated with fluctuation of magnetic order parameter near magnetic ordering temperature.

6.4 Conclusions

Effect of dilutely substituted cobalt on the dielectric properties in the wide temperature range 75K to 650K is investigated. The low temperature dielectric data are found a good fit to the Haverliak – Negami (HN) expression plus an additional term for the Maxwell Wagner (MW) type relaxations. The increase of the relaxation time towards low temperature suggests the slowing down of the dynamics of the material and the relaxation approached towards the ideal Debye type. The dielectric relaxations are well explained by polaronic variable range hopping model and a distinct transition from extrinsic to intrinsic behaviour is seen at 215K. The relaxation dynamics of the sample are further getting slower by the substitution of Cobalt. The extrinsic and non-Debye contribution is increased by the substitution of Co and hence suppresses spin reorientation transitions for x = 0.02 sample. These results very well explain the recently reported disappearance of hysteresis and appearance of linear behavior in the magneto-electric coupling coefficient for Co substituted $BiFeO_3$[40]. Moreover a clear picture in terms of nature (extrinsic or intrinsic) of various dielectric transitions (reported earlier) at low temperatures is also revealed. The pyroelectric active region in $BiFeO_3$ is found to be of diffusive nature. In summary, the present study reveals the various aspects of dielectricity in cobalt substituted $BiFeO_3$ and renders it for exploring its other aspects via spectroscopic technique, theoretical modeling, etc. The indications of relaxor behavior for BFCO2 are seen in the high temperature range

(~ 475K) and gradually shifts towards higher temperature with the increase in frequency. The maximum of the low temperature peak is found to be well fitted with the Vogel-Fulcher law which is the further confirmation of the relaxor behavior of the material. The freezing temperature is found to be T_f ~ 298K which is in accordance with our previous DC magnetization result for the BFCO2 sample (see chapter 3). The impedance data are analyzed by the use of Nyquist plot and the corresponding resistance, time constant and symmetric and asymmetric broadening parameters are obtained from the fitting of Nyquist plot. The nature of resistances implies the semiconducting nature of the sample. The relaxation dynamics are getting slower with the gradual increase in temperature is further confirmation of the relaxor behavior. This also seems plausible from the point of local fluctuations induced by dilute concentration of Cobalt in $BiFeO_3$. However, further investigations may be needed for the confirmation.

References

1. R. Ramesh and N. Spaldin, *Nature Mater.*, **6** 21 (2007)
2. H. Schmid, *Ferroelectrics*, **162** 19 (1994).
3. T. Kimura, T. Goto, H. Shintani, K. Ishizaka, T. Arima nad Y. Tokura, *Nature*, **426** 55 (2003).
4. M. Fiebig, *J. Phys. D*, **38** R123 (2005).
5. W. Eerenstein, N. D. Mathur, and J. F. Scott, *Nature*, **442** 759 (2006).
6. C. W. Nan, M. I. Bichurin, S. Dong, D. Viehland, and G. Srinivasan, *J. Appl. Phys.*, **103** 031101 (2008).
7. I. Sosnowska, T. Peterlin-Neumaier and E. Steichele, *J. Phys. C: Solid State Phys.*, **15** 4835 (1982).
8. S. A. T. Redfern, C. Wang, J. W. Hong, G. Catalan, and J. F. Scott, *J. Phys: Condens Matter.*, **20** 452205 (2008).
9. S. Kamba, D. Nuzhnyy, M. Savinov, j. Sebek, J. Petzelt, J. Prokleska, R. Haumont, J. Kreisel, *Phys. Rev. B* **75** 024403 (2007).
10. J. M. Caicedo, J. A. Zapata, M. E. Gomez, and P. Prieto, *J. Appl. Phys.*, **103** 07E306 (2008).

11. T. Kimura, Y. Sekio, H. Nakamura, T. Seigrist and A. P. Ramirez, *Nature Mater.*, **7** 291 (2008).
12. D. Choudhury, P. Mandal, R. Mathieu, A. Hazarika, S. Rajan, A. Sundaresan, U. V. Waghmare, R. Knut, O. Karis, P. Nordblad and D. D. Sarma, *Phys. Rev. Lett.*, **108** 127201 (2012).
13. A. Venimadhav, D. Chandrasekar and J. Krishna Murthy, *Appl. Nanosci.*, **3** 25 (2013).
14. R. Ranjith, A. K. Kundu, M. Filippi, B. Kundys, W. Prellier, B. Raveau, J. Laverdiere, M. P. Singh and S. Jandi, *Appl. Phys. Lett.*, **92** 062909 (2008).
15. S. R. Das, R. N. P. Choudhary, P. Bhattacharya, and R. S. Katiyar, P. Dutta, A. Manivannan, and M. S. Seehra, *J. Appl. Phys.*, **101** 034104 (2007).
16. V. A. Khomchenko, D. A. Kiselev, I. K. Bdikin, V. V. Shvartsman, P. Borisov, W. Keeman, J. M. Vieira and A. L. Kholkin, *Appl. Phys. Lett.*, **93** 262905 (2008).
17. P. Uniyal, K. L. Yadav, *J. Phys.: Condens. Mater*, **21** 012205 (2009).
18. V. A. Khomchenko, D. A. Kiselev, J. M. Vieira, Li Jian, A. L. Kholkin, A. M. L. Lopes, Y. G. Pogorelov, J. P. Araujo, and M. Maglione, *J. Appl. Phys.*, **103** 024105 (2008).
19. V. R. Palkar, D. C. Kundaliya, and S. K. Malik, *J. Appl. Phys.*, **93** 4337 (2003).
20. F. Chang, N. Zhang, F. Yang, S. Wang and G. Song, *J. Phys. D: Appl. Phys.*, **40** 7799 (2007).
21. Y. K. Jun and S. H. Hong, *Solid State Commun.*, **144** 329 (2007).
22. G. A. Smolenskii, I. E. Chupis *Soviet Physics – Uspekhi*, **25** 475 (1982).
23. M. K. Singh, R. S. Katiyar and J. F. Scott, *J. Phys: Condens Matter.*, **20** 252203 (2008).
24. J. F. Scott, M. K. Singh and R. S. Katiyar, *J. Phys: Condens Matter.*, **20** 322203 (2008).
25. A. Kumar, N. M. Murari and R. S. Katiyar, *Appl. Phys. Lett.*, **92** 152907 (2008).
26. B. Ramachandran, A. Dixit, R. Naik, G. Lawes and M. S. Ramachandra Rao, *J. Appl. Phys.*, **110** 104105 (2011).
27. B. Ramachandran, A. Dixit, R. Naik, G. Lawes and M. S. Ramachandra Rao, *Appl. Phys. Lett.*, **100** 252902 (2012).
28. R. Schmidt, J. Ventura, E. Langenberg, N. M. Nemes, C. Munuera, M. Varela, M. Garcia-Hernadez, C. Leon and J. Santamaria, *Phys. Rev. B*, **86** 035113 (2012).

29. J. Lu, A. Gunther, F. Schrettle, F. Mayr, S. Krohns, P. Lunkenheimer, A. Pimenov, V. D. Travkin, A. A. Mukhin and A. Loidl, *Eur. Phys. J. B*, **75** 451 (2010).
30. M. H. Cohen, J. B. Neaton, L. He and D. Vanderbilt, *J. Appl. Phys.* **94** 3299 (2003)
31. P. Lunkenheimer, V. Bobnar, A. V. Pronin, A. I. Ritus, A. A. Volkov and A. Loidl, *Phys. Rev. B* **66** 052105 (2002)
32. P. Lunkenheimer, R. Fichtl, S. G. Ebbinghaus and A. Loidl, *Phys. Rev. B* **70** 172102 (2004)
33. L. E. Cross, *Ferroelectrics*, **76** 241 (1987).
34. S. B. Krupanidhi, *Proc. Indian Acad. sci.*, **115** 775 (2003).
35. R. N. P. Choudhary D. K. Pradhan, C. M. Tirado, G. E. Bonilla and R. S. Katiyar, *J Appl. Phys.*, **100** 084105 (2006)
36. D. O'Neill, R. M. Bowman and J. M. Gregg, *Appl. Phys. Lett.*, **77** 1520 (2000).
37. S. K. Deshpande, S. N. Achary, R. Mani, J. Gopalakrishnan, and A. K. Tyagi, *Phys. Rev. B*, **84** 064301 (2011).
38. J. Ray, A. K. Biswal, S. Acharya, V. Ganesan and P. N. Vishawakarma, *J. Magn. Magn. Mater.*, **324** 4084 (2012).
39. R. Jarrier, X. Marti, J. Herrero-Albillos, P. Ferrer, R. Haumont, P. Gemeiner, G. Geneste, P. Berthet, T. Schulli, P. Cevc, R. Blinc, S. S. Wong, Tae-Jin Park, M. Alxe, M. A. Carpenter, J. F. Scott, G. Catalan, and B. Dkhil *Phys. Rev. B*, **85** 184104 (2012).
40. J. Ray, A. K. Biswal, P. D Babu, V. Siruguri and P. N. Vishawakarma, *J. Alloys. Comp.,***628** 32 (2015)
41. L. Zhang and Z. J. Tang, *Phys. Rev. B*, **70** 174306 (2004).
42. O. Bidault, M. Maglione, M. Actis, M. Kchikech, *Phys. Rev. B*, **52** 4191 (1995).
43. N. Hur, S. Park, P. A. Sharma, S. Guha and S. –W. Cheong, *Phys. Rev. Lett.*, **93** 107207 (2004).
44. V. Caignaert, A. Maignan, K. Singh, Ch. Simon, V. Pralong, B. Raveau, J. F. Mitchell, H. Zheng, A. Huq and L. C. Chapon, *Phys. Rev. B*, **88** 174403 (2013).
45. M. A. Subramanian, T. He, J. Chen, N. S. Rogado, T. G. Calvarse and A. W. Sleight, *Adv. Mater.*, **18** 1737 (2006).
46. H. J. Xiang and M. –H. Whangbo, *Phys. Rev. Lett.*, **98** 246403 (2007).

47. L. Y. Wang, Q. Li, Y. Y. Gong, D. H. Wang, Q. Q. Cao and Y. W. Du, *J. Am. Ceram, Soc.*, **97** 2024 (2014).
48. J. F. Scott, *J. Magn. Magn. Mater.*, **321** 1689 (2009).
49. J. Ray, A. K. Biswal, P. D Babu, V. Siruguri and P. N. Vishawakarma, *Under review*
50. A. K. Biswal, J. Ray, P. D. Babu, V. Siruguri, P. N. Vishwakarma, *J Appl. Phys.*, **113** 194106 (2014).

Chapter 7

Magnetic and dielectric study on $BiFe_{1-x}Co_xO_3$: x = 1, 0.5

This chapter describes magnetic and dielectric property of $BiFe_{1-x}Co_xO_3$: x = 1, 0.5 nanoparticles, prepared by sol-gel auto combustion method. The samples are crystallized in a cubic structure (space group I23) with the chemical formula $(Bi,Co)_{25}CoO_{40}$ (x = 1) and $(Bi_{13}Co_{5.5}Fe_{6.5})CoO_{40}$ (x = 0.5) as described in chapter 2. The DC magnetization measurement reveals that the BCO is paramagnetic and shows signs of magnetic ordering at 30K, which seems to be competing paramagnetic and antiferromagnetic behaviour. Interestingly, the Fe substituted BCFO shows large magnetic disorder (even at room temperature) with strengthening ferromagnetic ordering as the temperature is lowered. The low temperature dielectric and magnetodielectric measurement shows dominance of extrinsic contributions, throughout the temperature range for BCO. For BCFO, the behaviour may be divided under two regions viz., intrinsic (<260K) and extrinsic (>260K). The Haverliak - Negami equation is found to better describe the observed relaxation data.

7.1 Introduction

Multiferroics materials have drawn considerable attention[1, 2] due to their complex spin, charge and lattice interactions[3, 4]. Single phase multiferroics are very rare[5] and that’s why efforts are being made to improvise the multiferroic property of existing compounds by various chemical substitutions[6-8]. At the same time, researchers are also looking for alternate single phase multiferroics, which may be derived from the existing one via partial or complete substitution[9-11].

In this regard, considerable efforts are being made to obtain single phase bismuth cobaltite, as an analogue to bismuth ferrite, a well-known prototype single phase multiferroic compound. It has been found that bismuth cobaltite ($BiCoO_3$) prepared by high pressure technique, exhibits large spontaneous polarization and C-type antiferromagnetism having T_N ~ 470K in its tetragonal phase[12-15]. This compound is found to be isostructural with ferroelectric tetragonal $PbTiO_3$ with the space group P4mm[12]. Due to the large tetragonality (c/a= 1.27) in comparison to $PbTiO_3$ (c/a= 1.06), $BiCoO_3$ exhibits huge spontaneous polarization ($179\mu C/cm^{-2}$)[16]. Also, because of high tetragonal distortion, the corner shared CoO_5 pyramids are formed. Considering the above spectacular features of $BiCoO_3$ in its tetragonal phase, it is considered as a suitable multiferroic material[12].

In spite of being a promising multiferroic candidate, the complicated synthesis procedure for obtaining high quality single phase[12, 14], has restricted the reach of researchers to this compound for further studies. Thus the preparation of $BiCoO_3$ under ambient conditions is highly desired. Bucci[17] and Vasudevan et.al.[18] studied cubic (Im3) $BiCoO_3$ with the lattice parameter ~10.2 Å, prepared under ambient conditions using mixtures of various nitrates and oxides. They reported that in the cubic structure the material is a room temperature insulator with Neel temperature below 100K. In the present study, we have studied the magnetic and dielectric behaviour of the single phase BCO, prepared under ambient condition as a function of temperature, especially below 100K which was not done by Vasudevan et.al.[18]. In addition, we have also addressed partial substitution of Fe at Co site of BCO, as $BiFeO_3$ is a well-known multiferroic. The phase confirmation is done via Reitveld refinement of XRD data as described in chapter 2.

7.2 DC magnetization study

The temperature dependant DC magnetization at zero field cooled (ZFC) and field cooled warming (FCW) conditions are performed at 0.1T and 1 T respectively are shown in the fig. 7.1. For BCO as shown in fig. 7.1a, the magnetization data at 0.1 T shows a gradual increase with the decrease in temperature plus a cusp ~30K. The measurement repeated in 1T magnetic field also shows a similar behaviour with a higher magnitude (~10 times of the magnitude at 0.1T). The ZFC and FCW data in both magnetic fields exactly overlap over each other, thus ruling out the possibility of magnetic disorder. Cusp (~30K) of a similar nature has also been observed in the magnetization data of Co_3O_4 nanoparticles, where the behaviour has been ascribed to the competing interactions between octahedrally and tetrahedrally coordinated cobalt ions[20, 21]. In the present compound also, coexistence of cobalt at octahedral and tetrahedral positions has been confirmed by x-ray diffraction, and thus the observed cusp may be a manifestation of such competing interactions. The inset in fig. 7.1a shows the variation of the inverse of susceptibility as a function of temperature measured at 0.1T and 1T. A linear behaviour in accordance with Curie-Weiss law, from room temperature down to ~30K, reflects the paramagnetic nature of the sample above 30K. Linear extrapolation of the paramagnetic region to the intercept with temperature scale, gives θ ~ -79K in zero field and -78K in 1.3T magnetic field. The ratio of paramagnetic temperature θ with the magnetic ordering temperature 30K, gives a parameter called frustration parameter " f " = $\frac{|\theta|}{T_N}$ = 2.63, which shows a considerable deviation from unity, thus a measure of weak frustration[22- 24] present in the sample, probably due to competing interaction between Co in tetrahedral and octahedral environments. The frustration parameter value is in consistent with various other magnetic compounds having b.c.c. and rutile structure for which frustration parameter lies between 1 and 3 e.g . Co_3O_4 = 3, MnF_2 = 1.5, CoF_2 = 1.3[24]. The application of magnetic field minutely changes the frustration parameter implying that the magnetic field energy is insufficient to overcome the frustration potential.

In the case of BFCO as shown in fig. 7.1b, as the sample is cooled down, the ZFC at 0.1T decreases first slowly, then rapidly ~270K and ultimately saturates below 120K. Due to some technical problem in measurement, the FCW data couldn't be recorded, however from the nature of the graph, a bifurcation in ZFC and FCW may be expected below 325K. On the application of 1T magnetic field, the maxima position in ZFC (which is ~350K in 0.1T) has shifted to 175K. Below 175K, the FCW becomes flat in temperature, whereas ZFC decreases continuously thus resulting bifurcation in ZFC and FCW, which otherwise remains overlapped above 175K. Such behaviour which is commonly seen in nanoparticles[25], implies a ferromagnetic ground state for the sample, however due to slower dynamics below blocking temperature (here 175K), the ZFC and FCW bifurcates. In addition to this both ZFC and FCW shows an upturn at lowest temperatures, may be due to secondary phase seen as a hump in XRD (see chapter 2).

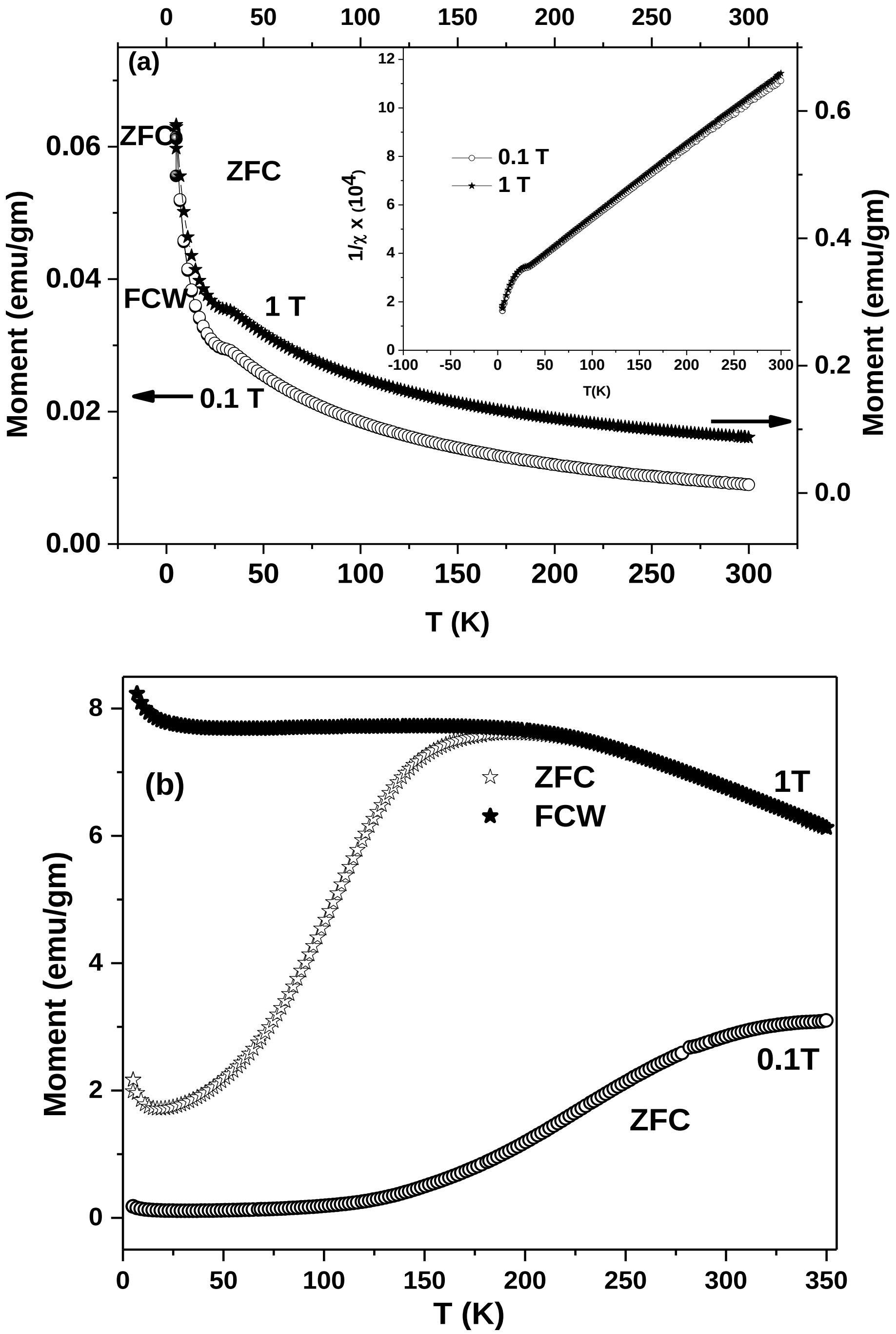

Fig. 7.1 The ZFC (open symbol) and FCW (solid symbol) magnetization curve of (a) $(Bi_{13}Co_{12})CoO_{40}$ (b) $(Bi_{13}Co_{5.5}Fe_{6.5})CoO_{40}$ as a function of temperature measured under a field of 0.1T and 1T respectively. The inset in (a) shows the plot of inverse of susceptibility as a function of temperature at 0.1T & 1T.

The magnetization (M) vs. field (H) measurement of BCO sample done at two different temperatures viz., 10K and 300K are shown in fig. 7.2a. The M-H behaviours at both the temperatures are in accordance with that of paramagnetic behaviour. However, in the inverse susceptibility plot (see inset of fig. 7.1a), a sudden decrease is observed at ~30K along with a negative intercept at θ ~ -79K of the Curie-Weiss extrapolation of without field data. This is an indication of antiferromagnetic interactions. Thus the M-H and M-T behaviour together reflects an overall paramagnetic behaviour with some antiferromagnetic ordering initiating below 30K. The Fe substitution in BCO significantly affects the magnetic ordering as seen in the M vs. H plot of BCFO at 300K and 5K (in fig. 7.2b). At 300K, the plot shows s-shaped graph saturation (5.816 μ_B/f.u.) but no hysteresis. When this measurement is done at 5K, the behaviour remains same with a addition of hysteresis and an increase in magnetization which now saturates at 8.566 μ_B/f.u. with coercive field 1.45T. Thus a transition from paramagnetic to ferromagnetic state is seen. The nature of the M-T plot in 1T magnetic field suggests the ferromagnetic ordering onset temperature to be above 200K. A high temperature M-T measurement may be required to locate the ferromagnetic onset temperature in this sample.

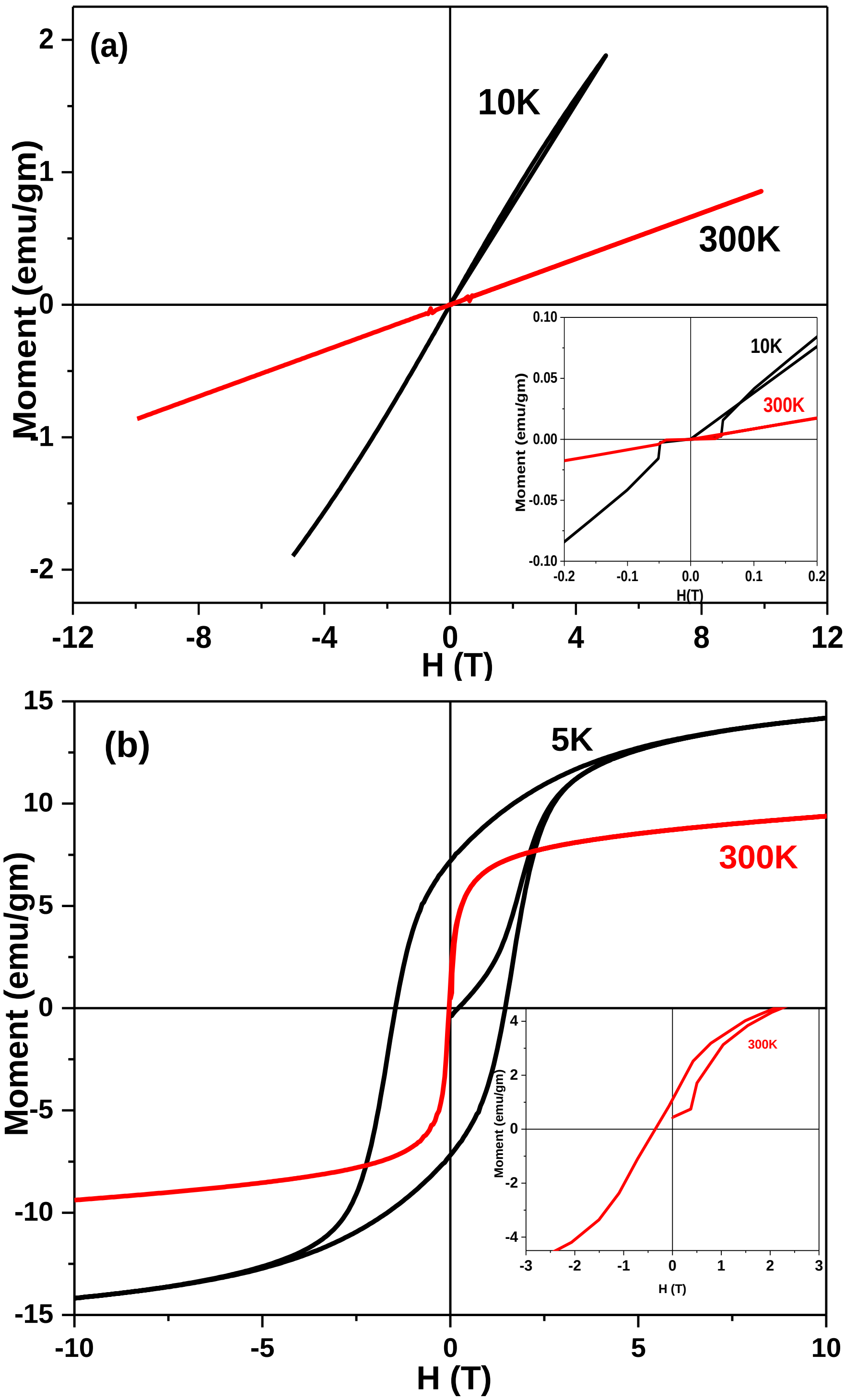

Fig. 7.2 The M-H loop of a) $(Bi_{13}Co_{12})CoO_{40}$ at 10K and 300K, (b) $(Bi_{13}Co_{5.5}Fe_{6.5})CoO_{40}$ at 5K and 300K. The inset shows the enlarged view of M-H loop near the origin to observe the existence of hysteresis.

7.3 Dielectric Study

The frequency dependent dielectric measurements are carried out for BCO and BCFO at various static low temperatures. Fig. 7.3a & c shows the temperature dependent relative dielectric permittivity (ε_r) and dielectric loss, extracted from the corresponding frequency dependence at various static low temperatures for BCO sample. The (ε_r) decreases monotonically with the decrease in temperature from room temperature value ~ 1400 to the low temperature value ~ 400. Significant dispersion seen at room temperature, gradually decreases for lower temperatures, but a complete dispersionless (intrinsic) region is yet to achieve even at 75K. A similar behavior is seen for $tan\delta$ with a difference that the low temperature region is less dispersive compared to (ε_r) (fig. 7.3b). The behavior for BCFO is similar but with a reduced dielectric value, and here the intrinsic region is seen at 200K. Interestingly, the intrinsic region shows a consistent dispersion down to the lowest temperature 75K. This consistent dispersion may be associated with the small amount of secondary phase seen in the XRD plot (see chapter 2). A very important observation for BCFO is the reduction in dielectric loss by at least ~15times as compared to BCO as shown in fig. 7.3d. This is an indication of possibility of permanent dipoles in the sample.

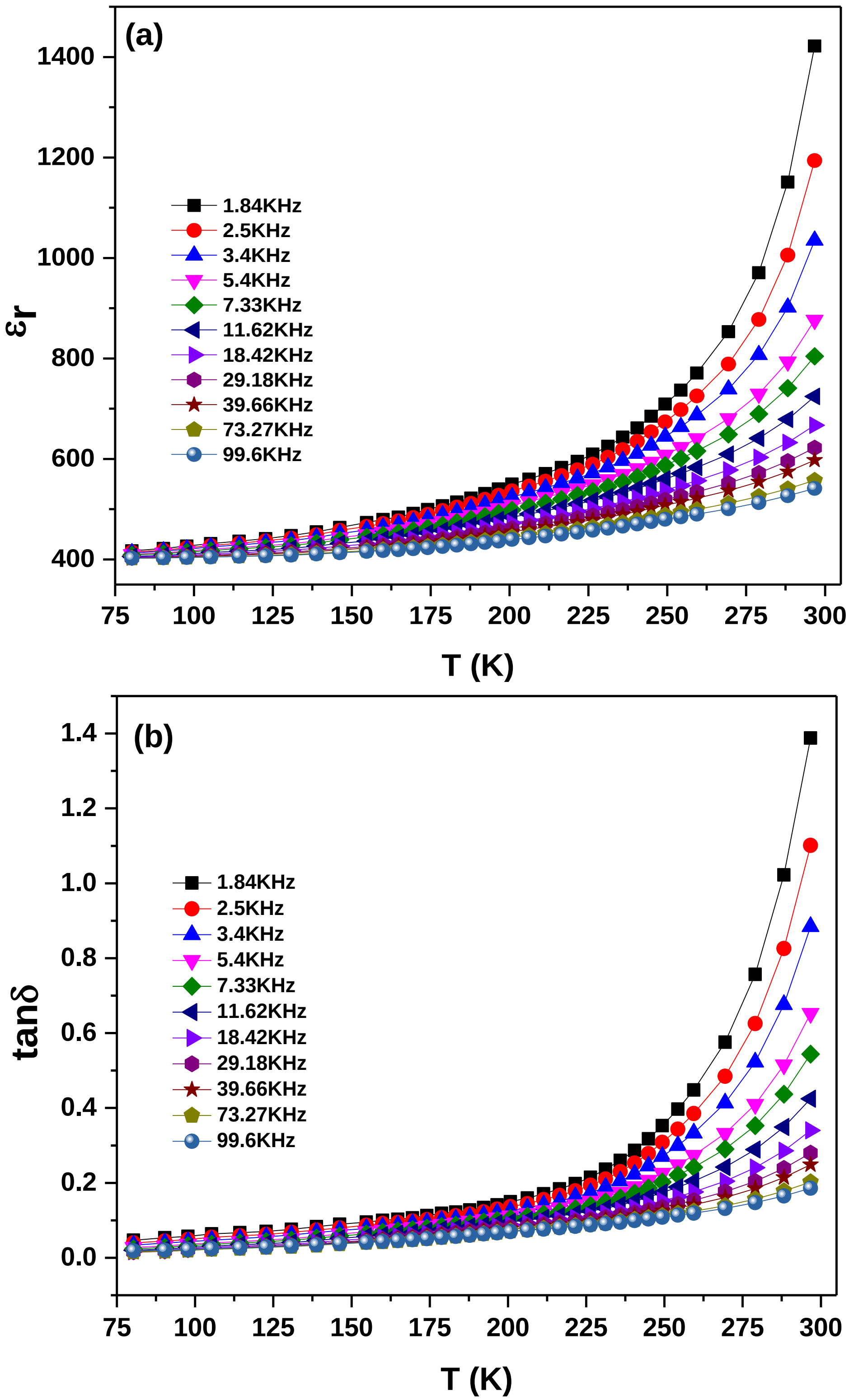
(a)
εr
1400
1200
1000
800
600
400
75
100
125
150
175
200
225
250
275
300
T (K)
1.84KHz
2.5KHz
3.4KHz
5.4KHz
7.33KHz
11.62KHz
18.42KHz
29.18KHz
39.66KHz
73.27KHz
99.6KHz
(b)
tanδ
1.4
1.2
1.0
0.8
0.6
0.4
0.2
0.0
75
100
125
150
175
200
225
250
275
300
T (K)
1.84KHz
2.5KHz
3.4KHz
5.4KHz
7.33KHz
11.62KHz
18.42KHz
29.18KHz
39.66KHz
73.27KHz
99.6KHz

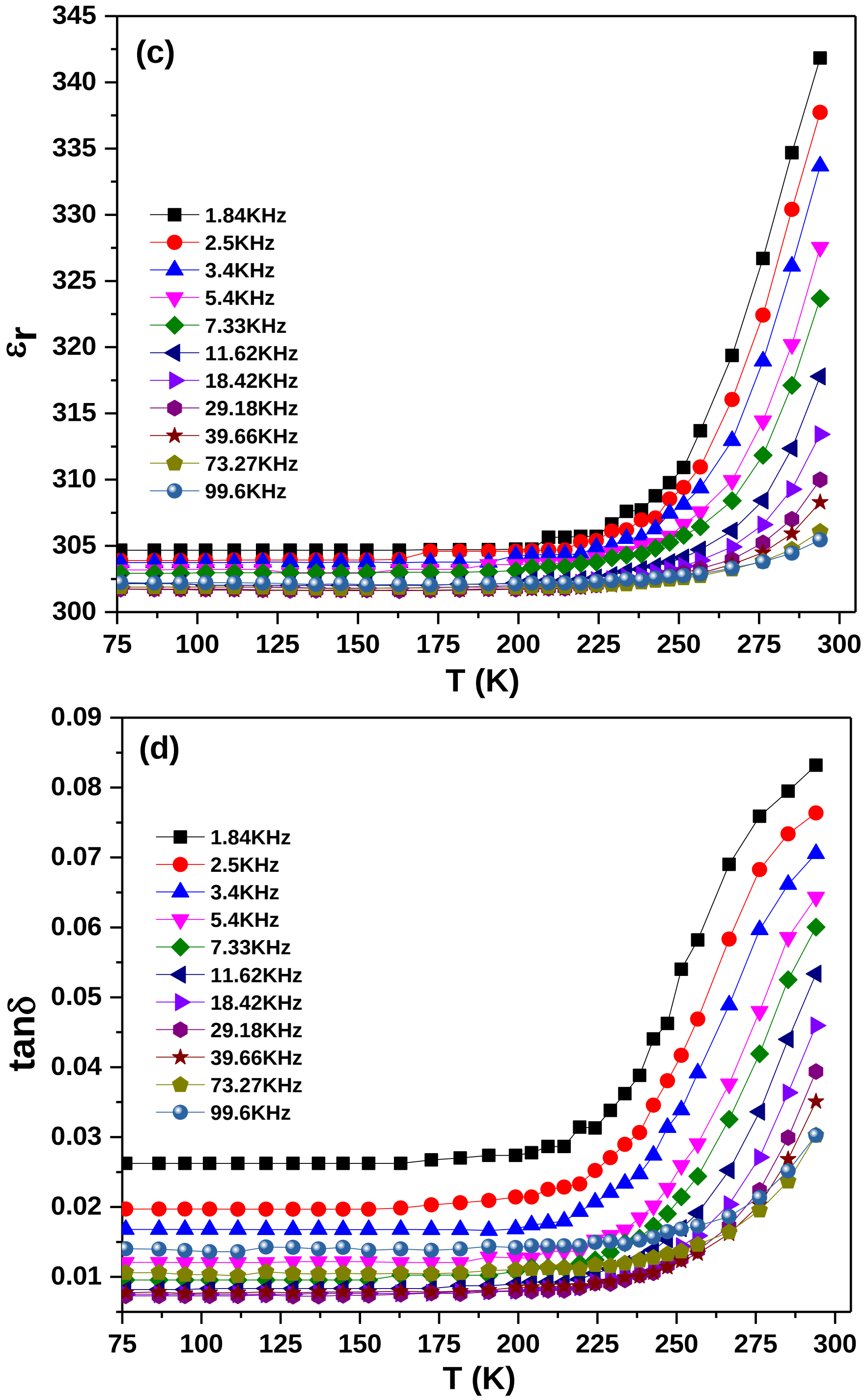

Fig. 7.3 a) & c) shows the temperature dependent relative dielectric permittivity of $(Bi_{13}Co_{12})CoO_{40}$ and $(Bi_{13}Co_{5.5}Fe_{6.5})CoO_{40}$, b) & d) shows the dielectric loss of $(Bi_{13}Co_{12})CoO_{40}$ and $(Bi_{13}Co_{5.5}Fe_{6.5})CoO_{40}$.

7.4 Magnetodielectric Study

To observe the effect of magnetic field on the electric dipoles and any possibility of magnetodielectricity, magnetic field of 1.3T is applied and the dielectric measurements repeated. To highlight even the smallest dielectric changes due to magnetic field, the data is plotted as magnetodielectricity (MD) (shown in fig. 7.4) and is expressed as eq. 7.1.

$$MD(\%) = \frac{\varepsilon(H)-\varepsilon(0)}{\varepsilon(0)} \times 100 \text{--- (Eq. 7.1)}$$

where the dielectric permittivity is $\varepsilon = \sqrt{((\varepsilon'^2) + (\varepsilon''^2))}$.It is observed that the maximum MD (in magnitude, which otherwise is negative) is obtained at 300K at low frequency and gradually decreases towards the higher frequency, thus reflects MD to be of ~1/ω behavior. The MD value gradually decreases towards the low temperature. In addition to this the MD is less than ~ 0.5% in the intrinsic region, suggesting that the magnetoelectric coupling in the intrinsic region is of very weak nature. The large value of MD at RT may be the extrinsic effect and further its ~1/ω behavior suggests the effect of either Maxwell-Wagner and/or Magnetoresistance effect to be playing significant role[26]. However, we did not find any significant changes in the loss spectra on the application of magnetic field which discards the possibility of Maxwell Wagner type polarization in the material. On the other hand, coexistence of Co^{3+} and Co^{4+} sites facilitate the hopping of the charge carriers and the probability of hopping decreases with lowering of temperature. As this contribution to the MD is more prominent near RT and negligible at lower temperatures, we believe this contribution to the MD is mainly from the finite conductivity or magnetoresistance effects. Partial substitution of Fe at Co sites in BCFO shows a drastic reduction in MD. Moreover, the data remain flat for larger temperature range (similar to the behavior of ε_r) and some temperature dependent negative MD values with dispersion is seen only near room temperature.

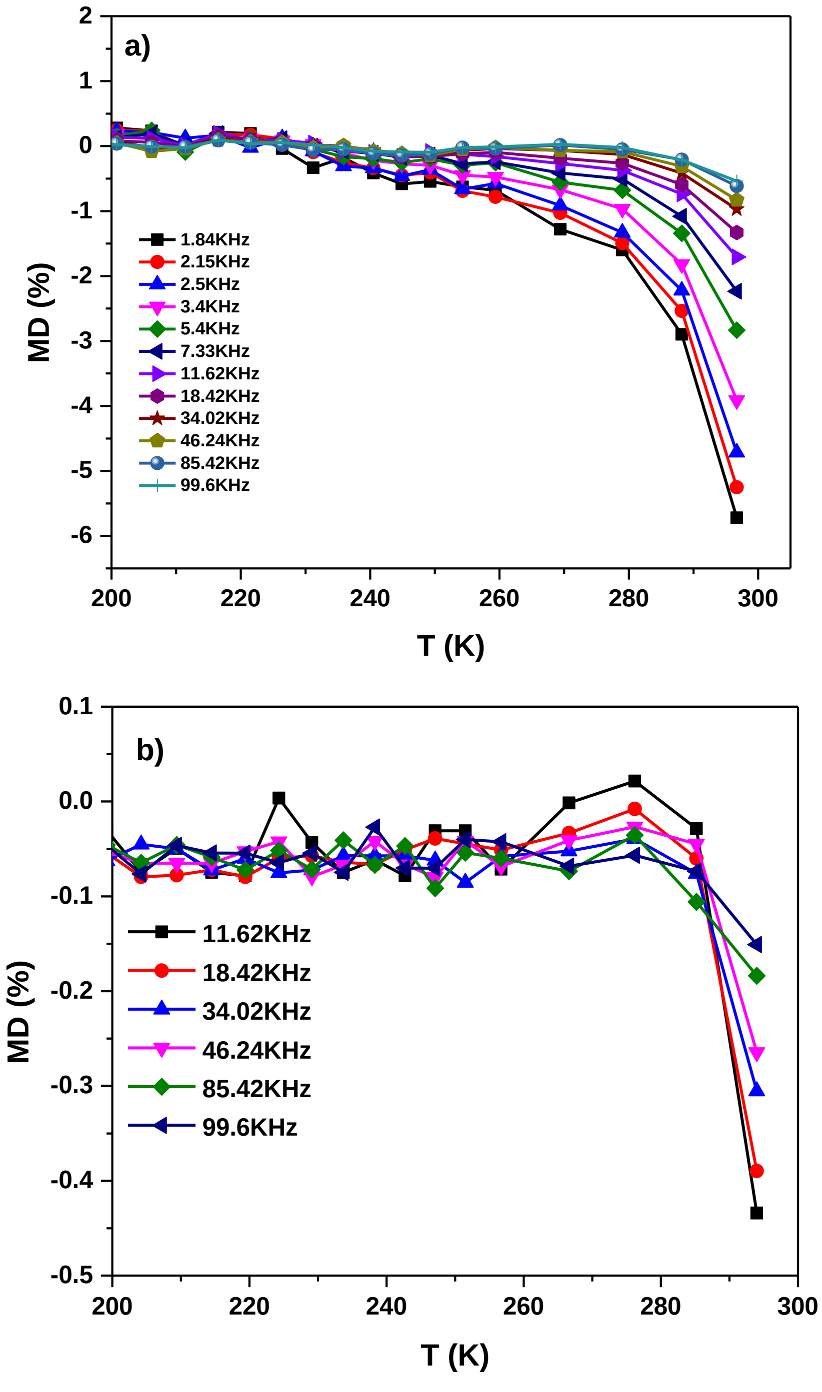

Fig. 7.4 Temperature dependent magnetodielectricity at selected frequencies for a) $(Bi_{13}Co_{12})CoO_{40}$& b) $(Bi_{13}Co_{5.5}Fe_{6.5})CoO_{40}$.

7.5 Impedance Spectroscopy Study

Finding the dielectric data to be dominated by extrinsic contributions, the data are analyzed further in complex impedance formalism. Cole-Cole plot of impedance data shows a single semicircle and the same in bode plot shows a peak in Z'', whose position shifts to lower frequencies for lower temperatures as shown in fig. 7.5. Simultaneous fitting of Bode and Cole-Cole plot is done using the impedance equivalent of Harverliak – Negami (HN) equation (eq. 7.2)[27].

$$Z^*(\omega) = \frac{R}{[1 + (i\omega\tau)^{\alpha}]^{\beta}} \text{------------------------------ (Eq. 7.2)}$$

where, R is the resistance, τ is the relaxation time, the parameter α and β are the broadness and asymmetry of the corresponding relaxation spectra. Values of α and β less than unity mark the deviation from Debye behavior. The solid lines in fig. 7.5a & b represents the fitting to the experimental data.

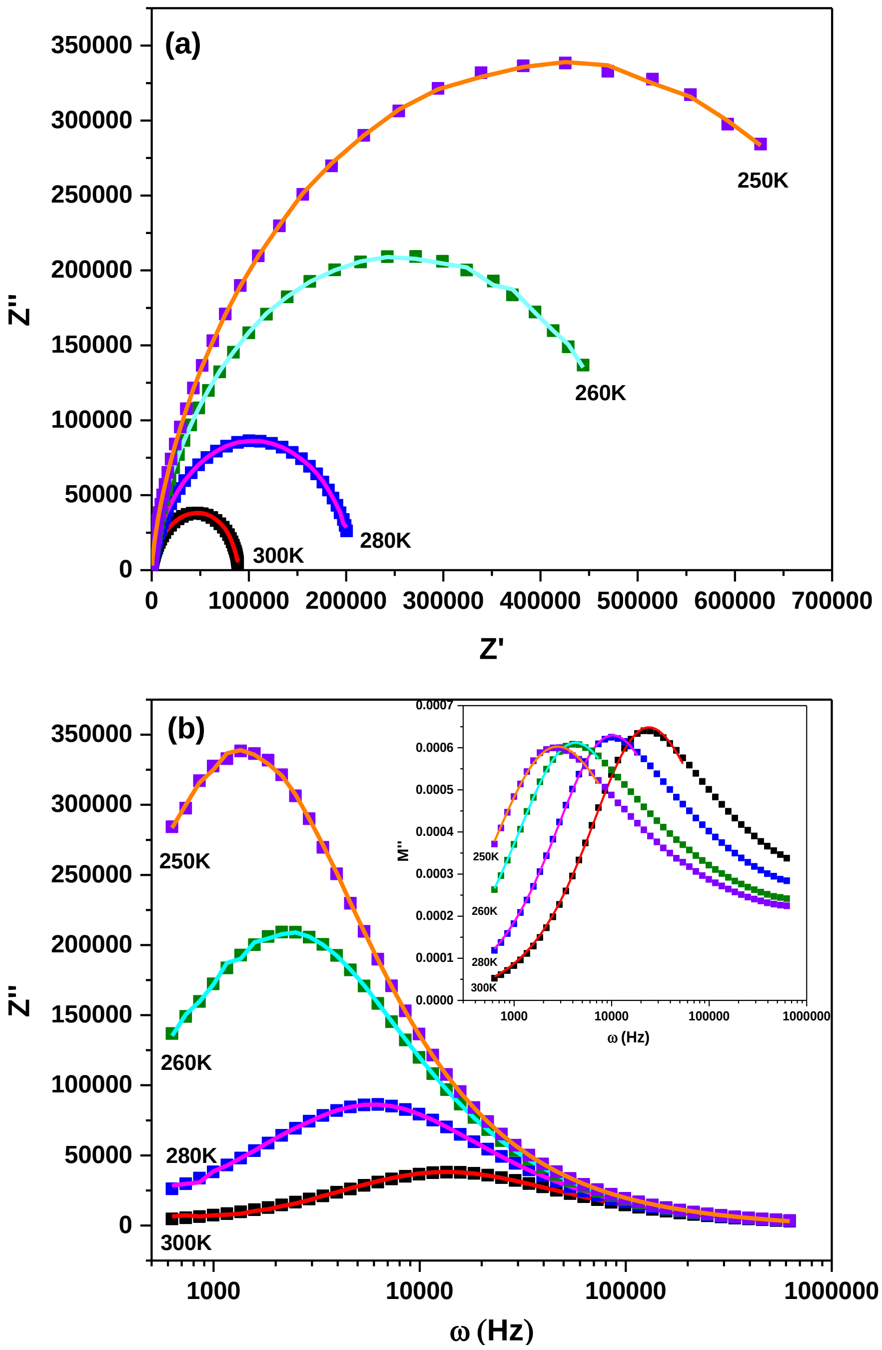

Fig. 7.5 shows the a) Cole-Cole plot and b) Bode plot of impedance at various temperatures of $(Bi_{13}Co_{12})CoO_{40}$. Inset shows the M'' vs. frequency plot for different representative temperatures.

The parameters ‘R’ and ‘τ’ are found to obey Arrhenius behavior. The linearity of the data when logarithmic resistance (lnR) plotted against the inverse of temperature (1000/T) confirms the Arrhenius type activated behavior as shown in fig. 7.6a. From the fit, the activation energies are calculated whose respective values in zero and 1.3T field are 0.262(5) eV and 0.259(5) eV. It is found that here also the effect of magnetic field is very less. Similarly from the temperature dependence of relaxation time (fig. 7.6b), the corresponding activation energies (in 0T and 1.3T) are 0.271(2) eV and 0.266(2) eV. Here too, insignificant role of magnetic field on the activation process is seen. The similarity in activation energies obtained from resistance and relaxation times implies a common mechanism of activation for conduction as well as relaxation.

Sometimes, modulus formalism is advantageous as it separates out the various spectral components of the material having similar resistances but have different capacitances. This formalism is complementary to the impedance formalism as in this process, even the smaller capacitance dominates and suppresses the electrode polarization where as in the impedance spectroscopy the total response is highlighted by the contribution of large resistances. The imaginary part of the modulus permits to study the electrical transport properties as well as the dipolar relaxations as a function of frequency and temperature. The inset of fig. 7.5b shows the M'' vs. frequency plot for different representative temperatures. The inset of fig. 7.5b shows the M'' vs. frequency plot at different representative temperatures. The single relaxation peaks are fitted to the Kohlarausch – Williams – Watts (KWW) function in frequency domain given by eq. 7.3 [28].

$$M'' = \frac{M_{max}''}{\left[1-\beta+\left(\frac{\beta}{1+\beta}\right)\left(\beta\left(\frac{\omega_{max}}{\omega}\right)+\left(\frac{\omega}{\omega_{max}}\right)^{\beta}\right)\right]} \text{------------------ (Eq. 7.3)}$$

Arrhenius fit to the obtained relaxation times yields the activation energies 0.268(4) eV and 0.267(4) eV in zero field and 1.3T magnetic field as shown in fig. 7.6b. Once again, these values are in good agreement with that obtained previously from the lnR and lnτ plots.

In the case of BCFO, the linear region in lnR and lnτ plot is fitted with Arrhenius relation as shown fig. 7.6c & d. A distinct slope change is observed at ~ 260K, which happens to be separating the intrinsic (< 260K) and extrinsic (>260K) regions (see fig 7.3c & d). The activation energies obtained from lnR plot in the extrinsic region are 0.198(8) eV (in 0T) and 0.27(1) eV (in 1.3T) whereas for intrinsic region the respective values are 0.047(5) eV and 0.05(5) eV. Similarly the activation energy obtained from the plot of $\ln\tau$ are 0.18(2) eV and 0.233(9) eV in the extrinsic region, whereas in intrinsic region it is 0.04(3) eV and 0.043(2) eV at 0T and 1.3T respectively. Corroboration of all the results suggests that the activation energy in extrinsic region is 0.2 – 0.25 eV whereas that in intrinsic regions is at least one order less at 0.04 – 0.05 eV. At temperatures > 260K, the relaxations are happening via conducting mechanism whose activation energy is ~0.2 eV. On the other hand, for temperatures < 260K the magnetoresistance effects are negligible and relaxations are happening via low energy (~0.04 eV) process. In a theoretical calculation done on NaCl lattice, Hatcher et.al., found an energy of 0.07 eV needed for relaxation via dipole-dipole interactions, on a contrary to other contributions which were at least two orders higher[29]. In the present scenario too, an association of 0.04 eV relaxations to the dipole-dipole interactions seems to be more plausible.

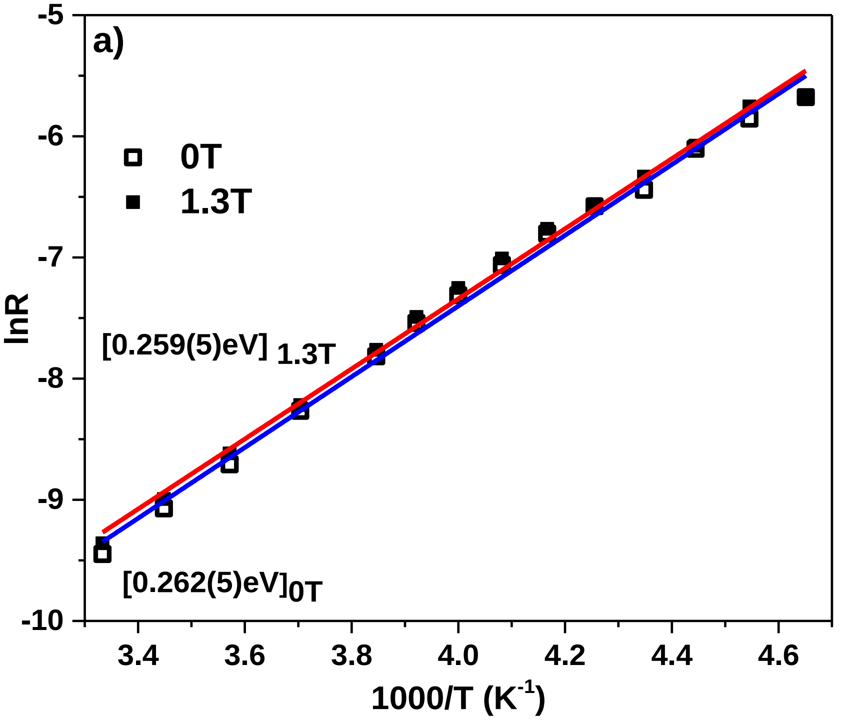
a)
-5
-6
-7
-8
-9
-10
lnR
3.4
3.6
3.8
4.0
4.2
4.4
4.6
1000/T (K-1)
0T
1.3T
[0.259(5)eV] 1.3T
[0.262(5)eV]0T

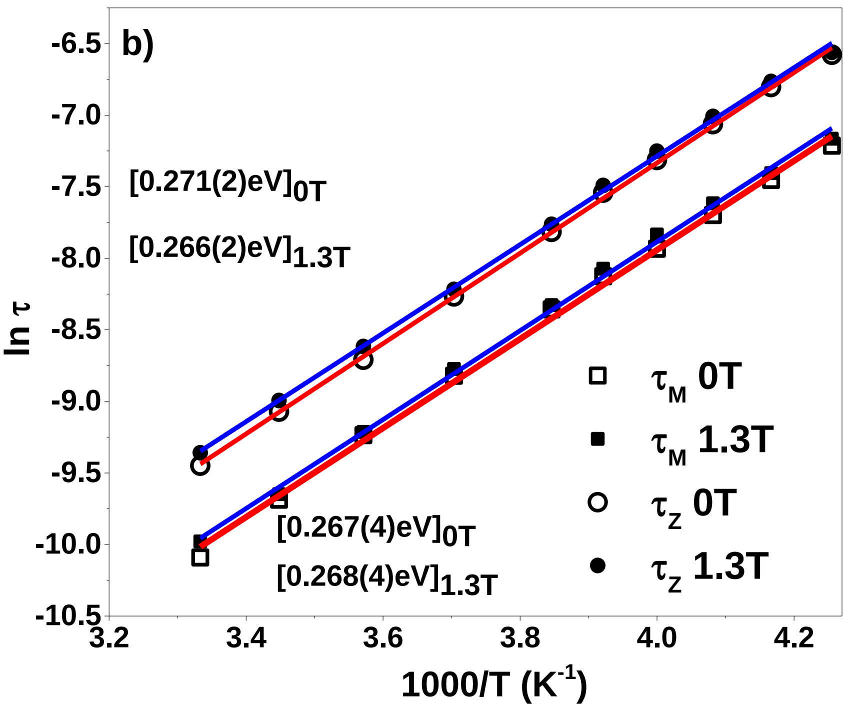
b)
-6.5
-7.0
-7.5
-8.0
-8.5
-9.0
-9.5
-10.0
-10.5
ln τ
3.2
3.4
3.6
3.8
4.0
4.2
1000/T (K-1)
[0.271(2)eV]0T
[0.266(2)eV]1.3T
[0.267(4)eV]0T
[0.268(4)eV]1.3T
τM 0T
τM 1.3T
τZ 0T
τZ 1.3T

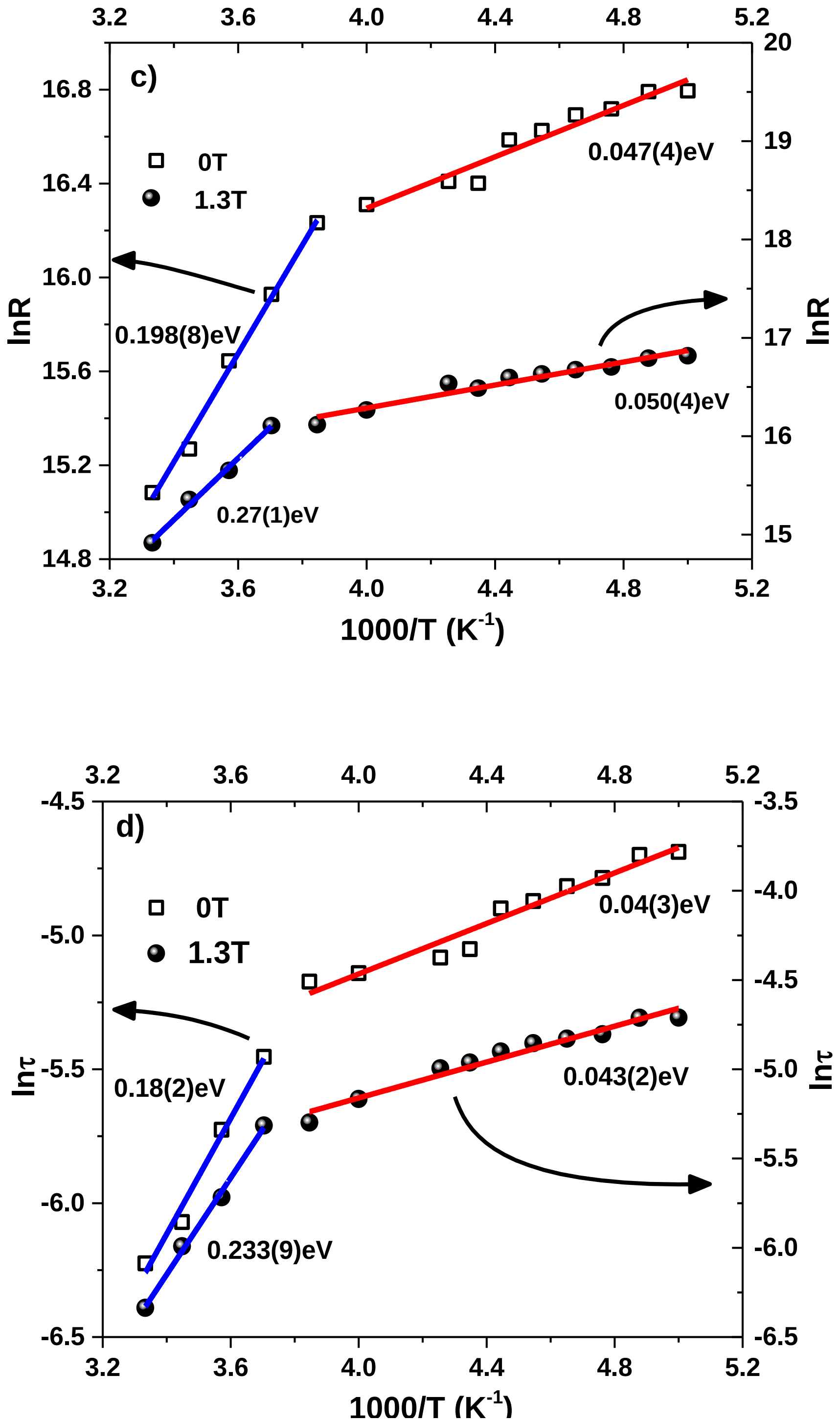

Fig. 7.6 a, b, c & d shows the logarithmic resistance (lnR) and relaxation time (lnτ) vs. 1000/T of ($Bi_{13}Co_{12}$)CoO_{40} and ($Bi_{13}Co_{5.5}Fe_{6.5}$)CoO_{40}.

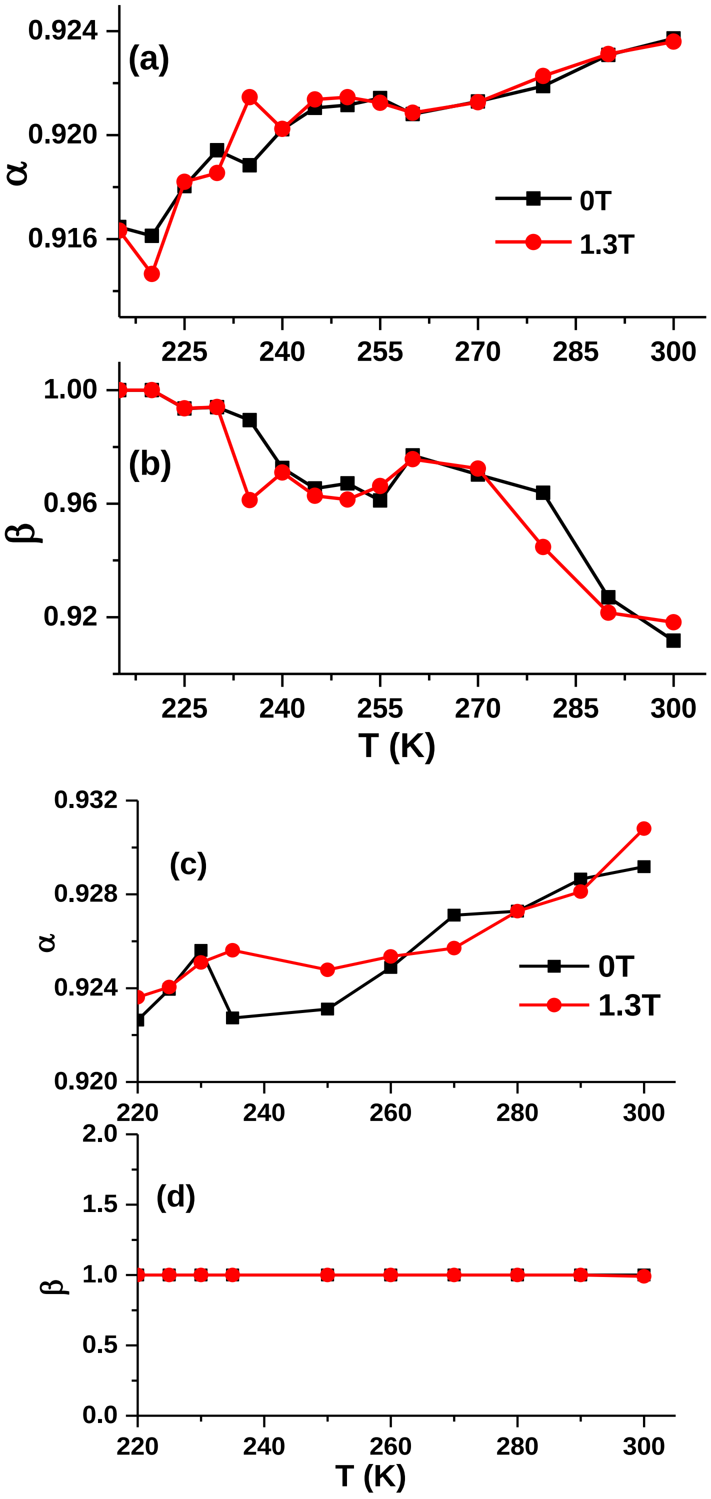

Fig. 7.7a, b, c & d shows the temperature dependent fitting parameter α and β of $(Bi_{13}Co_{12})CoO_{40}$ and $(Bi_{13}Co_{5.5}Fe_{6.5})CoO_{40}$ at 0T and 1.3T.

The deviation of broadening (α) and asymmetry (β) parameters from unity describes the non –Debye nature of relaxation. In fig. 7.7, α for both the samples, has values greater than 0.9 in the fitted temperature range, which shows a decreasing trend as temperature is lowered. In spite of similarity in α for both the samples, the asymmetry parameter β differs drastically: remains constant unity (hence HN relaxation reduces to Cole- Cole relaxation) for BCFO but increases from a room temperature value of 0.92 towards unity, as temperature is lowered. Since either α or β has value less than unity in the investigated temperature range, so the nature of relaxation is of Non –Debye type.

7.6 Conclusions

Bismuth cobaltite (BCO) nanoparticles and their Fe substituted counterparts (BCFO) are prepared by the sol-gel method. The XRD reveals cubic structure (as described in chapter 2) of the sample with coexistence of both octahedral and tetrahedral sites of cobalt in a unit cell. BCO is paramagnetic at room temperature and shows the magnetic ordering at 30K. No sign of magnetic disorderness is seen. On the other hand BCFO shows huge magnetic disorder with the ferromagnetic ground state. Dielectric measurements show lack of intrinsic dielectric in BCO and only extrinsic contributions whose activation energy is ~0.26eV. On the other hand BCFO shows both intrinsic and extrinsic regions of dielectric with the respective activation energies 0.18 – 0.27 eV and 0.04 – 0.05 eV.

References

1. M. Fiebig, *J. Phys. D: Appl. Phys.*, **38** R123 (2005)
2. W. Prellier, M. P. Singh and P. Murugavel, *J. Phys.: Condens. Matter*, **17** R803 (2005)
3. Y. Tokura and N. Nagaosa, *Science*, **288** 462 (2000)
4. E. Dagotto, *Science*, **309** 257 (2005)
5. N. A. Hill, *J. Phys. Chem. B*, **104** 6694 (2000)
6. P. Uniyal and K. L. Yadav, *J. Phys.: Condens. Mater*, **21** 012205 (2009)
7. V. A. Khomchenko, D. A. Kiselev, J. M. Vieira, Li Jian, A. L. Kholkin, A. M. L. Lopes, Y. G. Pogorelov, J. P. Araujo and M. Maglione, *J. Appl. Phys.*, **103** 024105 (2008)
8. V. R. Palkar, D. C. Kundaliya, and S. K. Malik, *J. Appl. Phys.*, **93** 4337 (2003)
9. T. Choi and J. Lee, *Appl. Phys. Lett.*, **84** 5043 (2004)
10. J. Magesh, P. Murugavel, R. V. K. Mangalam, K. Singh, Ch. Simon and W. Prellier, *Appl. Phys. Lett.*, **101** 022902 (2012)
11. S. S. Subramanian, K. Yamauchi, T. Ozaki, T. Oguchi and B. Natesan, *J. Phys : Condens. Matter.*, 25 385901 (2013)
12. A. Belik, S. Iikubo, K. Kodama, N. Igawa, S. Shamoto, S. Niitka, M. Azuma, Y. Shimakawa, M. Takano, F. Izumi and E. T. Muromachi, *Chem. Mater.*, **18** 798 (2006)
13. X. Ming, X. Meng, F. Hu, C-Z. Wang, Z-F, Huang, H-G, Fan and G. Chen, *J. Phys.: Condens. Matter*, **21** 295902 (2009)
14. K. Oka, M. Azuma, W. Chen, H. Yusa, A. A. Belik, E. T. Muromachi, M. Mizumaki, N. Ishimatsu, N. Hiraoka, M.Tsujimoto, M. G. Tuker, J. P. Attfield and Y. Shimakawa, *J. Am. Chem. Soc.*, **132** 9438 (2010)
15. M-Q. Cai, J-C. Liu, G-W. Yang, Y-L. Cao, X. Tan, X-Y. Chen, Y-G Wang, L-L. Wang and W-Y Hu, *J. Chem. Phys.*, **126** 154708 (2007)
16. Y. Uratani, T. Shishidou, F. Ishii and T. Oguchi, *Jpn. J. Appl. Phys.*, **44** 7130 (2005)
17. J. D. Bucci, *Ph.D. Thesis*, University of Missouri, Rolla (1971)

18. S. Vasudevan, C. N. R. Rao, A. M. Umarji and G. V. Subba Rao, *Mat. Res. Bull.*, **14** 451 (1979)

19. P. N. Vishwakarma, *Solid State Comm.*, **149** 115 (2009)

20. C. Nethravathi, S. Sen, N. Ravishankar, M. Rajamathi, C. Pietzonka and B. Harbrecht, *J. Phys. Chem. B*, **109** 11468 (2005)

21. W. L. Roth, *J. Phys. Chem. Solids* **25,** 1 (1964)

22. L. Balents, *Nature*, **464** 199 (2010)

23. A. P. Ramirez, *Annu. Rev. Mater. Sci.*, **24** 453 (1994)

24. A. H. Morrish, *The physical principles of magnetism*, IEEE Press, New York, 2001

25. T-J. Park, G. C. Papaefthymiou, A. J. Viescas, A. R. Moodenbaugh and S. S. Wong, *Nano Lett.*, **7** 766 (2007)

26. G. Catalan, *Appl. Phys. Lett.*, **88** 102902 (2006)

27. A. K. Biswal, J. Ray, P. D. Babu, V. Siruguri and P. N. Vishwakarma, *J. Appl. Phys.*, **115** 194106 (2014)

28. R. Bergman, *J. Appl. Phys.*, **88** 1356 (2000)

29. R. D. Hatcher and G. J. Dienes, *Phys. Rev.*, **134** A214 (1964)

Chapter 8

Future scope of the work

8.1 Future scope of work

In the present work, the phase pure Co substituted $BiFeO_3$ is prepared via sol-gel auto combustion method and the particle size is found to be of nano range. The effect of Co substitution on the various physical properties of $BiFeO_3$ is discussed in the respective chapters.

8.1 Future scope of the work:

This thesis investigates various physical properties of the Co substituted $BiFeO_3$. A lot of further studies on different aspects are possible for academic/fundamental interest and also for potential applications of the material.

- The study of the crystal structure from synchrotron radiation can be performed which will be useful for the better understanding of the structural transition.
- The time of flight measurement is necessary for the understanding about the spin canting.
- The temperature dependent magnetoelectric measurement can be done.
- The magnetodielectric study can be performed for Co substitute $BiFeO_3$ on the high temperature range.
- Magnetic, dielectric, magnetolelectric and magnetodielectric study of Co substituted $BiFeO_3$ crystallized both in the R3c and I23 space group ($0.03 \leq x \leq 0.3$) can be performed.

CURRICULAM VITAE

JASHASHREE RAY

Senior Research Fellow
Cryomagnetism Laboratory,
Department of Physics and Astronomy,
National Institute of Technology, Rourkela
Odisha, Pin-769008, India
Mobile: - 09861187122
Email: - jashashree@gmail.com

Residence: - c/o- Sj. Prasanna Kumar Ray
AT- College Square, P.O/ Dist. - Jagatsinghpur,
Odisha, Pin- 754103
Phone: - 09861173978

Education

- Ph.D, Physics, (submitted in December 2014)
  "Magnetic & Dielectric properties of Cobalt substituted $BiFeO_3$"
  Thesis submitted to National Institute of Technology, Rourkela, Odisha, India.
- M.Sc., Physics First Class (7.97)
  Department of Physics, National Institute of Technology, Rourkela. 2009.
- B.Sc., Physics First Class (81%)
  S. V. M College, Utkal University, Odisha. 2007.

Broad Field of Research

Experimental Condensed Matter Physics

Research Interests

- Transition Metal oxides

Studying the electric and magnetic properties in ferrites, cobaltites, manganese oxides and to find out the correlation among various order parameters.

- Superconductors

Instrumentation

- Design a setup for the measurement of resistivity, dielectric, magneto-dielectric in closed cycle refrigerator.
- Design a setup for measurement of magneto-electric coupling in a 2T electromagnet.
- Design a low cost setup for the thin film preparation in a spray pyrolysis method.
- Design a 6T superconducting magnet.

Experimental techniques used:

- X-ray diffraction.
- Neutron diffraction at DHRUVA reactor, BARC, Mumbai, India.
- Magnetoelectricity/ Magnetodielectricity by DC magnetic bias field up to 1.3T using an electromagnet (GMW 5403).
- High and low temperature resistance by Keithly Electrometer.
- Atomic Force microscopy (AFM).
- DC- magnetization using VSM.
- Impedance measurement by Lock- in amplifier and LCR meter.
- Closed cycle refrigerator for low temperature measurement.

Computational techniques used:

- **Rietveld refinement** using the **FULLPROF** program:

- Detailed **crystal structure analysis**, from the refinement of the **x-ray and neutronpowder diffraction** data, such as positions of the atoms in a unit cell, bond length and bond angle between the different atoms in a unit cell, **crystal structure**.

- Determination of the **magnetic structure** from the refinement of variable temperature neutron diffraction patterns.

- Data analysis using the **ORIGINC** programs.

Course work

- Techniques in advance characterization
- Special topics in Low temperature physics
- Problems in classical mechanics

Details of research experience

The multiferroic $BiFeO_3$ is a grey area of research since 19th century. The peculiar property and the underlying physics of this material captivates the urge of the researchers towards it. The material exhibits ferroelectric polarization (T_c= 1143K) and antiferromagnetic ordering (T_N= 643K) well above the room temperature. The stereochemically active $6s^2$ lone pair is responsible for the generation of ferroelectricity in the sample. In addition to this, the cycloidal spin arrangement of Fe^{3+} ions are superimposed on the G- type antiferromagnetism structure with a periodicity of 62nm, hence by cancelling the net magnetization. The peculiar arrangement of Fe^{3+} ions hinders it for practical applications. So researchers are trying to enhance the magnetization either by disrupting the spin cycloid via various chemical substitution or by the application of high magnetic field. The difficulty in the synthesis of the single phase $BiFeO_3$, the existence of weak magnetoelectric coupling and to minimize the loss allows the researchers to tune its property.

In my Ph. D work, I have undertaken a detailed study of magnetic and dielectric properties of Co substituted $BiFeO_3$. The nanoparticles of $BiFe_{1-x}Co_xO_3$ are prepared via sol-gel assisted auto-combustion method. XRD measurements confirms that the pristine sample is crystallized in the rhombohedral crystal structure (R3c). A structural transformation from rhombohedral structure (R3c) to cubic structure (I23) is observed from x= 0.35 onwards. So in the present work, we have only studied the single phase $BiFe_{1-x}Co_xO_3$ which constitutes the dilute concentration of $BiFe_{1-x}Co_xO_3$; x= 0, 0.01, 0.02 and higher concentration of $BiFe_{1-x}Co_xO_3$; x= 0.5, 1. Atomic force microscopy reveals average particle size is of 100 – 200 nm. The magnetic property is studied through the 14T VSM. Various magnetic properties like superparamagnetic, antiferromagnetic, ferrimagnetic etc. along with the peculiar spin and cluster glass behaviour is observed. To explain these magnetic behaviours successfully, a cycloidal spin model is proposed. Here it is observed that Co^{3+} ion undergoes a first order transition (Low spin to intermediate spin) which is a function of both magnetic field and temperature. To witness the effect of cobalt substitution in BFO at its best, temperature dependent neutron diffraction measurement is carried out. At room temperature, the Co^{3+} are found to be in intermediate spin state corresponding to magnetic moment 2.828 μ_B, whereas that of Fe^{3+} as $3.848\mu_B$. At low temperatures, signature of spin state transition from intermediate spin ($S = 1$) to low spin ($S = 0$) of Co^{3+} ion is observed. The Co^{3+} induced spin canting is also studied.

The magnetoelectric study is carried out in a homemade setup (based on the dynamic method) for the confirmation of magnetoelectric coupling. The substitution of Co induces the linear behavior in coupling coefficient with the dc magnetic field such that it is good enough for device applications especially where α must follow the applied magnetic field linearly, e.g., transistors, transducers, etc. Neutron diffraction studies show lattice stiffening due to cobalt substitution in $BiFeO_3$ and likely to be the cause of disappearance of hysteresis in α. Calculated value of polarization P (using the parameters derived from neutron diffraction) shows 19% drop in magnitude of P for cobalt substituted sample. Surprisingly, dielectric measurements also showed 18% decrease in dielectric constant ε' due to cobalt doping. Such a one to one correspondence in the three parameters viz., α, P and ε', reflects a strong interdependence so that variation in any one of them is reciprocated in the other. The dc electrical resistivity measurements, suggests variable range hopping (VRH) as the conduction mechanism at low temperatures. The low temperature dielectric data is found a good fit to the Haverliak – Negami (HN) expression plus an additional term for the Maxwell Wagner (MW) type relaxations. The dielectric relaxations is well explained by polaronic variable range hopping model and a distinct transition from extrinsic to intrinsic behavior is seen at 215K. The relaxation dynamics of the sample is further getting slower by the substitution of Cobalt. The indications of relaxor behavior for $x = 0.02$ are seen in high temperature range (above room temperature). $x = 1$ is found to be paramagnetic at room temperature and shows magnetic ordering at 30K. No sign of magnetic disorderness is seen. On the other hand $x = 0.5$ shows huge magnetic disorder with ferrimagnetic ground state. Dielectric measurements show lack of intrinsic dielectric in $x = 1$ and only extrinsic contributions whereas on the other hand $x = 0.5$ shows both intrinsic and extrinsic regions of dielectric with the variation of temperature.

Technical Programme

- As the work is based on the study of multiferroic properties so a magnetoelectric set up is designed for measuring the direct magnetoelectric coupling coefficient.
- The dielectric set up is designed for measuring the dielectric properties both at low (with closed cycle refrigerator) and high temperatures (a muffle furnace).
- To study the transport properties a low temperature resistivity set up is designed.
- The magnetic measurement and neutron diffraction measurement will be done at CSR Mumbai centre.

Sample preparation

I have the expertise in preparing the samples in chemical method as well as in solid state method. In my thesis work I have prepared the samples via sol-gel auto combustion method.

List of Published Papers:

Journals:

1. "Effect of Co substitution on the magnetic properties of $BiFeO_3$", **J. Ray**, A. K .Biswal, S. Acharya, V. Ganesan, D. K. Pradhan & P. N. Vishwakarma* *J. Magn. Magn. Mater.*, **324,** 4084 (2012).
2. "Low temperature magneto-dielectric measurements on $BiFeO_3$ lightly substituted by cobalt" **J. Ray**, A. K. Biswal & P. N. Vishwakarma*, *J. Appl. Phys.***,** **117,** 134102 (2015)
3. "Magnetoeletricity in $BiFeO_3$ and $BiFe_{0.98}Co_{0.02}O_3$ nano particles" **J. Ray**, A. K. Biswal, P. D. Babu, V. Siruguri & P. N. Vishwakarma*, *J. Alloys and Comp.*, **628**, 32 (2015).
4. "Magnetic and dielectric studies of Fe substituted sillenite phase Bismuth Cobaltite nanoparticles" **J. Ray**, A. K. Biswal, S. Kuila & P. N. Vishwakarma* *J. Alloys and Comp.*, **633**, 370 (2015)
5. "Study of $Bi_2Sr_2CaCu_2O_8/BiFeO_3$ nano-composite for electrical transport Applications" S. Acharya, A. K. Biswal, **J. Ray**, and P. N. Vishwakarma, *J. Appl. Phys.* **112**, 053916 (2012).
6. "Dielectric relaxation in La_2NiMnO_6 with signatures of Griffith Phase" A. K. Biswal, **J. Ray,** P. D. Babu, V. Siruguri, and P. N. Vishwakarma , *J. Appl. Phys.* **115**, 194106 (2014).
7. "Effect of Cu substitution on the magnetic and dielectric properties of La_2NiMnO_6" *J. Appl. Phys.* **117**, 17B728 (2015).
8. "Neutron diffraction studies on cobalt substituted $BiFeO_3$" **J. Ray**, A. K. Biswal, S. Acharya, P. D. Babu, V. Siruguri & P. N. Vishwakarma, *AIP Conf. Proc.* **1512**, 1124 (2013).

9. “Magnetic origin of dielectric transition in $BiFeO_3$” **J. Ray**, A. K. Biswal, P. D. Babu, V. Siruguri, and P. N. Vishwakarma, *AIP Conf. Proc.* **1591**, 1595 (2014).
10. “Signature of Griffith singularity in half doped $LaMn_{0.5}Cu_{0.5}O_3$” A. K. Biswal, **J. Ray**, P. D. Babu, V. Siruguri, and P. N. Vishwakarma *AIP Conf. Proc.* **1591**, 1630 (2014).
11. “Signature of relaxor behaviour in $BiFe_{0.98}Co_{0.02}O_3$” *AIP Conf. Proc.* **1665,** 140058 (2015).
12. “Gas sensing applications of La_2NiMnO_6” *AIP Conf. Proc.* **1665,** 140050 (2015)
13. “Near room temperature giant magnetodielectricity in $BiFeO_3/CoFe_2O_4$ composite” *AIP Conf. Proc.* **1665,** 140050 (2015).

Accepted:

1. “Neutron diffraction study of $BiFeO_3$ and $BiFe_{0.98}Co_{0.02}O_3$ nano particles” **J. Ray**, A. K. Biswal, P. D. Babu, V. Siruguri & P. N. Vishwakarma*, accepted in *Solid State comm.*

Conference/Symposia:

1. “Magnetic phase transition in Bismuth cobaltite nanoparticles” **poster presented at Joint Europian Magnetic Symposia-2012,** Parma, Italy**.**
2. “Neutron diffraction studies on cobalt substituted $BiFeO_3$” poster presented at **DAE SSPS-2012** at IIT Mumbai, India.
3. “Magnetic origin of dielectric transition in $BiFeO_3$” poster presented at **DAE SSPS-2013** at Thapar University, Patiala, India.
4. “Signature of relaxor behaviour in $BiFe_{0.98}Co_{0.02}O_3$” accepted at **DAE SSPS – 2014** at VIT University, Vellore, Tamilnadu.

Thanking You

Jashashree Ray